

**DEVELOPMENT AND EVALUATION OF A GIS-BASED
SPATIALLY DISTRIBUTED UNIT HYDROGRAPH MODEL**

by

Jennifer Leigh Kilgore

Thesis submitted to the Faculty of the
Virginia Polytechnic Institute and State University
in partial fulfillment of the requirements for the degree of

Master of Science
in
Biological Systems Engineering

Dr. Conrad D. Heatwole, Chair
Dr. Saied Mostaghimi
Dr. David F. Kibler
Dr. John V. Perumpral, Department Head

Keywords: GIS, unit hydrograph, hydrologic modeling, spatial modeling

December 10, 1997
Blacksburg, VA

Copyright 1997, Jennifer Leigh Kilgore

DEVELOPMENT AND EVALUATION OF A GIS-BASED SPATIALLY DISTRIBUTED UNIT HYDROGRAPH MODEL

by
Jennifer Leigh Kilgore

(ABSTRACT)

Synthetic unit hydrographs, which assume uniform rainfall excess distribution and static watershed conditions, are frequently used to estimate hydrograph characteristics when observed data are unavailable. The objective of this research was to develop a spatially distributed unit hydrograph (SDUH) model that directly reflects spatial variation in the watershed in generating runoff hydrographs.

The SDUH model is a time-area unit hydrograph technique that uses a geographic information system (GIS) to develop a cumulative travel time map of the watershed based on cell by cell estimates of overland and channel flow velocities. The model considers slope, land use, watershed position, channel characteristics, and rainfall excess intensity in determining flow velocities. The cumulative travel time map is divided into isochrones which are used to generate a time-area curve and the resulting unit hydrograph.

Predictions of the SDUH model along with the Snyder, SCS, and Clark synthetic unit hydrographs were compared with forty observed storm events from an 1153-ha Virginia Piedmont watershed. The SDUH model predictions were comparable or slightly better than those from the other models, with the lowest relative error in the peak flow rate prediction for 12 of the 40 storms, and a model efficiency of at least 0.90 for 21 of the storms. Despite the good predictions of the hydrograph peak flow rate and shape, the time to peak was underpredicted for 34 of the 40 storms.

Runoff from the 40 storms was also generated for two subwatersheds (C: 462 ha; D: 328 ha) in Owl Run to assess the effect of scale on the SDUH model. Peak flow rate predictions were more accurate for the entire watershed than for either subwatershed.

The time to peak prediction and model efficiency statistics were comparable for the entire watershed and subwatershed D. Subwatershed C had poorer predictions, which were attributed to a large pond in the main channel, rather than to scale effects.

The SDUH model provides a framework for predicting runoff hydrographs for ungauged watersheds that can reflect the spatially distributed nature of the rainfall-runoff process. Predictions were comparable to the other synthetic unit hydrograph techniques. Because the time to peak and model efficiency statistics were similar for the 1153-ha watershed and a 328-ha subwatershed, scale does not have a major impact on the accuracy of the SDUH model.

ACKNOWLEDGMENTS

I would like to thank Dr. Conrad Heatwole for his knowledge, advice and patience while serving as my major professor. Thanks also go to my other committee members, Dr. Saied Mostaghimi and Dr. David Kibler. Their knowledge and suggestions were a great help in the completion of this project. Nicole Cook and Kevin Brannan were extremely helpful in assembling the data set I used in this project. I would also like to thank the Department of Biological Systems Engineering for providing me with an excellent undergraduate and graduate education.

This study was funded, in part, by the Virginia Department of Conservation and Recreation, Division of Soil and Water Conservation, Richmond, Virginia.

Finally, my family and friends deserve many thanks for their support and encouragement. I would especially like to thank my parents and Aron. Without their constant faith in me, I never would have finished this project.

TABLE OF CONTENTS

1.0 Introduction	1
<i>Objectives</i>	<i>3</i>
2.0 Literature Review	4
2.1 <i>Runoff Prediction and the Unit Hydrograph.....</i>	<i>4</i>
2.2 <i>Lumped versus Distributed Models</i>	<i>9</i>
2.3 <i>Use of GIS in hydrology.....</i>	<i>10</i>
2.4 <i>Spatially Distributed Unit Hydrograph</i>	<i>12</i>
2.5 <i>Summary</i>	<i>13</i>
3.0 Methodology	14
3.1 <i>Study Overview.....</i>	<i>14</i>
3.2 <i>Model Development.....</i>	<i>15</i>
3.3 <i>Sensitivity Analysis</i>	<i>17</i>
3.4 <i>Traditional Synthetic Unit Hydrographs</i>	<i>18</i>
3.5 <i>Hydrology</i>	<i>26</i>
3.6 <i>Evaluation.....</i>	<i>29</i>
4.0 Model Development and Application.....	32
4.1 <i>Watershed Description</i>	<i>32</i>
4.2 <i>Topography.....</i>	<i>37</i>
4.3 <i>Channel Delineation.....</i>	<i>39</i>
4.4 <i>Flow velocity.....</i>	<i>41</i>
4.5 <i>Travel Time</i>	<i>46</i>
4.6 <i>Ponds.....</i>	<i>46</i>
4.7 <i>Cumulative Travel Time to the Outlet.....</i>	<i>47</i>

4.8 Unit hydrograph development.....	49
5.0 Results and Discussion	50
5.1 Comparison of Unit Hydrograph Techniques.....	50
5.2 Multiple Watershed Comparison.....	77
5.3 Sensitivity Analysis.....	95
5.4 Discussion.....	104
6.0 Summary and Conclusions.....	109
6.1 Summary.....	109
6.2 Conclusions.....	111
6.3 Recommendations for Future Research.....	112
7.0 References	113
Appendix A: Programs and Macro Files.....	119
Appendix B: Traditional Synthetic Unit Hydrographs.....	127
Appendix C: Comparison of Unit Hydrograph Techniques.....	131
Appendix D: Multiple Watershed Comparison.....	172
Vita.....	213

LIST OF ILLUSTRATIONS

Figure 3.1. SDUH Model Flow Chart.....	16
Figure 3.2. Traditional Synthetic Unit Hydrographs.....	25
Figure 4.1. Location of Owl Run Watershed.....	33
Figure 4.2. Owl Run land use (Spring/Summer 1992).....	34
Figure 4.3. Location of monitoring stations within Owl Run watershed (Mostaghimi et al., 1997).....	35
Figure 4.4. Map of Cells Used to Determine Slope of Cell E.....	37
Figure 4.5. Codes Used to Indicate Flow Directions.	38
Figure 4.6. Owl Run DEM-based stream network (red) and USGS blue-line stream network (blue).....	40
Figure 4.7: Manning’s roughness coefficient	42
Figure 4.8. Owl Run Stream Network.....	45
Figure 4.9. Algorithm used to develop the map of the cumulative travel times to the outlet for each grid cell in the watershed.	48
Figure 5.1. Observed and predicted hydrographs for storm #11 (November 9-10, 1990).....	52
Figure 5.2. Observed and predicted hydrographs for storm #21 (May 8, 1992).....	53
Figure 5.3. Observed and predicted hydrographs for storm #26 (July 27, 1992).....	54
Figure 5.4. Comparison of predicted versus observed peak flow rate for synthetic unit hydrograph techniques.	58
Figure 5.5. Observed and predicted hydrographs for storm #11 (Nov. 9-10, 1990).	79
Figure 5.6. Observed and predicted hydrographs for storm #21 (May 8, 1992).....	81
Figure 5.7. Observed and predicted hydrographs for storm #26 (July 27, 1992).....	83
Figure 5.8. Predicted vs. observed peak flow rates, entire Owl Run watershed.	87
Figure 5.9. Observed vs. predicted peak flow rates for subwatershed C.....	88
Figure 5.10. Observed vs. predicted peak flow rates for subwatershed D.....	89
Figure 5.11. Sensitivity of model response to variations in the channel flow threshold (CFT).....	97
Figure 5.12. Sensitivity of model response to variations in channel velocity.....	98
Figure 5.13. Sensitivity of model response to variations in overland flow velocity.....	99
Figure 5.14. Sensitivity of model response to variations in channel bottom width.....	100
Figure 5.15. Sensitivity of model response to variations in rainfall excess intensity.	101
Figure 5.16. Sensitivity of model response to variations in hydraulic residence time in the pond.....	102
Figure 5.17. Sensitivity of model response to variations in the time interval.....	103
Figure 5.18. Observed and predicted hydrographs for storm #7 (May 28-29, 1990).....	106
Figure 5.19. Observed and predicted hydrographs for storm #14 (August 9-10, 1990).....	106
Figure 5.20. Observed and predicted hydrographs for storm #18 (October 5-6, 1991).....	107
Figure 5.21. Observed and predicted hydrographs for storm #27 (July 31, 1992).....	107

LIST OF TABLES

Table 3.1. Base values used in the sensitivity analysis.....	17
Table 3.2. Summary of rainfall events.	28
Table 4.1. Summary of Owl Run land uses and Manning’s roughness coefficients.	43
Table 4.2. Summary of Manning’s roughness coefficients for channel cells.	46
Table 5.1. Observed peak flow rate and predicted peak flow rates (m ³ /s).....	56
Table 5.2. Relative error in peak flow rate for five unit hydrograph techniques.	57
Table 5.3. Observed and predicted time to peak (hours).	60
Table 5.4. Percent error in the time to peak for each storm.	61
Table 5.5. Model efficiency for each unit hydrograph technique.	63
Table 5.6. Average R ² values for unit hydrograph technique with and without storm #4.	64
Table 5.7. Number of events each method had the highest and lowest R ² values.....	64
Table 5.8. Number of events that had high R ² values.	64
Table 5.9. Bias in Hydrograph Shape Prediction.	67
Table 5.10. Sum of absolute Residuals (SAR) and total sum of absolute residuals (TSAR).	68
Table 5.11. Sum of squared residuals (SSR) and total sum of squared residuals (TSSR).	69
Table 5.12. Relative error in peak flow rate based on rainfall volume.....	71
Table 5.13. Relative error in the time to peak based on rainfall volume.	71
Table 5.14. Average model efficiency (R ²) based on rainfall volume.....	71
Table 5.15. Error in peak flow rate based on average rainfall excess intensity.	73
Table 5.16. Error in time to peak based on average rainfall excess intensity.	73
Table 5.17. Average model efficiency (R ²) based on average rainfall excess intensity.	73
Table 5.18. Seasonal effects on the prediction of peak flow rate.....	75
Table 5.19. Seasonal effects on time to peak prediction.	75
Table 5.20. Seasonal effects on average model efficiency.	75
Table 5.21. Predicted and observed peak flow rates (m ³ /s).....	85
Table 5.22. Percent error in peak flow rate for subwatersheds C and D and the whole watershed.....	86
Table 5.23. Time to Peak (hours).....	91
Table 5.24. Relative error and MARE for time to peak predictions; Owl Run and subwatersheds C and D.	92
Table 5.25. Model efficiencies for Owl Run and subwatersheds C and D.	94

1.0 Introduction

The human race has been trying to control water for thousands of years. Archeologists believe that the Egyptians built a dam across the Nile river in 4000 B. C. There is also evidence that there were extensive irrigation canals in Egypt around 3200 B. C. For appropriate design and management of hydraulic structures, engineers must be concerned with the peak discharge and the time to peak for large storm events. This type of information is needed for a wide variety of design applications, including dams, spillways, and culverts. Unfortunately, many streams are ungauged and do not have flow records. Even when stream gauges are in place, the record is often too short to accurately predict extreme events (Ajward, 1996).

In many cases, runoff characteristics may be estimated using rainfall-runoff models. Precipitation data is generally more available than stream flow data because there are a larger number of gauging stations and usually longer periods of record than are available for stream flow data.

Many researchers have developed rainfall-runoff models that attempt to accurately predict runoff hydrographs, peak flow rates, and times to peak. Early models were based on empirical equations. Sherman (1932) proposed the “unitgraph” or unit hydrograph technique. It was one of the first attempts to predict an entire hydrograph instead of just the peak flow rate and time to peak. In the following years, numerous researchers attempted to improve on the unit hydrograph method by using increasingly complex models to develop the hydrograph shape. Some of the techniques proposed included treating the watershed as a cascade of linear reservoirs, using nonlinear reservoirs or using statistical procedures. In Todini’s (1988) assessment, the techniques produced mathematically correct hydrographs; however, they lost their connections with

the “real world” and increasingly became “mathematical games played by algebrists”.

During the 1960’s, researchers tried to develop models that produced accurate results, but also had a physical interpretation. Todini (1988) provides a summary of many of the physically-based rainfall-runoff models developed during the 1960’s and 1970’s.

As computing power has improved, hydrologists have developed more complex models. During the 1980’s and 1990’s, many distributed parameter models were introduced. Distributed parameter models have the ability to incorporate information about the spatial variability of soils, land use, topography, or any other parameter in the modeling scenario. Many distributed parameter models have large input data requirements and require substantial computing power; however, they have the ability to model processes occurring within the watershed as well as at the outlet.

In order to manage the enormous amount of data required for distributed models, hydrologists are increasingly turning to geographic information systems (GIS). GISs may be used to combine topographic information with other data such as soils, land use, surface cover, in order to create hydrologic models (DeVantier and Feldman, 1993). GISs have been used in a wide variety of hydrologic applications ranging from determining the drainage pattern in a watershed for nonpoint source modeling (Kao, 1992) to simulating surface runoff from flash floods (Julien et al., 1995).

Maidment (1993b) suggested a unit hydrograph technique that could combine the advantages of distributed modeling with the power of GIS. He applied the method to a hypothetical 36 grid-cell watershed. The time-area curve method was used to develop the synthetic unit hydrograph. While the time-area technique is a fairly standard method, the procedure to determine the isochrones is new. An isochrone is a line of equal travel time. Instead of estimating isochrone lines based only on the distance from the watershed outlet, the GIS model can route the runoff over the elevation surface and account for differences in runoff velocity due to changing slope, land use, and surface conditions. Unlike conventional time-area methods, the GIS model can also account for features such as detention ponds or wetlands that can slow runoff.

Although Maidment’s results were inconclusive, Muzik (1995) and Ajward

(1996) successfully applied his technique to two large mountainous watersheds in the Canadian Rockies. To date, this unit hydrograph technique has not been evaluated on agricultural catchments or on moderately-sized watersheds.

Objectives

The overall goal of this study was to develop and evaluate a method for predicting direct runoff hydrographs for moderately-sized ungauged watersheds. Specific objectives were:

- Develop a spatially distributed unit hydrograph model suitable for ungauged basins based on the spatial analysis functions in a raster GIS;
- Evaluate the accuracy of the model by comparing the results with traditional synthetic unit hydrographs and with observed flow data from a Virginia Piedmont watershed;
and
- Evaluate the effectiveness of the model at different spatial scales.

2.0 Literature Review

2.1 Runoff Prediction and the Unit Hydrograph

2.1.1 Background

Rainfall-runoff modeling began in the second half of the nineteenth century in response to three major engineering problems (Todini, 1988):

1. urban sewer design,
2. land reclamation drainage system design, and
3. reservoir spillway design.

At first, many engineers applied empirical equations developed in one region to many other areas and situations (Todini, 1988). They assumed that the conditions were "close enough." The other popular technique was the "rational method" to predict peak flow rates (Todini, 1988). Developed for small watersheds, the rational method is based on land use and rainfall intensity. It was the first attempt to "rationally" predict runoff from rainfall. During the 1920's, the need arose to have an analogous procedure that predicts the peak flow rate for larger watersheds. A modification of the rational method was developed based on the concept of isochrones. Isochrones are areas with equal travel times. The modified rational method was used to solve many of the same types of problems as the original rational method, however it generally produced more realistic, accurate solutions (Todini, 1988).

Sherman (1932) introduced the unit hydrograph based on the principle of

superposition. It was one of the first tools available to hydrologists to predict entire hydrographs instead of just peak discharges (Todini, 1988).

The procedure to develop a unit hydrograph for a storm with a single peak is fairly simple. After the baseflow is removed from the total runoff hydrograph, the direct runoff hydrograph remains. The total runoff volume is determined by integrating the direct runoff hydrograph. In order to obtain the unit hydrograph, each ordinate of the direct runoff hydrograph is divided by the runoff volume.

Theoretically, unit hydrographs developed from different storms should be identical, however that is rarely the case in practice. In order to develop an average response, Ponce (1989) recommended developing unit hydrographs from at least five different storm events. Linsley et al. (1975) suggest that an average response may be determined by calculating the average peak flow rate and time to peak, then sketching a hydrograph shape such that it contains 1 unit of runoff, passes through the average peak, and has a shape similar to the unit hydrographs developed from the individual storm events.

2.1.2 Unit Hydrograph Theory

The unit hydrograph is a linear response function of the watershed. It assumes that the time base of the hydrograph remains constant regardless of the amount of runoff resulting from different storms with the same duration. When using the unit hydrograph theory, it is assumed that the runoff response from a storm with a runoff depth other than 1 unit may be obtained by multiplying the runoff depth by the ordinates of the unit hydrograph that was developed for that duration.

Because the unit hydrograph is a linear function, the applicability of superposition is assumed. In order to calculate the runoff response from complex storm events, a series of unit hydrographs are constructed for a number of lagged volumes of rainfall excess. The set of unit hydrographs are lagged and summed to develop the composite runoff hydrograph. The composite hydrograph is a linear combination of the unit hydrograph ordinates.

2.1.3 Unit Hydrograph Limitations

Assumptions

Unit hydrograph theory contains a number of assumptions that can limit its use. They are (Chow et al., 1988):

1. *The excess rainfall has a constant intensity within the effective duration.* When the unit hydrograph is developed using gauged data, the storms selected for analysis should have a short duration because they are the most likely to have a uniform intensity and produce a single-peaked hydrograph.
2. *The excess rainfall is uniformly distributed throughout the entire drainage area.* This assumption may pose difficulties for larger watersheds. For watersheds above a certain size, the assumption of uniform rainfall is no longer valid.
3. *The base time of the direct runoff hydrograph is constant based on a given duration of rainfall.* This assumption implies that the unit hydrograph model cannot account for differences in the watershed response to different rainfall intensities.
4. *The ordinates of all direct runoff hydrographs with the same base time are proportional to the total amount of direct runoff represented by each hydrograph.*
5. *The hydrograph resulting from excess rainfall reflects the unique characteristics of the watershed.* The unit hydrograph model cannot reflect variations in the watershed response due to changes in the season, land use or channel characteristics.

The unit hydrograph is assumed to be a constant response function of the watershed as long as there are no major changes in the land use. Traditional unit hydrograph models cannot account for differences in the watershed response due to seasonal conditions or rainfall intensities.

Area

While many authors agree that the unit hydrograph is only applicable for a limited range of watershed sizes, they disagree about what the extent actually is. Sherman (1932) used the unit hydrograph theory on watersheds ranging from 1300 km² to 8000 km². Linsley et al. (1975) recommended that the unit hydrograph only be used on watersheds less than 5000 km², while Ponce (1989) suggested that it should only be applied on midsize catchments between 2.5 km² and 250 km². Because the unit hydrograph model assumes that rainfall is uniform over an entire area, it is not applicable to large watersheds. Small catchments tend to reflect variations in the rainfall excess more than larger watersheds, because they have less channel storage than larger watersheds, thus the small catchments are less appropriate for unit hydrograph analysis (Huggins and Burney, 1982).

Watershed Linearity

One of the most significant limitations of the unit hydrograph theory is the assumption of linearity. In fact, the watershed is a highly nonlinear system (Huggins and Burney, 1982). Due to the assumption of linearity, the unit hydrograph method is not applicable for watersheds that have appreciable storage effects (Gray, 1973). In addition, the unit hydrograph theory may not be applicable to small watersheds because they tend to exhibit a nonlinear response more than larger areas (Huggins and Burney, 1982). In practice, the linearity assumption is useful because the equations are relatively simple and the results are acceptable for most engineering purposes (Bedient and Huber, 1992).

Superposition

The unit hydrograph theory is based on the idea of superposition. The hydrograph ordinates for a complex storm event are the sum of the ordinates of the incremental hydrographs that are developed for each period of rainfall excess.

2.1.4 Synthetic Unit Hydrographs

Because Sherman's unit hydrograph is based on observed rainfall and runoff data, it is only applicable for gauged basins. Unfortunately, the majority of watersheds are ungauged. Primarily based on empirical equations, synthetic unit hydrographs attempt to extend the application of unit hydrograph theory to ungauged catchments. Synthetic unit hydrographs try to relate the unit hydrograph shape to watershed characteristics such as basin length and area (Yen and Lee, 1997). Because synthetic methods do not rely on observed runoff data, they may be applied to ungauged watersheds.

Types of Synthetic Unit Hydrographs

Chow et al. (1988) suggested that there are three major types of synthetic unit hydrographs. They can be:

1. based on hydrograph characteristics such as peak discharge and time to peak (Snyder, 1938);
2. based on a dimensionless unit hydrograph (SCS, 1972);
3. based on watershed storage (Clark, 1945).

Snyder (1938) proposed the first unit hydrograph technique that was applicable to ungauged areas, based on a study of watersheds located in the Appalachian mountains. In his approach, the time to peak is estimated from watershed length, the distance from the outlet to the watershed centroid, and a regional coefficient, while the predicted peak flow rate is calculated using the watershed area, the time to peak, and a storage coefficient. In order to sketch the hydrograph shape, the hydrograph width is estimated at 50% and 75% of the peak discharge. The widths are generally distributed such that 1/3 is placed before the peak and 2/3 is placed after the peak.

The SCS unit hydrograph is based on a dimensionless hydrograph. The time to peak is estimated based on the duration of effective rainfall and the lag time between the centroid of the excess rainfall and the time to peak. The lag time is calculated using the watershed length, the average slope, and a factor based on watershed storage. The peak

flow rate is based on the watershed area and the time to peak. A triangle is commonly used to estimate the unit hydrograph shape.

Clark (1945) developed a unit hydrograph model that combined a watershed time-area diagram with a linear reservoir at the basin outlet. The shape of Clark's (1945) unit hydrograph is developed from the travel time through the basin, as well as the watershed shape and storage characteristics. In order to create a unit hydrograph, Clark divided the basin into isochrones, then developed a time-area histogram. The time-area curve was assumed to be the inflow into a hypothetical reservoir. The direct runoff hydrograph at the watershed outlet can be predicted by routing the inflow hydrograph through a reservoir that has the same storage characteristics as the watershed.

2.2 Lumped versus Distributed Models

Traditionally, hydrologic models have considered watersheds to be homogeneous, with weighted averages or mean values used as inputs to these “lumped” models. Distributed parameter models account for the spatial variability in a watershed by considering the areal variations in watershed characteristics such as soils and land use when applying the model. Lumped models cannot account for spatial variability within a watershed, and generally use representative or mean values to describe watershed characteristics such as slope and soil type. Although distributed parameter models may be more accurate, they require large amounts of data and computing power (Larson et al., 1982). Until the 1980's hydrologists usually had to settle for lumped models because computing power was prohibitively expensive. As computers became more powerful and less expensive, hydrologists started to take advantage of the advances in computing capabilities. Instead of using lumped parameter models, many hydrologists began using distributed parameter models.

Distributed parameters models offer the possibility of a significant improvement over lumped models because they can model the spatial variability of hydrologic parameters. Instead of having one value for the watershed slope or land use, distributed parameter models like AGNPS (Young et al., 1985) and ANSWERS (Beasley and Huggins, 1981) can model the interactions within a watershed area. Distributed

parameter models can account for the structure of processes and parameters involved in the movement of water and pollutants over and through a landscape (McDonnell, 1996).

2.3 Use of GIS in hydrology

As the interest in distributed hydrologic models increased, there was also an increase in the use of GIS for modeling and spatial analysis (McDonnell, 1996).

Maidment (1993a) suggested a scheme to classify the different uses of GIS in hydrology:

1. Hydrological inventory and assessment,
2. Hydrological parameter determination,
3. Loosely coupled GIS and hydrological models,
4. Integrated GIS and hydrological models.

2.3.1 Hydrological inventory and assessment

Measuring the spatial extent of hydrologic variables from paper maps may be tedious, labor-intensive and error-prone (McDonnell, 1996). A GIS may be used as a way to automatically derive the required information. It can be used as a method to integrate, visualize, and derive spatial and nonspatial data (McDonnell, 1996).

Gustafsson (1993) used remotely sensed imagery as well as field and geophysical data to identify areas for groundwater exploration in Botswana. Gurnell et al. (1993) used a GIS for the ecological analysis of the Blackwater River in the United Kingdom.

2.3.2 Hydrologic parameter determination

The use of GIS for model parameter estimation is a very active area of research (McDonnell, 1996). Distributed parameter models require large amounts of data. A GIS may be used to manage and manipulate the large quantities of data that distributed models demand. Values such as slope and cumulative area above a point may be difficult to estimate with paper maps and manual methods, however they are easily determined with a GIS. Chieng and Luo (1993) used a GIS to route runoff through a watershed. They developed a more accurate time of concentration for use with the Rational Method.

Arc/Info has been used to develop the geomorphic input parameters for the WAHS model (Bhaskar et al., 1992; Hill et al., 1987). Wolfe (1992) used GRASS to overlay soils and land use maps to develop a map of hydrologic response units. This map was used as input for the FESHM model. GIS-based systems have also been used to develop parameter estimates for the Penn State Runoff Model (PSRM), PRSM, and SPUR (Shamsi, 1996; Jeton and Smith, 1993; Sasowsky and Gardner, 1991).

2.3.3 Loosely Coupled Hydrologic Models

One of the major limitations of the integration of GIS and hydrologic models is that current GIS technology cannot represent the continuous temporal element of modeling. It can only represent time as a series of “snapshots” (McDonnell, 1996). One of the most popular ways to use GIS in hydrologic modeling is a loosely coupled system where the model and GIS maintain two separate databases and interact through some form of a file exchange or conversion process. Many common hydrologic models have been coupled with GISs. AGNPS has been used in conjunction with a GIS by many researchers (Tim and Jolly, 1994; Srinivasan and Engel, 1991; Lee et al., 1990). ANSWERS has also been combined with a GIS in many applications (Rewerts and Engel, 1991). SWAT is a continuous, basin-scale hydrologic model that has been coupled with a GIS (Rosenthal et al., 1995; Srinivasan and Arnold, 1994).

2.3.4 Integrated GIS-hydrologic models

In an integrated GIS-hydrologic model, both components share one database and there is no data export between the two. The major limitation of this type of system is that current GISs often have limited modeling capabilities. Drayton et al. (1992) developed an integrated model that calculated the runoff volume and hydrograph for a watershed. The model uses satellite imagery and digital elevation data for the model inputs. The model estimates the runoff volume based on the SCS curve number method, then routes it through the watershed. The model assumes that the travel time through each grid cell is constant. It does not account for different travel times due to slope, surface roughness, or flow direction. It also does not account for differences in travel times due

to different storm intensities. Once the travel time from each cell to the outlet is determined, a hydrograph is generated by accumulating the runoff from each cell.

Zollweg et al. (1996) developed an integrated soil-moisture based rainfall-runoff model in GRASS. The model consists of soil moisture balance and runoff generation submodels. In order to model the soil moisture balance, the soil profile is divided into 3 zones. The amount of water stored in the surface zone is dependent on evapotranspiration, precipitation, interflow, percolation, and surface runoff. In addition, interflow and drainage are used to estimate the soil moisture storage for the two subsurface zones. On days with precipitation, the runoff submodel is used. The runoff submodel estimates the storm hydrograph based on the rainfall amount, rainfall intensity, and initial soil moisture conditions. SMOReMod predicts the volume of runoff based on the soil moisture storage that is available during each 30-minute time step. The runoff is routed to the watershed outlet based on the optimal flow path and the travel time through each cell in the path. The model was tested using 77 storm events from a small agricultural watershed in Pennsylvania. Zollweg et al. (1996) compared the predictions from the SMOReMod model with the observed values and the results from the distributed curve number method (Muzik, 1988). They found that SMOReMod predicted the peak flows with good accuracy, however it generally underpredicted the total runoff volume. The model also failed to accurately predict the baseflow between runoff events.

2.4 Spatially Distributed Unit Hydrograph

The “spatially distributed unit hydrograph” proposed by Maidment (1993b) is similar to the geomorphic instantaneous unit hydrograph (Rodriguez-Iturbe and Valdes, 1979), except that it uses a GIS to describe the connectivity of the links and the watershed flow network instead of probability arguments. Maidment calculated the flow distance from each cell to the watershed outlet. The travel time from each cell to the watershed outlet was calculated by dividing each flow length by a constant velocity. He developed a time-area curve based on the travel time from each grid cell. Maidment (1993b) evaluated his methodology on a hypothetical watershed that consisted of 36 grid

cells. His results were inconclusive; the time-area histogram did not result in the expected S-hydrograph shape. The poor results were blamed on the small size of the watershed.

Muzik (1995) applied Maidment's procedure to a 229 km² watershed in the Canadian Rockies. He estimated the flow velocity through each grid cell by combining the continuity equation and Manning's equation. The resulting time-area curve had the expected S-hydrograph shape. A unit hydrograph can be derived from the time-area curve by applying the standard S-curve technique (Chow et al., 1988). In order to test the model, a 1-hour unit hydrograph was derived and convoluted with a storm event that had an intensity of 3.7 mm/hr. Based on a visual estimation, the predicted hydrograph showed good agreement with the observed hydrograph.

Ajward (1996) applied the spatially distributed unit hydrograph to two large watersheds in the Canadian Rockies, comparing the predictions from the spatially distributed unit hydrograph with the observed hydrograph for eight rainfall events. He found that the model generally gave good predictions of the peak flow rate and the time to peak. He also found that the best predictions were produced when a unit hydrograph developed from a storm with a similar intensity to the test event was used. An "average" unit hydrograph always gave less accurate predictions of time to peak and peak flow rate than a unit hydrograph that was developed with an intensity that was close to the average intensity of the test event.

2.5 Summary

This chapter presented the history of the unit hydrograph theory, including some of the basic assumptions and limitations inherent in this type of hydrologic model. In addition, several types of unit hydrograph models were presented. The uses of GISs in hydrology were also summarized. These uses can be loosely classified in four categories: hydrological inventory and assessment; hydrological parameter determination; loosely coupled GIS and hydrological models; and integrated GIS and hydrological models.

3.0 Methodology

The following chapter presents an overview of the methodology used to accomplish the goals of this research project. A brief description of the model development is presented here; a more complete discussion may be found in Chapter 4. In addition to a description of the model development, this chapter also discusses the “traditional” unit hydrographs that were used in this project as well as the comparison criteria used to evaluate each of the unit hydrograph techniques.

3.1 Study Overview

In order to meet the goals of this study, a spatially distributed unit hydrograph (SDUH) model was developed such that it only relied on USGS DEM data and land use information for input parameters. The developed model is essentially a time-area unit hydrograph technique. A raster GIS was used to calculate the travel time from each point in the watershed to the outlet. Based on the cumulative travel time from each point, 1-hour isochrones were developed and the unit hydrograph was created.

The SDUH model was compared with four traditional synthetic unit hydrograph techniques in order to evaluate how well the new model performed in relation to the existing methods. The models included in this study were the Snyder, SCS, and Clark synthetic unit hydrographs. Forty storm events from the Owl Run watershed located in Fauquier County, Virginia were used to test the unit hydrograph techniques.

3.2 Model Development

The GIS software Idrisi was used for this study. Idrisi is a geographic information and image processing software system developed by the Graduate School of Geography at Clark University (Eastman, 1995). Although Idrisi has both raster and vector capabilities, the raster data structure was used for this study. Raster based systems generally have much more analytical power. In addition, the raster data structures tend to allow rapid evaluations of problems that involve mathematical combinations of data from multiple images.

The basic modeling approach was to use the raster GIS functions to calculate the travel time from each point in the watershed to the outlet by determining the flow path and the travel time through each cell along the path. The travel time through each individual cell along the flow path was summed to estimate the cumulative travel time to the outlet. The model accounts for differences in overland and channel velocity, slope, and land use. Runoff is routed over the elevation surface. The total travel time to the outlet from each grid cell is estimated based on the runoff pathway and the travel time through each grid cell along the path. Figure 3.1 is a flow chart of the model. A detailed description of the model development may be found in Chapter 4. Macro files developed for the model implementation may be found in Appendix A.

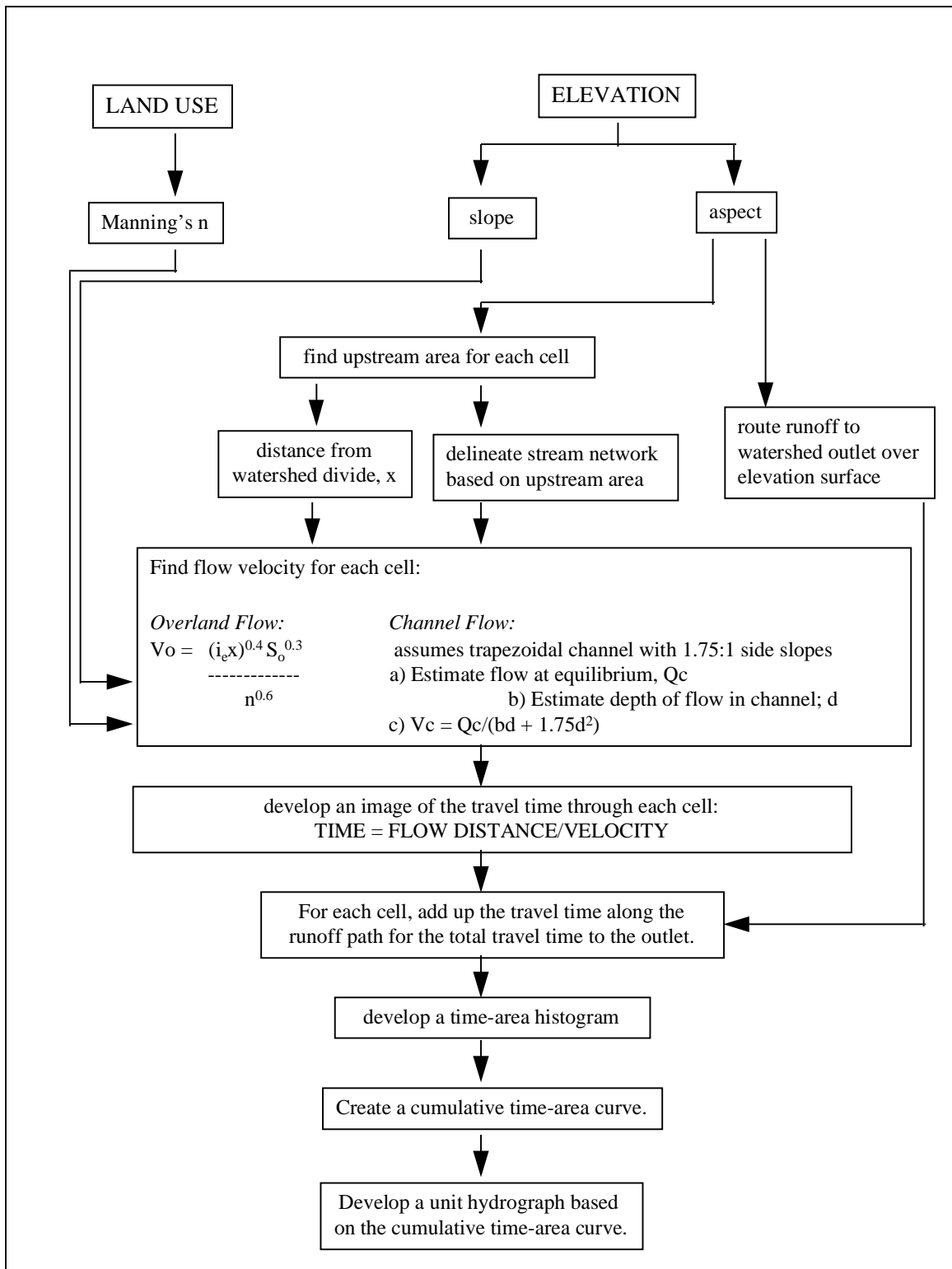


Figure 3.1. SDUH Model Flow Chart.

Because the model is meant to be used on ungauged watersheds, the only data that is required for the model is readily available to scientists and engineers working with ungauged basins. In order to use this spatially distributed unit hydrograph model (SDUH model), the only data that is required is elevation data (usually in the form of a DEM) and land use information. For this study, a 30-m resolution DEM was used for the elevation data. The land use information was collected as part of the Owl Run Watershed/Water Quality monitoring project (Mostaghimi et al., 1989).

3.3 Sensitivity Analysis

In order to assess the SDUH model's sensitivity to different parameters, a series of sensitivity analyses were performed. Performing sensitivity analyses is a method to identify the input parameters that have the biggest impact on model predictions. As each variable was allowed to vary, all others were held constant. The 'base' scenario used for the sensitivity analyses is summarized in Table 3.1. As each parameter was evaluated, the impacts on the peak flow rate, the time to peak and the overall hydrograph shape were examined.

Table 3.1. Base values used in the sensitivity analysis.

Parameter	Value
channel flow	20 cells
threshold	(1.8 ha)
channel velocity	values calculated in section 4.4.2
overland velocity	values calculated in section 4.4.1
channel width	values calculated in section 4.2.5
intensity of rainfall excess	2.54 mm/hr (0.10 in./hr)
hydraulic residence time in pond	1 hour

The channel and overland flow velocities were investigated by multiplying the 'base' value by 0.5, 1.0, 1.5, and 2.0 in order to evaluate how the peak flow rate, time to peak and general hydrograph shape were affected by the changes in these parameters. In addition, the effect of the channel width was evaluated. Because there is a good deal of

uncertainty in the estimates of the channel dimensions, the model's sensitivity to changes in the bottom width were evaluated. The bottom width was varied by multiplying the width by 0.5, 1.0, 1.5, and 2.0. The effects of the changes on the peak flow rate, the time to peak and the overall hydrograph shape were evaluated. The model's sensitivity to the channel flow threshold was studied because there is no good way to quantify the threshold where overland flow becomes channel flow. Channel flow thresholds of 10, 20, 40, and 60 cells were tested. As the channel flow threshold increased, the amount of area that was assumed to be controlled by overland flow also increased. In order to test the SDUH model's responsiveness to different excess rainfall intensities, unit hydrographs were developed for 1.27 mm/hr (0.05 in./hr), 2.54 mm/hr (0.10 in./hr), 3.81 mm/hr (0.15 in./hr), and 5.08 mm/hr (0.20 in./hr). In order to investigate the effects of the pond routing, hydraulic residence times of 30 minutes, 1 hour, 1.5 hours and 2 hours were tested.

3.4 Traditional Synthetic Unit Hydrographs

In order to compare the spatially distributed unit hydrograph model with existing techniques, a Snyder synthetic unit hydrograph, a SCS synthetic unit hydrograph, and a Clark instantaneous unit hydrograph were developed for the Owl Run watershed. A listing of the parameters used to create each synthetic unit hydrograph, as well as the ordinates for each traditional unit hydrograph may be found in Appendix B. Because the synthetic unit hydrographs used in this study are based on empirical equations, the ordinates were calculated using English units. Once the unit hydrographs were developed, they were converted to metric units for convolution with the rainfall events.

3.4.1 Snyder Synthetic Unit Hydrograph

Snyder (1938) was the first to propose a unit hydrograph technique that could be used on ungauged basins. His method was developed based on a number of watersheds in the Appalachian Highlands that ranged in size from 10 mi² to 10,000 mi².

The basin lag is calculated by:

$$t_p = C_t(LL_c)^{0.3} \quad [1]$$

where t_p = basin lag (hours)

C_t = slope coefficient

L = length of main stream from the outlet to the divide (mi.)

L_c = length along the main stream to a point nearest the watershed centroid (mi.)

The peak discharge is calculated by :

$$Q_p = \frac{640C_p A}{t_p} \quad [2]$$

where Q_p = peak flow rate (cfs)

C_p = storage coefficient

A = basin area (mi²)

In general the base time of the unit hydrograph is estimated by:

$$T_b = 3 + \frac{t_p}{8} \quad [3]$$

where: T_b = base time for the unit hydrograph (days)

t_p = basin lag (hours)

Because Owl Run is a small watershed, the time base of the unit hydrograph was assumed to be (Bedient and Huber, 1992):

$$T_b = 5t_p \quad [4]$$

The duration of the rainfall excess that produced the peak flow rate and basin lag time was calculated by equation [5] (Bedient and Huber, 1992):

$$D = t_p/5.5 \quad [5]$$

where: D = rainfall excess duration (hours)

Based on equation [5], the rainfall excess duration was 0.67 hours. In order to convert the Snyder unit hydrograph to a 1-hour rainfall excess interval, equation [6] was used to

estimate the new basin lag:

$$t'_p = t_p + 0.25(D' - D) \quad [6]$$

where: t'_p = new basin lag (hours)

D' = new rainfall excess duration (hours) = 1 hour

The peak flow rate for the new rainfall excess duration may be calculated by:

$$Q_p = \frac{640C_p A}{t'_p} \quad [7]$$

The new base time of the unit hydrograph may be estimated by:

$$T_b = 5t'_p \quad [8]$$

Based on the peak flow rate, the time to peak and the base time, four other unit hydrograph ordinates were estimated. Bedient and Huber (1992) suggested that the width of the hydrograph could be calculated at 50% of the peak flow rate and 75% of the peak flow rate using:

$$W_{50} = \frac{770}{\left(\frac{Q_p}{A}\right)^{1.08}} \quad [9]$$

and

$$W_{75} = \frac{440}{\left(\frac{Q_p}{A}\right)^{1.08}} \quad [10]$$

where W_{50} = width of the unit hydrograph at 50% of the peak flow rate (hours)

W_{75} = width of the unit hydrograph at 75% of the peak flow rate (hours)

Q_p = peak flow rate (cfs)

A = watershed area (mi^2)

The widths are distributed such that one third of the time lies before the peak and 2/3 of the width lies after the peak flow rate.

Based on the seven ordinates calculated above, the other ordinates of the unit

hydrograph were determined by sketching an approximate shape, and ensuring that the resulting unit hydrograph contained 1 inch of direct runoff.

In order to determine the C_t and C_p parameters in the Snyder unit hydrograph method, it is generally suggested that a nearby watershed be used to calibrate these values. Unfortunately, there was no data available from a nearby watershed that had a similar size and shape. In this study, two Snyder unit hydrographs were created based on two different estimates of those values. C_t usually ranges from 1.8 to 2.2, while C_p usually falls between 0.4 to 0.8 (Viessman et al., 1977). The first Snyder synthetic unit hydrograph used the average value from the suggested ranges for C_t and C_p . For the second Snyder technique, two observed storms were used to calibrate C_t and C_p .

In order to calibrate the Snyder parameters, two storms were selected that represent a range of seasons and storm sizes. Specific details about these storms are summarized in Appendix B. For each of the storm events, the ‘unit’ peak flow rate was estimated by dividing the observed peak flow rate by the depth of rainfall excess. The ‘unit’ peak flow rates and the observed times to peak were averaged for mean values. The average time to peak and ‘unit’ peak flow rate were substituted into equations [1] and [2]. The resulting equations were solved for calibrated C_t and C_p values. The calibrated C_t and C_p values were then considered input; a new peak flow rate and time to peak were calculated using equations [1] and [2] and the development of the Snyder unit hydrograph continued normally. Although the resulting Snyder hydrograph is not really “synthetic” since observed data were used in its development, it represents the best possible Snyder unit hydrograph for this watershed.

3.4.2 SCS Synthetic Unit Hydrograph

The time of concentration for Owl Run was estimated using the three-part segmental approach described in Chapter 3 of TR-55, Urban Hydrology for Small Watersheds (SCS, 1986). The longest flow path through the watershed to the outlet was identified and divided into three sections: overland flow, shallow concentrated flow, and channel flow. The watershed’s time of concentration was estimated based on the travel time through each of these sections. The overland flow travel time is calculated by (SCS,

1986):

$$T_o = \frac{0.007(nL)^{0.8}}{P_2^{0.5} S^{0.4}} \quad [11]$$

where: T_o = overland flow travel time (hours)
 n = Manning's roughness coefficient
 L = flow length (ft)
 P_2 = 2-year, 24-hour rainfall event (in.)
 S = slope (ft/ft)

The travel time through the shallow concentrated flow portion of the travel path was estimated based on the flow length and the average velocity estimated using Figure 3.1 in TR-55 (SCS, 1986).

In order to estimate the travel time through the main channel in Owl Run, the stream was divided into four segments based on differences in the channel slope and the bottom width. For the channel flow portion of the flow path, Manning's equation is used to estimate the average flow velocity:

$$V = \frac{1.49r^{2/3} S^{1/2}}{n} \quad [12]$$

where: V = average channel velocity (ft/s)
 r = hydraulic radius (ft); $r = A/P$

The channels were assumed to be trapezoidal with 1.75:1 side slopes. The cross-sectional area is:

$$A = bd + 1.75d^2 \quad [13]$$

and the wetted perimeter is:

$$P = b + 4d \quad [14]$$

The channel section was assumed to have a depth of 4 feet and a bottom width that increased from 5 feet to 20 feet along the main channel. The channel dimension estimates were based on a site visit and the recommendation of Mr. Tony Pane, the watershed coordinator for the Owl Run Watershed/Water Quality monitoring project (Mr. Tony Pane, personal communication, 1997).

The time to the peak flow rate is calculated by:

$$T_R = \frac{D}{2} + t_p \quad [15]$$

where T_R = time of rise (hours)
 D = rainfall excess duration (hours)
 t_p = lag time from centroid of rainfall to peak flow rate (hours)

The peak flow rate was calculated by:

$$Q_p = \frac{484A}{T_R} \quad [16]$$

where Q_p = peak flow rate (cfs)
 A = watershed area (mi²)

The time base of the unit hydrograph was estimated using:

$$Vol = \frac{Q_p T_R}{2} + \frac{Q_p B}{2} \quad [17]$$

where $Vol.$ = runoff volume (cfs-hr)
 Q_p = peak flow rate (cfs)
 B = time of recession (hours)

Because the runoff volume is 1 inch, equation [16] may be solved for the recession time. The total base time for the entire unit hydrograph is the sum of the time of rise and the recession time.

3.4.3 Clark Instantaneous Unit Hydrograph

The Clark unit hydrograph is very similar to the SDUH model, because they are both based on the time-area method to derive unit hydrographs. The major difference between the two methods is that the Clark unit hydrograph is routed through a linear reservoir at the watershed outlet to account for watershed storage. The hydraulic residence time in the watershed is assumed to be equal to the watershed's time of concentration.

In order to calculate the watershed's isochrones, the travel time to the watershed outlet was calculated for 50 points in the watershed using the same procedure used to estimate the time of concentration for the SCS unit hydrograph. Based on the travel time from each of these points, the isochrones were drawn. The area of each isochrone was determined and a time-area curve was developed.

Summary

Four 'traditional' synthetic unit hydrographs were developed for Owl Run. Two different Snyder unit hydrographs, an SCS unit hydrograph and a Clark instantaneous unit hydrograph were developed. These synthetic unit hydrographs are summarized in Figure 3.2. Although they are all synthetic unit hydrographs, there is substantial variability in the peak flow rate, the time to peak, and the base time. The unit hydrograph peak flow rate ranges from 12.53 m³/s to 20.53 m³/s. The time to peak shows less variability with a range of 3 hours up to 6 hours. The base time varies from 10 hours for the SCS unit hydrograph up to 24 hours for the calibrated Snyder unit hydrograph.

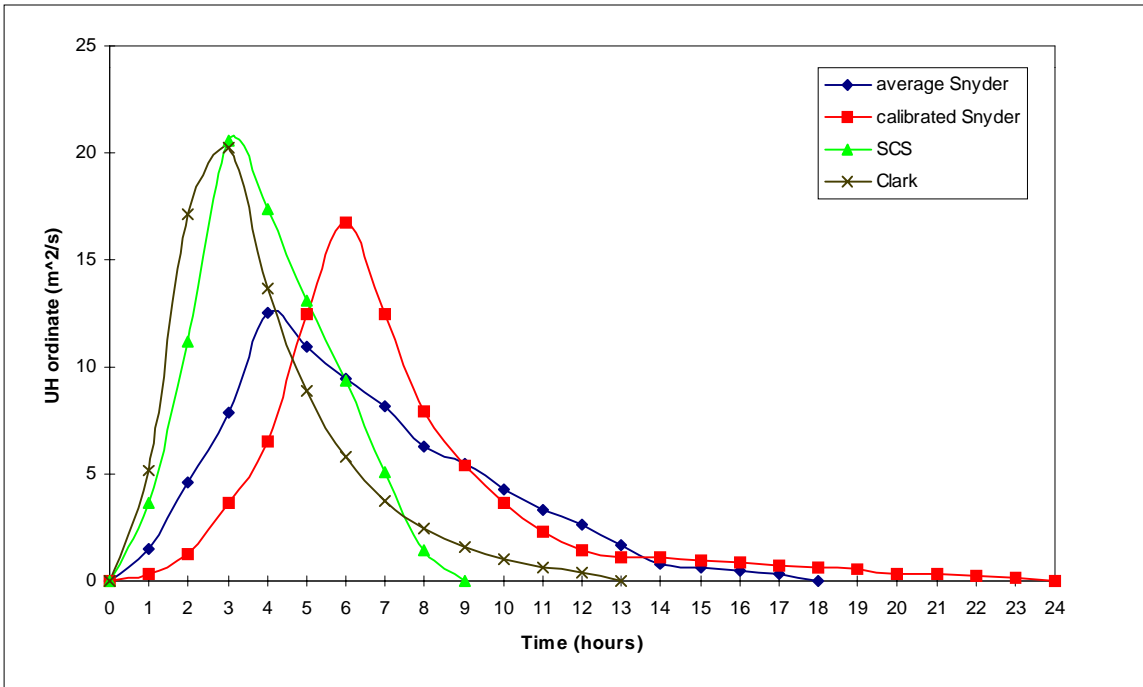


Figure 3.2. Traditional Synthetic Unit Hydrographs.

3.5 Hydrology

3.5.1 Storm selection

As part of a 10-year water quality monitoring project, rainfall and runoff data were collected for the period of 1986 through 1996 for the Owl Run watershed (Mostaghimi et al., 1989). For the purposes of this study, the data from 1990 through 1993 were used. The storms included in this study met the following criteria:

- isolated storm event
- at least 6.35 mm (0.25 inches) of rainfall
- peak flow rate larger than 0.283 m³/s (10 cfs)
- occur between April and November

A storm event was considered to be over when there was a period of at least 6 hours without rainfall. The storms included in this study were selected because they had significant rainfall amounts and observable runoff peaks. Because the model developed in this study cannot account for snowmelt, storms from the winter months were excluded in this study. Ajward (1996) used similar guidelines to select storms. The above criteria resulted in forty storm events with a range of average intensities, rainfall volumes, and peak runoff rates (Table 3.1).

3.5.2 Baseflow Separation

Because unit hydrographs only model direct runoff hydrographs, they do not account for baseflow. The observed hydrographs were separated into baseflow and surface flow so that the observed and predicted hydrographs could be compared. Baseflow separation is considered to be somewhat arbitrary and there is no reliable method to accurately separate baseflow from surface runoff (Bedient and Huber, 1992). For larger runoff events, the baseflow contribution has little impact on the peak discharge and runoff hydrograph. For this study a constant-slope baseflow separation technique

was used to divide the observed hydrographs into a baseflow hydrograph and a direct runoff hydrograph (McCuen, 1989). The points used to identify the ends of the direct runoff hydrograph were the first sign of hydrograph rise and the point of inflection on the falling limb of the hydrograph.

3.5.3 Determination of rainfall excess

The total runoff volume for each storm was determined by integrating the direct runoff hydrograph. Once the volume of rainfall excess was determined, the corresponding phi-index line was calculated and applied to the rainfall pattern (Gray, 1970). While this technique insures that the rainfall excess volume is exact, it does not reflect the time distribution of the rainfall excess.

Table 3.2. Summary of rainfall events.

			Rainfall Volume	Rainfall Duration	Runoff volume	Avg. Rainfall Excess intensity	Peak Flow Rate	Time to Peak
			(mm)	(hours)	(mm)	(mm/hr)	(m³/s)	(hours)
1	1990	April 1	6.6	3	0.9	0.9	0.50	5
2		April 2	13.3	7	4.1	4.1	3.13	4
3		April 14-15	21.0	7	3.2	1.6	1.34	6
4		April 29-30	26.2	24	2.2	2.2	0.60	4
5		May 9-10	37.9	21	8.3	4.1	4.25	4
6		May 25-26	25.0	21	1.4	1.4	0.44	5
7		May 28-29	52.4	17	23.7	1.8	11.02	17
8		July 13-14	31.2	6	1.7	1.7	1.22	3
9		October 18	40.1	7	1.1	1.1	0.58	4
10		October 22-23	49.9	26	4.4	1.1	1.47	12
11		November 9-10	52.3	15	6.0	1.5	2.75	10
12	1991	June 18	59.1	5	1.4	1.4	1.71	3
13		July 25-26	49.4	20	4.5	4.5	3.02	6
14		August 9-10	82.0	10	15.7	3.9	12.95	8
15		September 4-5	52.8	15	2.6	2.6	2.57	3
16		September 17-18	47.0	5	2.8	2.8	2.21	5
17		September 24	37.1	9	2.9	2.9	1.93	2
18		October 5-6	14.4	6	2.3	2.3	1.92	2
19		November 21-22	26.6	22	1.5	1.5	1.12	3
20	1992	April 21	48.4	17	13.6	2.8	9.00	14
21		May 8	10.5	4	0.8	0.8	0.42	5
22		June 5	22.2	19	1.0	1.0	0.46	5
23		June 30	24.4	4	1.0	1.0	1.04	3
24		July 3-4	16.4	8	1.2	1.2	0.76	4
25		July 24	30.2	2	2.1	2.1	1.66	3
26		July 27	40.0	5	15.1	7.5	12.35	4
27		July 31	22.9	3	3.1	3.1	3.07	4
28		August 4	17.4	2	0.6	0.6	0.54	3
29		September 2	33.6	6	0.6	0.6	0.46	7
30		September 5-6	18.2	13	0.7	0.7	0.38	6
31		September 10-11	18.0	6	3.0	3.0	1.60	5
32		November 2-3	17.5	7	1.4	1.4	0.83	6
33		November 12	17.8	8	3.2	1.6	1.90	8
34		November 22-23	29.9	5	16.0	8.0	13.20	4
35	1993	April 1	11.3	12	1.2	0.6	0.92	4
36		April 9-10	38.8	19	12.8	2.1	6.63	13
37		April 16	56.1	6	32.8	10.9	32.26	4
38		May 5	64.9	4	19.7	19.7	13.78	3
39		June 8	20.9	5	0.6	0.6	0.35	5
40		November 27-28	137.5	25	60.5	6.0	35.18	11

3.6 Evaluation

In order to evaluate how well each unit hydrograph technique predicts an observed hydrograph, a series of statistics were used. The hydrographs were evaluated based on a visual comparison, an evaluation of the peak flow rate, the time to peak prediction, the model efficiency, the bias, the sum of squared residuals, and the sum of absolute residuals. Based on the results of these tests, the predictive capabilities of each technique were assessed.

The relative error in the peak flow rate was calculated by:

$$rel.error = \frac{q_{ps} - q_{po}}{q_{po}} \quad [18]$$

where q_{ps} = simulated peak flow rate
 q_{po} = observed peak flow rate

In order to compare the five unit hydrograph techniques' prediction capabilities, the mean arithmetic relative error (MARE) was calculated by:

$$MARE = \frac{\sum_{i=1}^n |rel.error|}{n} \quad [19]$$

where n = number of events

While the MARE emphasizes outliers, the LMARE statistic places less importance on the extreme values. The LMARE was calculated by:

$$LMARE = \frac{\sum_{i=1}^n \log_{10} |rel.error|}{n} \quad [20]$$

Good predictions result in MARE values that are close to zero and LMARE values that are negative.

Nash and Sutcliffe (1970) first proposed the dimensionless coefficient of model efficiency (R^2). Since then it has gained wide acceptance (Green and Stephenson, 1986).

If the R^2 value equals 0, the model efficiency statistic may be interpreted that the model prediction is as accurate as using an average of the observed data. An R^2 value of 1 indicates a perfect fit between the simulated and observed hydrographs. The model efficiency was calculated for each storm event by:

$$R^2 = \frac{F_o^2 - F^2}{F_o^2} \quad [21]$$

where:

$$F_o^2 = \sum_{i=1}^n [q_o(t) - \bar{q}_o]_i^2$$

$$F^2 = \sum_{i=1}^n [q_o(t) - q_s(t)]_i^2$$

$q_o(t)$ = observed flow rate at time t

$q_s(t)$ = simulated flow rate at time t

\bar{q}_o = average observed flow rate for each time t

n = number of pairs of ordinates compared in a single event

The bias of each technique was estimated by:

$$B = \sum_{i=1}^n (q_o(t) - q_s(t))_i \quad [22]$$

The sum of absolute residuals (SAR) was calculated by:

$$SAR = \sum_{i=1}^n |q_o(t) - q_s(t)|_i \quad [23]$$

and the total sum of absolute residuals (TSAR) was calculated by:

$$TSAR = \sum_{j=1}^m SAR_j \quad [24]$$

where:

m = number of storm events

The sum of squared residuals (SSR) is one of the most common statistics used to evaluate hydrograph shapes (Green and Stephenson, 1986). It was calculated by:

$$SSR = \sum_{i=1}^n (q_o(t) - q_s(t))_i^2 \quad [25]$$

The total sum of squared residuals (TSSR) was also calculated for each technique:

$$TSSR = \sum_{j=1}^m SSR_j \quad [26]$$

The unit hydrograph techniques were compared based on these statistics. The results of these comparisons may be found in Section 5.1.

4.0 Model Development and Application

4.1 Watershed Description

The SDUH model was applied to the Owl Run watershed. It is an 1153 hectare watershed located in Fauquier County, Virginia (Figure 4.1). Over 90% of the land area is in some form of agricultural land use (Figure 4.2). The land slope in the watershed is generally between 2% and 7%, however, in some locations, the slope may be as large as 25% (Wang, 1991). Because Owl Run was included in a Chesapeake Bay program to study the impact of animal waste best management practices (BMPs), it was continuously monitored from 1986 through 1996. In addition to hydrologic data, detailed biological, soil and water quality, and land use data have been collected as a part of the Owl Run Watershed/Water Quality Monitoring project (Mostaghimi et al., 1989).

The soils in the watershed are typically shallow silt loams. The major soil series in the watershed are Penn, Bucks, and Montalto associations. The Penn soils are shallow and excessively drained soils that occur on undulating or rolling relief. The Buck soil series (16% of the watershed) is moderately deep well-drained upland soils. The Montalto soils are moderately shallow, well-drained soils with slopes ranging from 2-14%. All of the soils in the watershed are relatively fertile because they are well supplied with organic matter and plant nutrients (Mostaghimi et al., 1989).

There are eight precipitation stations and four runoff monitoring stations located throughout the watershed (Figure 4.3). Usually, there are over 100 rainfall events per year, although only 40% of them generally produce runoff. The average annual rainfall is evenly distributed throughout the year, but the largest runoff events generally occur

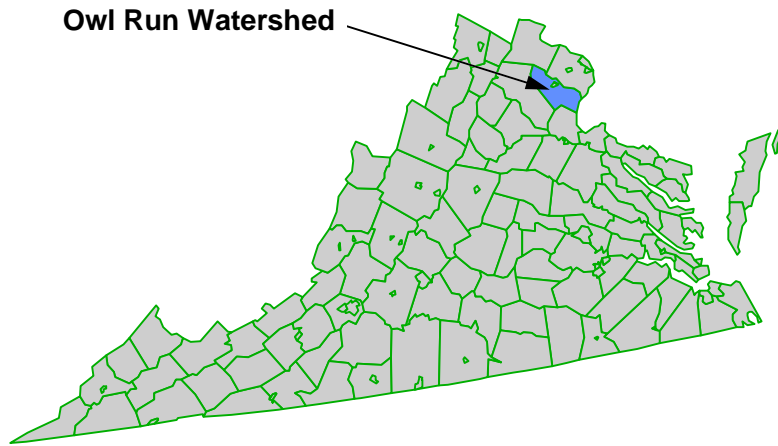


Figure 4.1. Location of Owl Run Watershed.

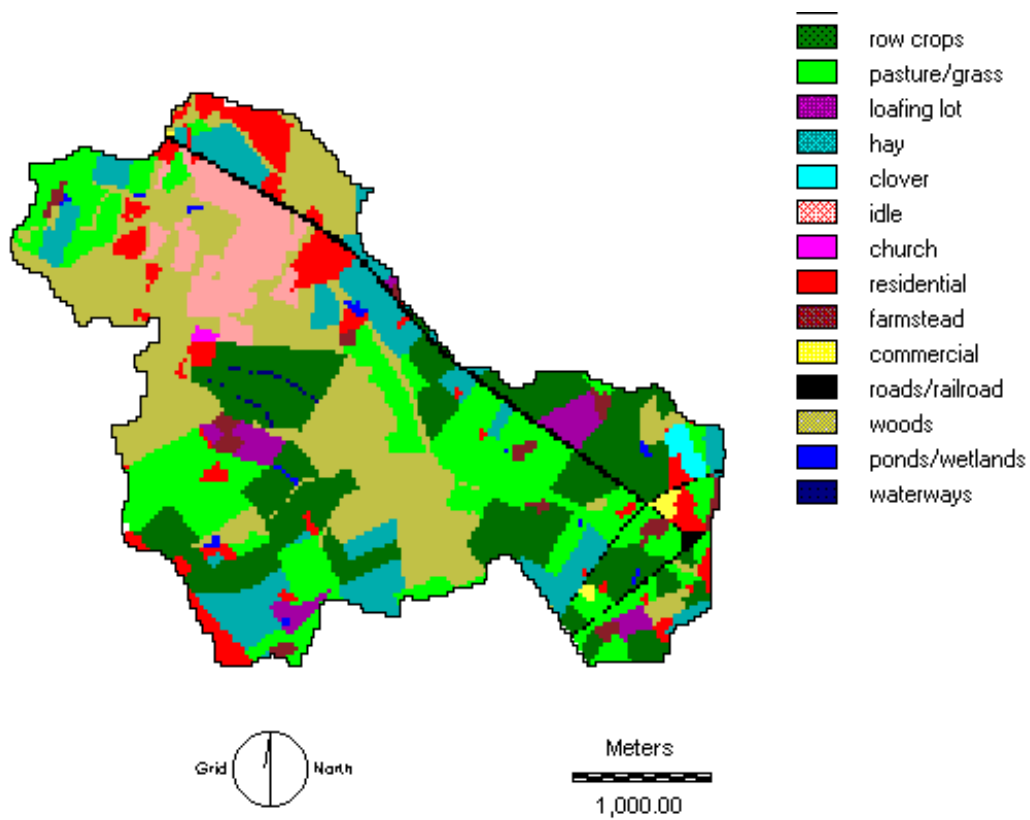


Figure 4.2. Owl Run land use (Spring/Summer 1992).

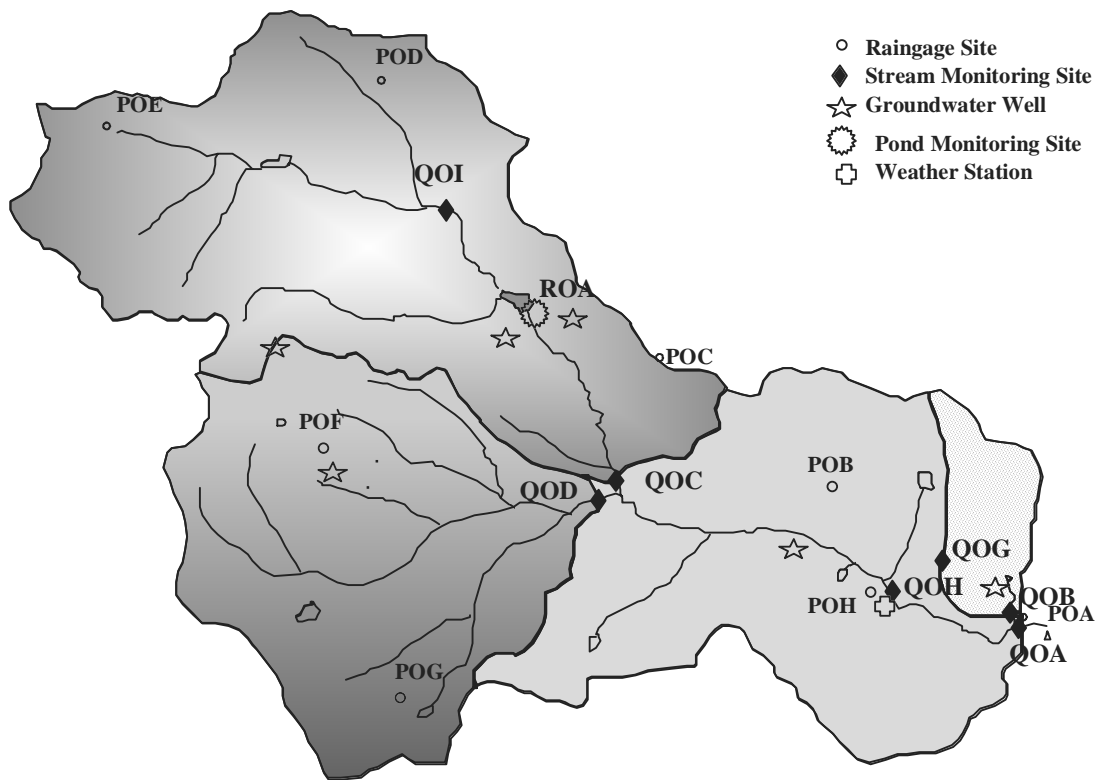


Figure 4.3. Location of monitoring stations within Owl Run watershed (Mostaghimi et al., 1997).

during the summer because of the high rainfall intensities associated with thunderstorms. Typically, there is little base flow between storm events (Wang, 1991).

The land use data used in this study was collected as part of the Owl Run Watershed/Water Quality Monitoring project and was stored in a raster GIS format (11.1 m resolution). Approximately 26% of the land is forested, while much of the remaining area is used for corn, hay or pasture. Residential and commercial areas account for approximately 9% of the watershed.

The elevation data used in this study was a USGS digital elevation model (DEM). Nearly all DEMs have “pits” in the data where every neighboring cell has a higher elevation than the center cell. Frequently, these are the result of the process used to develop the DEMs and are not actual watershed features (Martz and Garbrecht, 1993). In order to correct the pits, Jenson and Domingue’s method (1988) was used. The depressions were filled to the height of the lowest neighboring cell. Martz and Garbrecht (1993) report that this procedure has been satisfactorily tested on a wide variety of watersheds.

In order to evaluate the accuracy of the SDUH model at different scales, it was also applied to subwatersheds C and D in Owl Run (Figure 4.3). Subwatershed C is approximately 462 ha with slopes generally between 1% and 6%, however; some slopes are as high as 25%. Approximately 37% of the land in subwatershed C is forested. Much of the remaining area is used for hay and pasture. There are three small ponds and one large pond in subwatershed C.

Subwatershed D is slightly smaller than subwatershed C with an area of 327 ha. Most of the slopes are between 1% and 7%; however, they may be as high as 19%. Approximately half of subwatershed D is either forested or used for corn production. The remaining areas are mainly used for pasture, hay, and residential areas.

4.2 Topography

4.2.1 Slope

In order to calculate the slope of each grid cell, the tangent of the angle that has the maximum downhill slope is estimated by:

$$\text{slope of E} = \sqrt{\left(\frac{B - A}{2 * \text{resolution}}\right)^2 + \left(\frac{C - D}{2 * \text{resolution}}\right)^2} \quad [27]$$

where: A= elevation of cell A (Figure 4.4)

B = elevation of cell B (Figure 4.4)

C = elevation of cell C (Figure 4.4)

D = elevation of cell D (Figure 4.4)

resolution = 30 m for this study

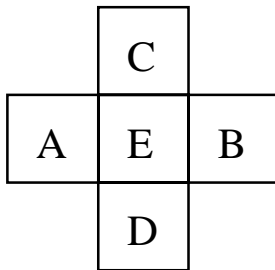


Figure 4.4. Map of Cells Used to Determine Slope of Cell E.

4.2.2 Aspect and Flow Direction

The aspect and flow direction was determined for each grid cell using a technique developed by Jenson and Domingue (1988). With this algorithm, the elevation of the cell of interest is compared with the elevation of the eight neighboring cells. It is assumed that the flow direction is in the direction of the steepest elevation drop. Based on this drop, the center cell is assigned a code that indicates the flow direction (Figure 4.5). In order to determine the steepest elevation drop, the difference in elevation between each neighbor cell and the center cell is divided by the distance from the center cell. The

corners were divided by $\sqrt{2}$, while the orthogonal cells were divided by 1. If the elevation of the center cell is lower than each surrounding cell, the flow direction is assigned a negative number and is assumed to have an undefined flow direction. If two cells on opposite sides have an equal weighted elevation drop, the flow direction is randomly assigned to one of them. If there are three cells in a row that have equal elevation drops, the flow direction is assigned to the center cell.

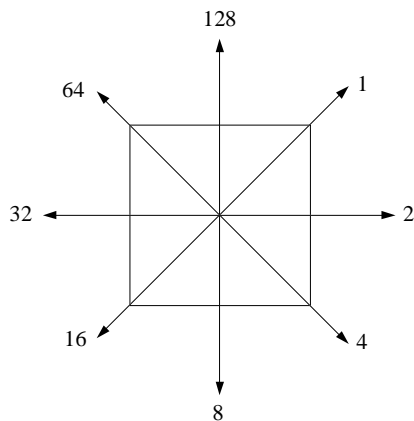


Figure 4.5. Codes Used to Indicate Flow Directions.

4.2.3 Flow Distance

An estimate of the length of flow through each grid cell is necessary to determine the amount of time it takes for runoff to travel through the cell for a given flow velocity. The length of flow for each cell was assigned based on the flow direction. If the flow direction was 1, 4, 16, or 64 (Figure 4.5); the flow length was assigned to be 42 meters, otherwise it was assigned to be 30 meters.

4.2.4 Upstream Area

An algorithm developed by Jenson and Domingue (1988) was used to calculate the area upstream of each grid cell. This technique counts the number of cells that flow into each cell based on the flow direction.

4.2.5 Channel Dimension Estimate

Based on a site visit and the recommendation of the watershed coordinator for the Owl Run Watershed/Water Quality monitoring project (Tony Pane, personal communication, 1997), the channels in the watershed were assumed to be trapezoidal with 1.75:1 side slopes. The bottom width of each channel cell was estimated based on measurements at five points in the watershed. At the other locations, linear interpolation was made based on the upstream area above each cell.

4.3 Channel Delineation

The watershed channels were delineated based on the upstream area above each cell. It was assumed that any upstream area smaller than the threshold value did not produce enough runoff to support a channel. The area required to develop a channel depends on regional and watershed characteristics such as climatic conditions, soil properties, surface cover, and slope characteristics (Martz and Garbrecht, 1992). Any cells that were not determined to be part of the stream network were assumed to be controlled by overland flow. Cells that did not have any other cells flowing into them were considered to be ridge cells. Many researchers have delineated stream networks based on the upstream area (Martz and Garbrecht, 1992; Jenson and Domingue, 1988; Mark, 1984).

For this watershed, a channel flow threshold of 1.8 hectares (20 cells) was chosen. All cells with less upstream area were assumed to be dominated by overland flow. If the contributing area is idealized as a semi-circular region, an area of 1.8 hectares results in a maximum flow distance (radius) of 107 meters. This channel threshold follows the recommendations by Huggins and Burney (1982) that overland flow can only exist for the first 100 meters along the flow path before the runoff concentrates into small rills. Figure 4.6 shows the stream network that results from the channel flow threshold of 20 cells. There was good agreement between the stream network derived using the GIS and

the upstream area technique and the blue-line stream network digitized from a 7.5 minute USGS quadrangle. The GIS-based stream network shows many more streams than the USGS blue line network. Many of the GIS streams represent ephemeral and intermittent streams that are too small to be represented on the USGS map.

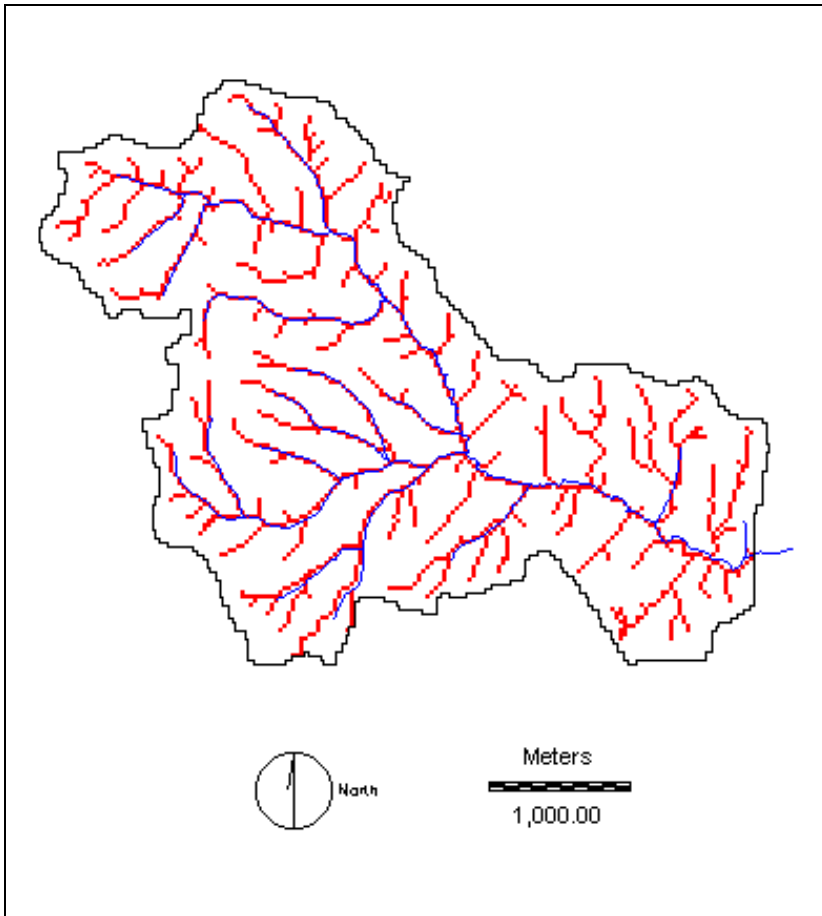


Figure 4.6. Owl Run DEM-based stream network (red) and USGS blue-line stream network (blue).

4.4 Flow velocity

In order to calculate the travel time through each cell, the runoff velocity is required.

4.4.1 Overland Flow Velocity

The runoff velocity for areas with overland flow may be estimated using a kinematic wave approximation. The depth of flow at equilibrium is given by (Overton and Meadows, 1976):

$$y = \left(\frac{i_e n x}{\sqrt{S_o}} \right)^{0.6} \quad [28]$$

where y = depth of runoff flow at equilibrium (m)
 i_e = rainfall excess intensity (m/s)
 n = Manning's roughness coefficient
 x = distance along the flow plane (m)
 S_o = slope (m/m)

The equilibrium depth of flow from equation [27] may be used in Manning's equation to calculate the equilibrium runoff velocity.

$$V_o = \frac{(i_e x)^{0.4} S_o^{0.3}}{n^{0.6}} \quad [29]$$

where: V_o = overland flow velocity (m/s)

The distance along the flow plane was estimated based on the distance of each grid cell from the closest ridge cell. For cells identified as ridge cells, the distance was assigned to be half the length of a grid cell (15 m).

The land use data for Owl Run was used to estimate the Manning's roughness coefficient for the overland cells. Because many published tables of Manning's roughness coefficients do not include most of the specific land uses found in Owl Run, a number of assumptions were made to estimate values. The assumptions are summarized

with the roughness coefficients in Table 4.1. A map of the Manning's roughness values may be found in Figure 4.7.

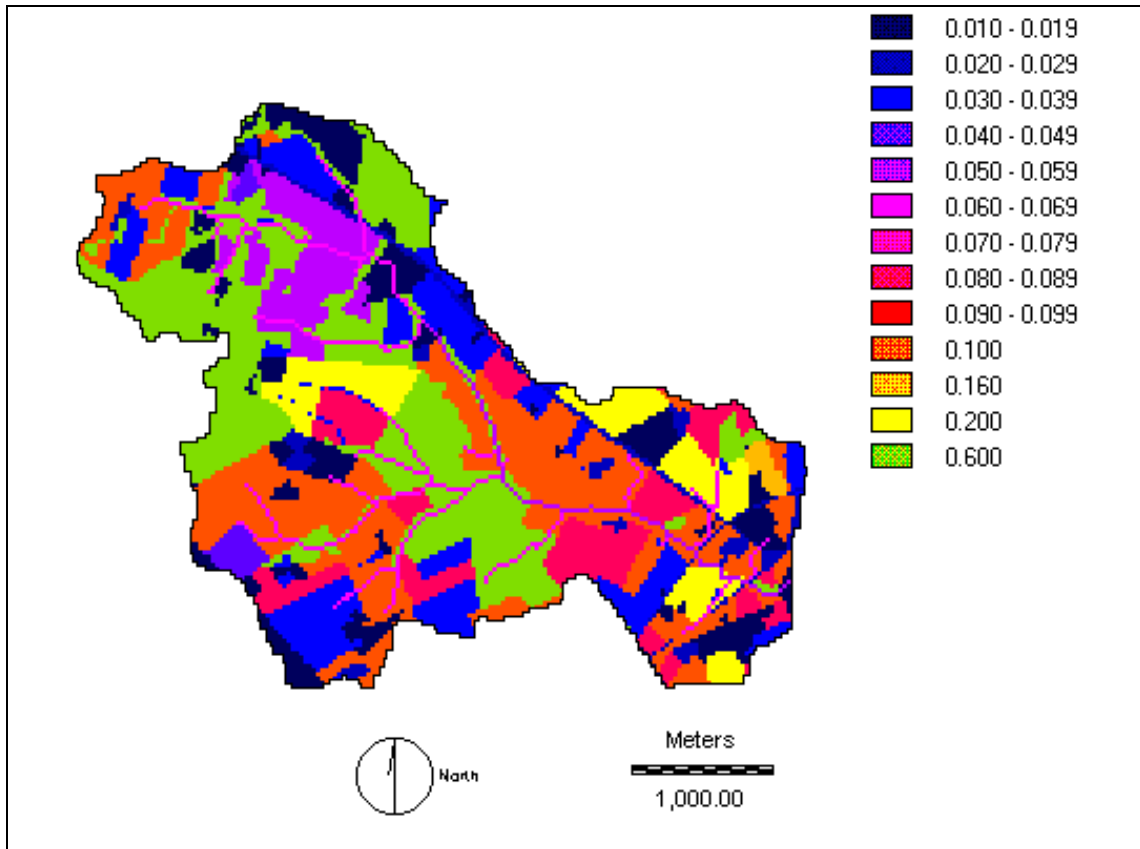


Figure 4.7: Manning's roughness coefficient

Table 4.1. Summary of Owl Run land uses and Manning's roughness coefficients.

Land Use	Code	Manning's n	Notes/Sources*
alfalfa	alf	0.040	normal, mature field crop, (1)
barley	ba	0.032	small grain (2)
church	ch	0.038	¾ good grass (3); ¼ concrete (2)
clover	clo	0.160	(2)
commercial	cm	0.015	(2)
commercial 1	cm1	0.015	(2)
commercial 2	cm2	0.015	(2)
conventional corn	co	0.080	(2)
farmstead	fa	0.025	½ short grass (2); ½ gravel (3)
full season beans	fsb	0.040	normal, mature field crop, (1)
grass	gr	0.046	(3)
hay	ha	0.035	
idle	id	0.050	(3)
light industry	li	0.013	street pavement, (2)
loafing lot	lo	0.040	lower end of grass/pasture range (3)
minimum till corn	mco	0.200	(2) upper end of row crop range
min. till corn residue	mcr	0.070	(3) cornstalk residue (4 t/ac.)
minimum till sorghum	mso	0.200	upper end of row crop range, (2)
minimum till small grain	mtsg	0.400	(2) upper end of small grain range
no-till bean residue	nbr	0.040	(2)
no-till corn residue	ncr	0.200	upper end of row crop range, (2)
no report	nr	--	
no-till beans	ntb	0.200	upper end of row crop range, (2)
no-till corn	ntc	0.200	upper end of row crop range (2)
oats	oat	0.032	good, across slope small grain, (3)
outside watershed	out	--	
pasture	pa	0.100	middle of grass/pasture range (3)
plowed	plw	0.055	(3)
pond	po	0.080	same as waterway
road/rail road	rdr	0.020	gravel surface, (3)
residential	res	0.015	
soybean residue	sbr	0.070	(3)
strip conventional corn	sco	0.090	½ pasture, ½ corn
strip conv. corn residue	scor	0.070	cornstalk residue (3)
small grain	sg	0.032	(2)
strip no-till corn residue	snc	0.200	same as notill corn residue
strip no-till corn	sntc	0.200	upper end of row crop range, (2)
sorghum	so	0.086	½ good across slope small grain (3); ½ conventional corn (2)
strip small grain	ssg	0.100	
summer annual	sua	0.086	same as sorghum
wetland	wet	0.125	sluggish river reach, very weedy, fair condition (4)
wheat	wh	0.032	(2)
woodland	wo	0.600	(2)
waterway	ww	0.08	(4)

*Sources:

1. Gray (1973)
2. Novotny and Olem (1994)
3. Engman (1986)
4. Brater and King (1976)

4.4.2 Channel Flow Velocity

To estimate the equilibrium runoff velocity through channel cells, the equilibrium flow rate was calculated using (Ajward, 1996):

$$Q = i_e A_{drain} \quad [30]$$

where Q = equilibrium flow rate (m^3/s)
 i_e = intensity of rainfall excess (m/s)
 A_{drain} = upstream area (m^2)

Manning's equation is given by:

$$Q = \frac{1}{n} \sqrt{S_o} \frac{A^{5/3}}{P^{2/3}} \quad [31]$$

where: Q = equilibrium flow rate from equation [29]
 A = channel cross-sectional area (m^2)
 P = wetted perimeter (m)

When equations [13] and [14] are substituted into equation [31], the resulting equation is:

$$Q = \frac{\sqrt{S_o} (bd + 1.75d^2)^{5/3}}{n (b + 4d)^{2/3}} \quad [32]$$

The slope used in the above equation is the slope of the corresponding cell derived from the DEM data. Equation [32] may be solved for the equilibrium flow depth, d , because it is the only unknown. A C program was written to solve for the depth of flow (Appendix A). Once the equilibrium depth of flow is estimated, the runoff velocity through each channel cell may be calculated by:

$$V_{channel} = \frac{Q}{(bd + 1.75d^2)} \quad [33]$$

Because the hydraulic roughness changes dramatically along the stream network, the stream network was divided into three sections based on the upstream area. The first section consists of stream channel cells with upstream areas between 1.8 ha (20 cells) and 18 ha (200 cells). The second section of the stream network contains stream channel

cells with upstream areas between 18 ha and 360 ha (4000 cells). The third stream channel division contains cells that have upstream areas larger than 360 ha. The Manning's roughness coefficient used for each stream section is shown in Table 4.2. The two larger channel sections roughly correspond to the intermittent and permanent streams shown on the USGS quad sheet. The stream network divisions are illustrated in Figure 4.8.

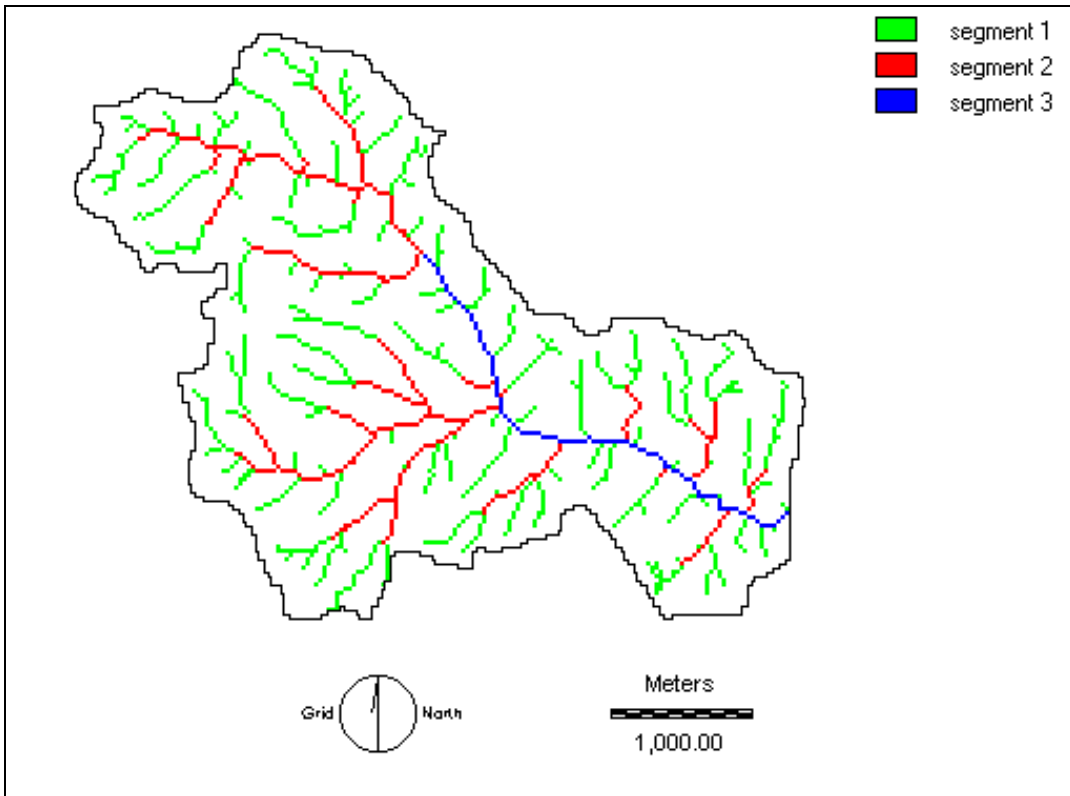


Figure 4.8. Owl Run Stream Network.

(segment 1: land use n , segment 2: $n = 0.06$; segment 3: $n=0.05$)

Table 4.2. Summary of Manning's roughness coefficients for channel cells.

Section	Upstream area (ha)	Manning's n	Notes
shallow concentrated flow	1.8 - 18	corresponding land use n	
intermittent stream	18 - 360	0.06	Brater and King (1976)
permanent stream	360 and up	0.05	Brater and King (1976)

4.5 Travel Time

The travel time through each grid cell may be calculated as flow distance divided by flow velocity. For both surface and channel flow, the flow distance was determined based on the flow direction. If the runoff flowed in directions 1, 4, 16 or 64 (Figure 4.5), the flow distance was assumed to be 42 meters. If the runoff flowed in directions 2, 8, 32, or 128, the flow distance was assumed to be 30 meters. The runoff travel time through each grid cell was calculated by:

$$t_{cell} = D/V \quad [34]$$

where t_{cell} = equilibrium travel time through grid cell (s)

D = flow distance through the cell (m)

V = equilibrium velocity (m/s)

4.6 Ponds

One of the strengths of the SDUH model is that it can account for ponds and wetlands that can significantly alter direct runoff hydrograph timing and shape. Two techniques were used to model the ponds and wetlands. For large ponds, the Muskingum routing method was used to route the runoff hydrograph. This technique accounts for both the time delay and the hydrograph attenuation resulting from the pond effects.

In order to ensure numerical stability for the Muskingum method, the following constraint must be met (Dr. David Kibler, class notes: CE 4304 Hydrology, Fall 1996):

$$2Kx \leq \Delta t \leq K$$

where K = travel time constant
 x = weighting factor
 Δt = time step (1 hour)

In the Owl Run watershed, a number of small ponds had short hydraulic residence times that could not meet the criteria for numerical stability. In these cases, a large Manning's n -value of 0.08 was assigned to those cells, resulting in low flow velocities and long travel times. This roughness coefficient corresponds with a weedy, sluggish river in bad condition (Brater and King, 1976). This method can account for the time delay, but does not attenuate the direct runoff hydrograph.

For the largest pond in Owl Run, Muskingum routing was used to route the runoff hydrograph through the pond. For each rainfall excess intensity, the travel time through the pond was estimated by assuming that the pond was a channel with a bottom width of 10 meters and a depth of 1 meter. These dimensions approximate the dimensions of the pond. Based on this travel time, the average hydraulic residence time was estimated (Muskingum K value). The Muskingum weighting factor was assumed to be 0.2, because a weighting factor of 0.0 produced too much attenuation in the outflow hydrograph. The Muskingum routing calculations were performed using a spreadsheet.

4.7 Cumulative Travel Time to the Outlet

The GIS was used to find the optimal path over the elevation surface to the watershed outlet. Once the path was determined, the GIS was used to sum the travel times through each cell in the optimal path. The total travel time is the sum of the times to travel through each cell along the route. Zollweg et al. (1996) used a similar procedure in the SMoRMod model.

The algorithm used to develop the cumulative travel time is summarized in Figure 4.9. For each grid cell in the watershed, the optimal flow path was found by routing the runoff over the elevation surface. Once the optimal path was found, the travel time through each cell along the path was summed for a cumulative travel time to the outlet. The process was repeated for each cell in the watershed.

In order to develop the cumulative travel time map, a program in C and a DOS batch file were written (Appendix A). If a cell was in the watershed, the program ran a batch file of Idrisi for DOS (version 4.1) commands. If the cell was not in the watershed, the C program moved to the next grid cell and began the process again.

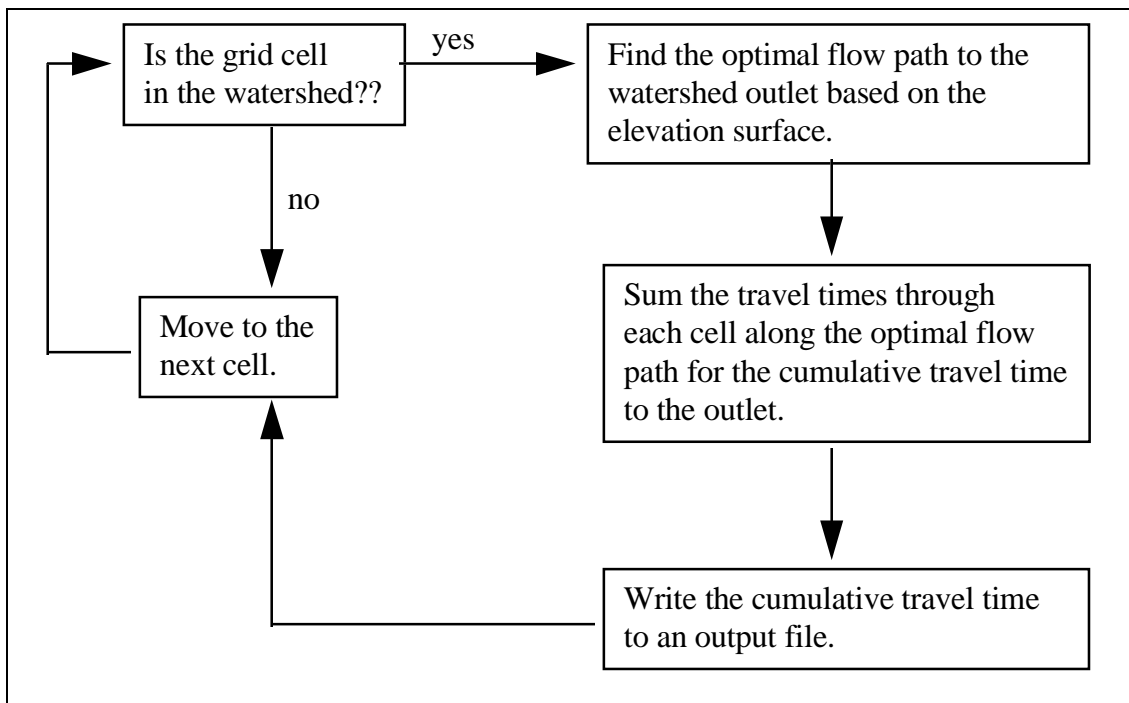


Figure 4.9. Algorithm used to develop the map of the cumulative travel times to the outlet for each grid cell in the watershed.

4.8 Unit hydrograph development

Once the cumulative travel time to the outlet was determined for each grid cell, the watershed was divided into 1-hour isochrones. A unit hydrograph was developed using the procedure presented by Maidment (1993b) and Ajward (1996). After the watershed was divided into isochrones, a time-area histogram was developed. Based on the time-area histogram, a cumulative time-area curve was created. The unit hydrograph ordinate at each time interval was the incremental area for that time step divided by the time interval.

5.0 Results and Discussion

Each of the unit hydrograph techniques described in chapters 3 and 4 were used to predict the direct runoff hydrographs for each of the forty storm events. For each event, the relative error in the peak flow rate, the percent error in time to peak, the bias, sum of squared residuals, sum of absolute residuals and the model efficiency were calculated. The results are summarized and discussed in this chapter.

5.1 Comparison of Unit Hydrograph Techniques

Green and Stephenson (1986) suggested that predicted hydrographs be shifted so that the best possible agreement is found between the observed and predicted hydrographs. They argue that it is not fair to penalize a hydrograph with a good fit, simply because there may be a time discrepancy between the two hydrographs. The predicted hydrographs in this study were shifted in time so that each had the best visual fit with the observed hydrograph for the model efficiency, bias, sum of squares residuals and sum of absolute residuals calculations.

5.1.1 Visual Comparison

An ASCE task committee (1993) has recommended that both visual and statistical comparisons be made between the observed and predicted hydrographs whenever possible. Visual comparisons of simulated and observed hydrographs can provide a fast and comprehensive way to evaluate the overall accuracy of the model output. In fact, the visual comparison may have more practical significance than a statistical analysis (Green

and Stephenson, 1986).

In general, the SDUH model shows the most variation between storm events, because it has the capability to account for differences in the watershed response due to the intensity of rainfall excess. Overall, the two Snyder techniques performed better for the spring storms than the other methods; however, they generally did a worse job for the summer and fall events. The other three unit hydrograph techniques predicted the summer and fall hydrographs better than the spring storms. In general, the SDUH model does the best job of predicting the observed hydrograph shape. Three sample storms are discussed here; they were chosen because they represent a range of storm sizes and seasons. Graphs for all 40 storm events are presented in Appendix C.

Storm #11: November 9-10, 1990:

Storm #11 (November 9-10, 1990) was a large rainfall event with 52.3 mm of rain and a peak flow rate of 2.75 m³/s. None of the unit hydrograph techniques did a very good job of predicting the observed hydrograph (Figure 5.1). Each of the unit hydrograph techniques predict that there was an initial peak flow rate followed by a “hump” due to the second period of rainfall excess. The observed hydrograph showed that there was a slower rise to the peak flow rate. Because the phi-index method was used to estimate the rainfall excess, the volume of rainfall excess is exact, however, it cannot account for the time distribution of the rainfall excess. There probably should have been less rainfall excess during the first few hours of the storm and more rainfall excess towards the end of the storm event. In the watershed, surface storage and interception must be satisfied before runoff will occur. The phi-index method does not account for these processes.

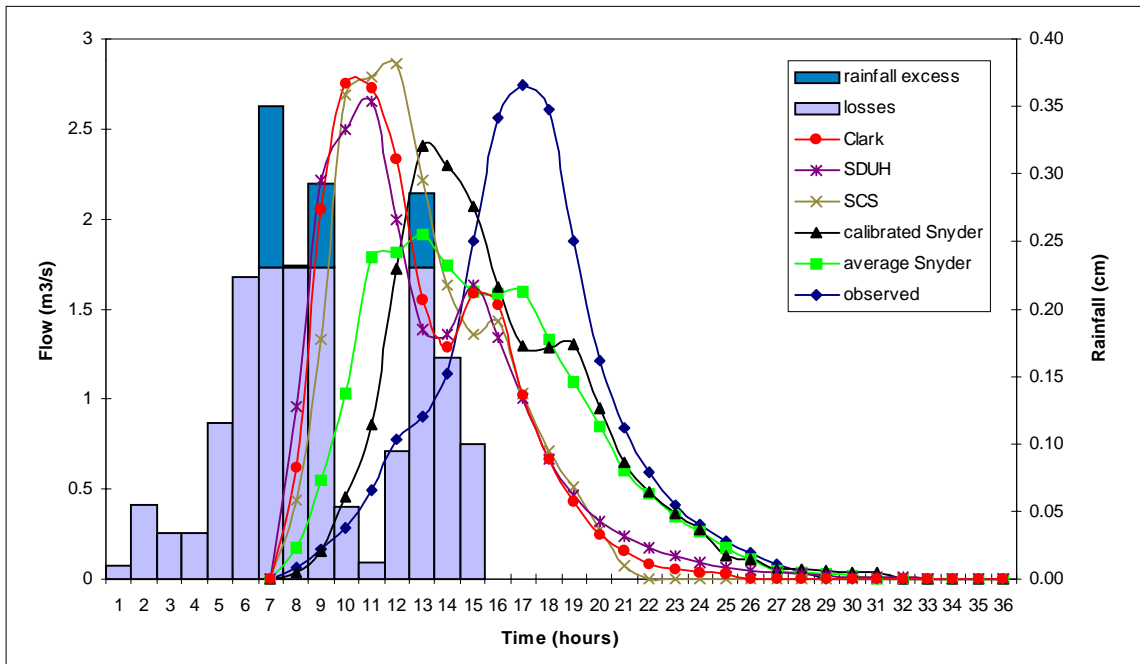


Figure 5.1. Observed and predicted hydrographs for storm #11 (November 9-10, 1990).

Storm #21 May 8, 1992:

Storm #21 (Figure 5.2) was a small spring storm with a low rainfall excess intensity of 0.838 mm/hr. The SDUH method did the best job of predicting the observed hydrograph, however it showed a time shift to the left of approximately one hour. If the SDUH hydrograph was delayed, there would be good agreement between the two.

With the exception of the average Snyder and SDUH models, the other unit hydrograph techniques showed far too little attenuation. The SDUH, Clark, and SCS models tended to show a time shift to the left, while the two Snyders were “late”, with a time shift to the right. The SDUH and observed peak flow rates were substantially lower than the other unit hydrograph techniques.

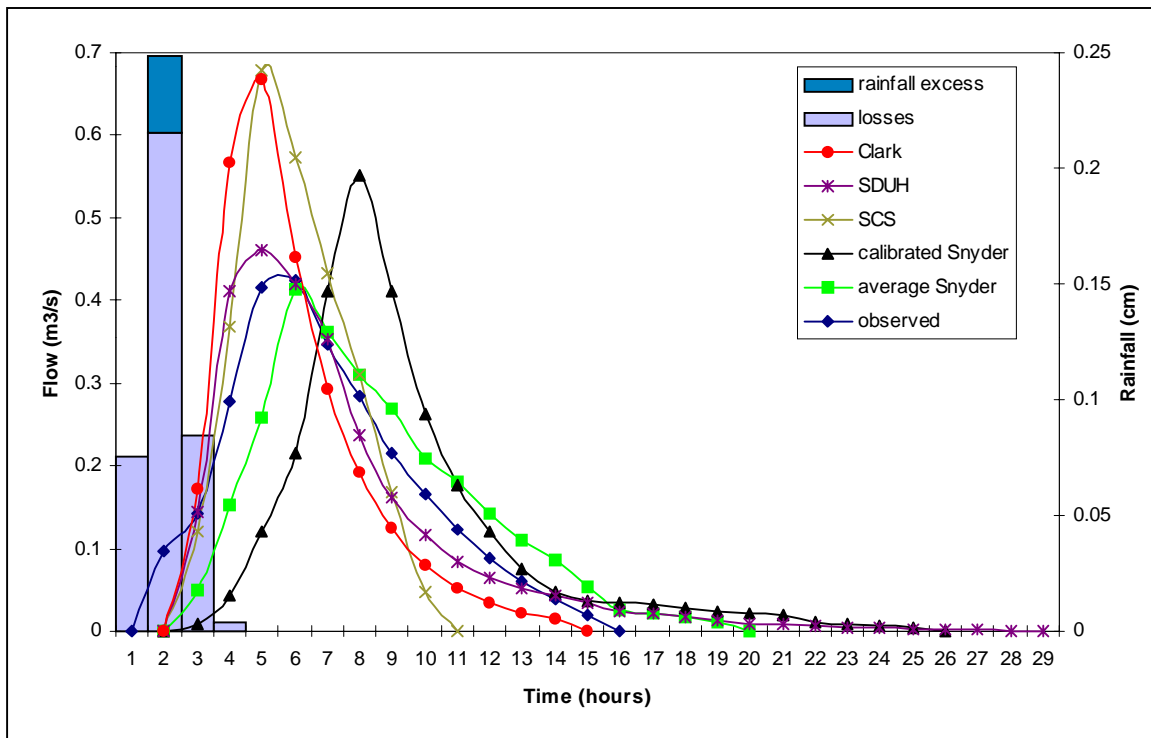


Figure 5.2. Observed and predicted hydrographs for storm #21 (May 8, 1992).

Storm #26; July 27, 1992:

Storm #26 was a large storm with a high observed peak flow rate and a large average rainfall excess intensity of 7.518 mm/hr (Figure 5.3). The SDUH model does the best job of predicting the hydrograph shape; it shows a similar amount of attenuation as the observed hydrograph. The SDUH model also predicts a peak flow rate that is closer to the observed value than the other unit hydrograph methods. The Clark method did a good job of predicting the observed hydrograph shape at both tails, however it did not perform as well around the hydrograph peak. Both Snyder techniques had too much attenuation, therefore they underpredicted the peak flow rate and overpredicted the time to peak.

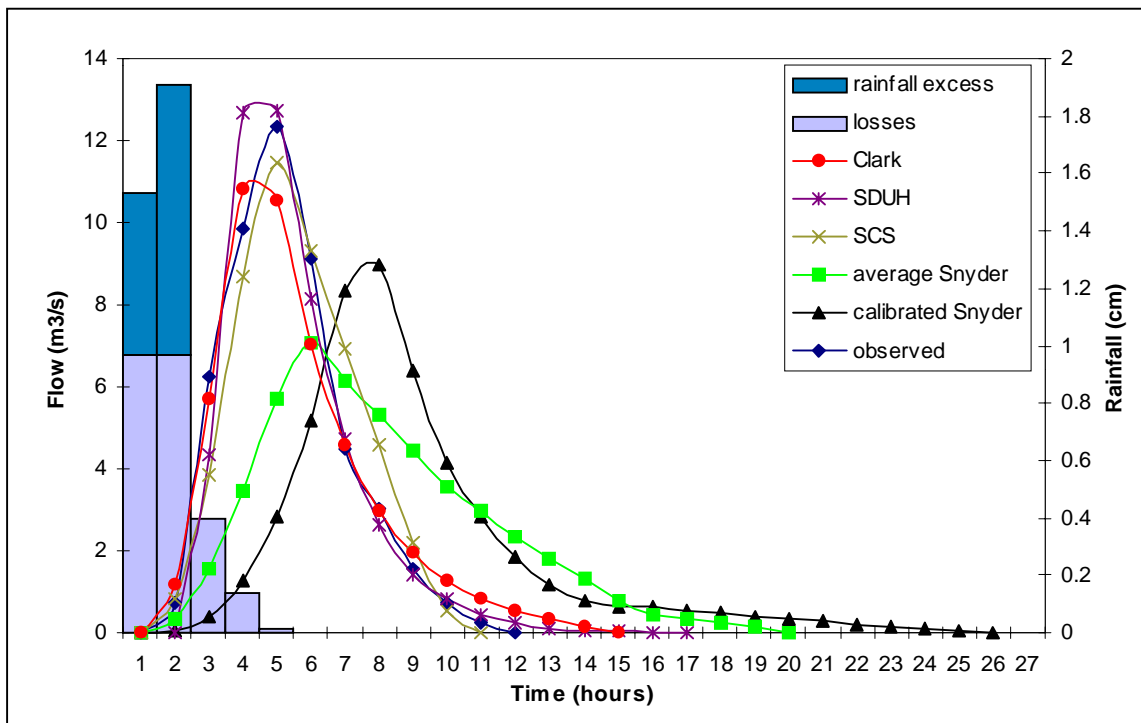


Figure 5.3. Observed and predicted hydrographs for storm #26 (July 27, 1992).

5.1.2 Peak Flow Rate

The peak flow rate prediction for each unit hydrograph model and the observed peak flow rates are summarized in Table 5.1. The relative error in the peak flow rate can be found in Table 5.2. The calibrated Snyder had the lowest MARE (equation [19]) value for the peak flow rate prediction, followed closely by the SDUH model. The other techniques also had similar relative errors. Of the five unit hydrograph techniques, the SDUH model had the lowest relative error for twelve of the 40 events. The average Snyder had the lowest relative error for nine events, while the SCS and Clark methods had the lowest relative error for 7 storms each. Although the calibrated Snyder had the lowest average relative error, it had the lowest relative error for only 5 storms.

The LMARE statistic (equation [20]) indicated that the SDUH method did the best job of predicting the peak flow rate, followed closely by the Clark unit hydrograph. The average Snyder method had the worst LMARE value of -0.541.

Figure 5.4 shows the predicted versus observed flow rates for each of the five unit hydrograph techniques. In general, the unit hydrograph techniques tended to underpredict the peak flow rate. The two Snyder methods did the worst job of predicting the peak flow rates, especially at the higher observed values. For the larger storms, the SDUH method did the best job of predicting the peak flow rate.

With the exception of the SDUH technique, the other unit hydrograph predictions stayed in the same order. The two Snyder methods had the lowest predictions, followed by the Clark unit hydrograph, then the SCS unit hydrograph.

Table 5.1. Observed peak flow rate and predicted peak flow rates (m³/s).

Storm	Observed	SCS	Average Calibrated Snyder	Calibrated Snyder	Clark	SDUH
1	0.496	0.733	0.447	0.595	0.722	0.515
2	3.132	3.293	2.011	2.679	3.248	3.795
3	1.342	2.464	1.518	1.940	2.297	2.118
4	0.598	1.736	1.059	1.413	1.710	1.642
5	4.250	6.193	3.840	4.783	6.063	6.796
6	0.442	1.121	0.685	0.912	1.104	0.858
7	11.018	9.212	6.388	7.583	8.883	8.475
8	1.221	1.209	0.824	1.099	1.192	1.206
9	0.578	0.867	0.530	0.705	0.855	0.609
10	1.473	2.350	1.693	1.807	2.129	1.894
11	2.747	2.860	1.917	2.413	2.755	2.656
12	1.708	1.104	0.674	0.898	1.087	0.864
13	3.019	3.608	2.203	2.937	3.557	4.335
14	12.947	8.589	6.032	6.878	8.127	9.231
15	2.566	2.138	1.305	1.739	2.107	2.234
16	2.206	2.277	1.388	1.852	2.246	2.469
17	1.931	2.322	1.419	1.889	2.291	2.520
18	1.920	1.841	1.124	1.498	1.815	1.855
19	1.119	1.254	0.765	1.019	1.238	1.127
20	8.996	7.810	5.052	6.609	8.212	8.158
21	0.422	0.677	0.413	0.552	0.668	0.462
22	0.462	0.844	0.515	0.688	0.833	0.583
23	0.988	0.714	0.436	0.581	0.705	1.589
24	0.762	0.980	0.598	0.796	0.966	0.750
25	1.659	1.685	1.028	1.371	1.662	1.589
26	12.349	11.460	7.076	8.957	10.845	12.734
27	3.067	2.526	1.543	2.056	2.492	2.752
28	0.535	0.510	0.312	0.416	0.504	0.430
29	0.462	0.493	0.300	0.399	0.484	0.340
30	0.382	0.578	0.351	0.470	0.569	0.430
31	1.597	2.415	1.475	1.965	2.382	2.631
32	0.830	1.141	0.697	0.929	1.127	1.042
33	1.903	2.438	1.526	1.994	2.413	0.634
34	13.199	12.700	7.790	10.163	12.171	11.035
35	0.920	0.881	0.547	0.682	0.858	0.634
36	6.626	4.143	3.016	3.429	4.151	3.928
37	32.256	25.412	15.685	20.167	24.115	29.464
38	13.776	15.945	9.733	12.975	15.724	23.248
39	0.351	0.473	0.289	0.385	0.467	0.331
40	35.175	28.396	20.720	22.849	27.575	30.577

Table 5.2. Relative error in peak flow rate for five unit hydrograph techniques.

Storm	SCS	Average Snyder	Calibrated Snyder	Clark	SDUH
1	0.480	-0.097	0.200	0.457	0.040
2	0.052	-0.358	-0.145	0.037	0.212
3	0.835	0.131	0.445	0.711	0.578
4	1.905	0.773	1.365	1.863	1.749
5	0.457	-0.097	0.125	0.426	0.599
6	1.538	0.551	1.064	1.500	0.942
7	-0.164	-0.420	-0.312	-0.194	-0.231
8	-0.009	-0.325	-0.100	-0.023	-0.012
9	0.500	-0.083	0.221	0.480	0.054
10	0.596	0.150	0.227	0.446	0.287
11	0.041	-0.302	-0.122	0.003	-0.033
12	-0.353	-0.605	-0.474	-0.363	-0.494
13	0.195	-0.270	-0.027	0.178	0.436
14	-0.337	-0.534	-0.469	-0.372	-0.287
15	-0.167	-0.491	-0.322	-0.179	-0.129
16	0.032	-0.371	-0.160	0.018	0.119
17	0.202	-0.265	-0.022	0.186	0.305
18	-0.041	-0.414	-0.220	-0.055	-0.034
19	0.122	-0.316	-0.089	0.106	0.008
20	-0.132	-0.438	-0.265	-0.087	-0.093
21	0.604	-0.020	0.309	0.584	0.094
22	0.828	0.117	0.491	0.804	0.264
23	-0.278	-0.559	-0.413	-0.287	0.607
24	0.286	-0.216	0.045	0.268	-0.015
25	0.015	-0.381	-0.174	0.002	-0.043
26	-0.072	-0.427	-0.275	-0.122	0.031
27	-0.176	-0.497	-0.330	-0.187	-0.102
28	-0.048	-0.418	-0.222	-0.058	-0.196
29	0.067	-0.350	-0.135	0.049	-0.264
30	0.511	-0.081	0.230	0.489	0.126
31	0.512	-0.076	0.230	0.491	0.647
32	0.375	-0.160	0.119	0.358	0.256
33	0.281	-0.198	0.048	0.268	-0.667
34	-0.038	-0.410	-0.230	-0.078	-0.164
35	-0.043	-0.406	-0.258	-0.068	-0.311
36	-0.375	-0.545	-0.482	-0.374	-0.407
37	-0.212	-0.514	-0.375	-0.252	-0.087
38	0.157	-0.294	-0.058	0.141	0.688
39	0.347	-0.177	0.097	0.331	-0.056
40	-0.193	-0.411	-0.350	-0.216	-0.131
MARE:	0.339	0.331	0.281	0.328	0.295
LMARE:	-0.694	-0.541	-0.696	-0.760	-0.806

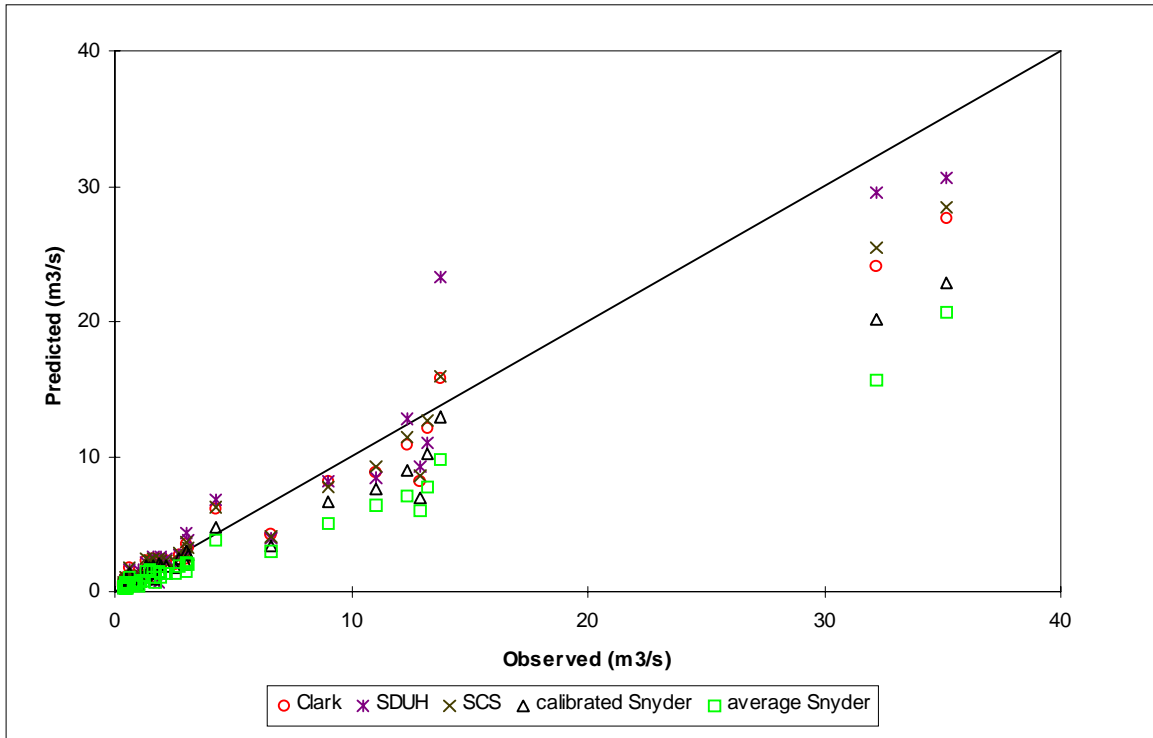


Figure 5.4. Comparison of predicted versus observed peak flow rate for synthetic unit hydrograph techniques.

5.1.3 Time to Peak Flow Rate

The time to peak flow rate was calculated for each event; the observed and predicted times to peak are summarized in Table 5.3. It is recognized that the 1-hour time step is not very precise for this analysis. The SCS technique did the best job of predicting the time to peak, followed closely by the Clark and average Snyder methods (Table 5.4). The calibrated Snyder method did the worst job of predicting the time to peak flow rate.

The two Snyder methods generally overpredicted the time to peak. The SCS and Clark methods underpredicted the time to peak for approximately half of the storm events. The SDUH model underpredicted the time to peak for 34 out of the 40 events. The SCS method did the best job of predicting the time to peak. It had the lowest MARE and it underpredicted the time to peak as often as it overpredicted it. The SCS method correctly predicted the time to peak flow rate for 15 storms. The LMARE statistic was not calculated for the time to peak flow rate because of all the exact predictions. When the relative error is equal to zero, the LMARE statistic is undefined.

Table 5.3. Observed and predicted time to peak (hours).

	Observed	SCS	Average Snyder	Calibrated Snyder	Clark	SDUH
1	5	3	4	6	3	3
2	4	3	4	6	3	2
3	6	4	5	7	4	3
4	4	3	4	6	3	2
5	4	4	5	7	3	3
6	5	3	4	6	3	2
7	17	16	17	19	16	15
8	3	3	4	6	3	2
9	4	3	4	6	3	3
10	12	7	8	10	6	6
11	10	5	6	6	3	4
12	3	3	4	6	3	2
13	6	3	4	6	3	2
14	8	7	8	10	7	6
15	3	3	4	6	3	2
16	5	3	4	6	3	2
17	2	2	4	6	3	2
18	2	3	4	6	3	2
19	3	3	4	6	3	2
20	14	15	16	17	14	13
21	5	4	5	7	4	4
22	5	4	5	7	4	3
23	3	3	4	6	3	4
24	4	3	5	7	4	3
25	3	3	4	6	3	2
26	4	4	5	7	4	3
27	4	4	5	7	4	3
28	3	3	4	6	3	3
29	7	3	4	6	3	3
30	6	3	4	6	3	3
31	5	3	4	6	3	2
32	6	3	5	7	4	3
33	8	8	9	11	8	7
34	4	4	5	7	4	5
35	4	4	5	7	3	4
36	13	4	14	7	4	3
37	4	5	6	8	5	3
38	3	3	4	6	3	1
39	5	3	4	6	3	3
40	11	12	13	14	11	10

Table 5.4. Percent error in the time to peak for each storm.

	SCS	Average Snyder	Calibrated Snyder	Clark	SDUH
1	-0.400	-0.200	0.200	-0.400	-0.400
2	-0.250	0.000	0.500	-0.250	-0.500
3	-0.333	-0.167	0.167	-0.333	-0.500
4	-0.250	0.000	0.500	-0.250	-0.500
5	0.000	0.250	0.750	-0.250	-0.250
6	-0.400	-0.200	0.200	-0.400	-0.600
7	-0.059	0.000	0.118	-0.059	-0.118
8	0.000	0.333	1.000	0.000	-0.333
9	-0.250	0.000	0.500	-0.250	-0.250
10	-0.417	-0.333	-0.167	-0.500	-0.500
11	-0.500	-0.400	-0.400	-0.700	-0.600
12	0.000	0.333	1.000	0.000	-0.333
13	-0.500	-0.333	0.000	-0.500	-0.667
14	-0.125	0.000	0.250	-0.125	-0.250
15	0.000	0.333	1.000	0.000	-0.333
16	-0.400	-0.200	0.200	-0.400	-0.600
17	0.000	1.000	2.000	0.500	0.000
18	0.500	1.000	2.000	0.500	0.000
19	0.000	0.333	1.000	0.000	-0.333
20	0.071	0.143	0.214	0.000	-0.071
21	-0.200	0.000	0.400	-0.200	-0.200
22	-0.200	0.000	0.400	-0.200	-0.400
23	0.000	0.333	1.000	0.000	0.333
24	-0.250	0.250	0.750	0.000	-0.250
25	0.000	0.333	1.000	0.000	-0.333
26	0.000	0.250	0.750	0.000	-0.250
27	0.000	0.250	0.750	0.000	-0.250
28	0.000	0.333	1.000	0.000	0.000
29	-0.571	-0.429	-0.143	-0.571	-0.571
30	-0.500	-0.333	0.000	-0.500	-0.500
31	-0.400	-0.200	0.200	-0.400	-0.600
32	-0.500	-0.167	0.167	-0.333	-0.500
33	0.000	0.125	0.375	0.000	-0.125
34	0.000	0.250	0.750	0.000	0.250
35	0.000	0.250	0.750	-0.250	0.000
36	-0.692	0.077	-0.462	-0.692	-0.769
37	0.250	0.500	1.000	0.250	-0.250
38	0.000	0.333	1.000	0.000	-0.667
39	-0.400	-0.200	0.200	-0.400	-0.400
40	0.091	0.182	0.273	0.000	-0.091
MARE:	0.213	0.259	0.588	0.230	0.347

5.1.4 Model Efficiency

The model efficiencies for each of the five unit hydrograph techniques were calculated using equation [21] and are summarized in Table 5.5. The two Snyder techniques have the highest average R^2 values, followed by the SDUH method. The Clark and SCS techniques have the lowest average R^2 values. The average R^2 value may be skewed by the extremely poor results for Storm #4. Without this event, the average R^2 values improve for each of the five unit hydrograph techniques (Table 5.6).

The SDUH method has the highest R^2 value for 12 of the 40 storm events, more than for any other method (Table 5.7). The two Snyder techniques and the Clark method had a similar number of events with the highest R^2 value. The SCS method had the highest model efficiency for two events and the lowest for 12 storms. The average Snyder method also did not predict the hydrograph shape very well. Among the five unit hydrograph techniques, it had the lowest R^2 value for 20 storms.

Each of the techniques had an R^2 of at least 0.95 for approximately the same number of events. The calibrated Snyder and the SDUH technique predicted events with a model efficiency of at least 0.90 for at least twice as many events as the other techniques.

According to the R^2 statistic, the SDUH and the calibrated Snyder methods did the best job of predicting the hydrograph shape. Their average R^2 values were higher than the other techniques. In addition, they both had many more events with R^2 values of at least 0.90. The SDUH method had the highest R^2 value for more events than any other technique (12). The calibrated Snyder and the Clark methods followed with 9 events.

Table 5.5. Model efficiency for each unit hydrograph technique.

Storm	SCS	Average Snyder	Calibrated Snyder	Clark	SDUH
1	0.579	0.940	0.958	0.691	0.942
2	0.947	0.660	0.941	0.964	0.909
3	0.137	0.963	0.821	0.321	0.693
4	-3.375	-0.249	-1.023	-2.981	-2.547
5	0.463	0.939	0.854	0.653	0.407
6	-1.669	0.609	0.060	-1.498	-0.959
7	0.705	0.676	0.767	0.634	0.808
8	0.950	0.864	0.949	0.930	0.984
9	0.325	0.907	0.937	0.591	0.948
10	0.540	0.950	0.771	0.691	0.896
11	0.832	0.661	0.679	0.768	0.831
12	0.702	0.708	0.842	0.811	0.873
13	0.701	0.455	0.478	0.701	0.520
14	0.674	0.616	0.725	0.619	0.776
15	0.897	0.661	0.837	0.876	0.949
16	0.840	0.725	0.907	0.739	0.886
17	0.926	0.835	0.931	0.857	0.916
18	0.878	0.733	0.938	0.982	0.922
19	0.913	0.797	0.948	0.866	0.921
20	0.832	0.808	0.903	0.921	0.923
21	0.416	0.968	0.927	0.423	0.942
22	-0.578	0.920	0.700	-0.099	0.629
23	0.773	0.685	0.882	0.914	0.897
24	0.731	0.879	0.913	0.639	0.905
25	0.944	0.794	0.950	0.897	0.938
26	0.912	0.742	0.937	0.956	0.953
27	0.797	0.691	0.926	0.944	0.918
28	0.963	0.808	0.940	0.882	0.727
29	0.829	0.716	0.761	0.976	0.932
30	0.297	-0.020	0.903	0.681	0.946
31	0.673	0.892	0.894	0.734	0.709
32	0.685	0.899	0.969	0.789	0.913
33	0.863	0.868	0.258	0.833	0.911
34	0.794	0.762	0.934	0.955	0.943
35	0.955	0.819	0.523	0.957	0.959
36	0.331	0.552	0.546	0.311	0.544
37	0.860	0.719	0.833	0.883	0.875
38	0.954	0.806	0.921	0.874	0.250
39	0.443	0.928	0.950	0.742	0.966
40	0.866	0.829	0.854	0.862	0.883
average	0.533	0.738	0.769	0.607	0.708

Table 5.6. Average R^2 values for unit hydrograph technique with and without storm #4.

	With Storm #4	Without Storm #4
SCS	0.533	0.633
average Snyder	0.738	0.763
calibrated Snyder	0.769	0.815
Clark	0.607	0.699
SDUH	0.708	0.792

Table 5.7. Number of events each method had the highest and lowest R^2 values.

	lowest R^2 value	highest R^2 value
SCS	12	2
average Snyder	20	8
calibrated Snyder	2	9
Clark	3	9
SDUH	3	12

Table 5.8. Number of events that had high R^2 values.

	Number of Events (out of 40)	
	$R^2 \geq 0.95$	$R^2 \geq 0.90$
SCS	4	9
average Snyder	3	8
calibrated Snyder	4	20
Clark	6	10
SDUH	4	21

5.1.5 Shape Statistics

When the predicted hydrographs were compared with the observed data on an ordinate-by-ordinate basis, the SCS, Clark, and SDUH model predicted the hydrograph shape better than the two Snyder methods.

Bias

The SCS and SDUH techniques tended to underpredict the hydrograph ordinates, while the two Snyder methods and the Clark method tended to overpredict the hydrograph ordinates (Table 5.9). The SCS and SDUH technique had the smallest average bias estimates. They were -0.047 and -0.097, respectively. The SCS method had the smallest bias estimate of the five techniques for 38 of the 40 storm events used in this study. The calibrated Snyder method showed the most bias in the estimation of the hydrograph ordinates. Its average bias was 0.230. The SCS and SDUH models tended to overpredict the observed hydrograph ordinates, while the Clark and two Snyder methods tended to underpredict the hydrograph ordinates.

Sum of absolute residuals (SAR) and total sum of absolute residuals (TSAR)

The Clark method had the lowest TSAR, followed by the SDUH and the SCS techniques (Table 5.10). The two Snyder methods had the highest TSAR values. In general, the average Snyder method had the smallest SAR values for spring storms, while the Clark and SDUH methods generally did the best job for summer and fall storms. In an ordinate by ordinate comparison of observed and predicted hydrographs, the Clark method did the best job of predicting the hydrograph shape. The two Snyder methods did the worst job of predicting the shape.

Sum of squared residuals (SSR) and total sum of squared residuals (TSSR)

According to the TSSR, the Clark and SDUH methods did the best job of predicting the hydrograph shape (Table 5.11). The two Snyder techniques had the highest TSSR values. The average Snyder method had the highest SSR values for nearly half of the storm events. The calibrated Snyder, Clark and SDUH methods each had relatively low SSR values for most of the storms. The calibrated Snyder and Clark methods each had the highest SSR values for only three events each. The SDUH method had the highest SSR value for five storms.

Table 5.9. Bias in Hydrograph Shape Prediction.

Storm	SCS	Average Snyder	Calibrated Snyder	Clark	SDUH
1	-0.001	0.027	0.024	0.029	-0.001
2	-0.005	-0.561	0.109	0.130	-0.012
3	-0.004	0.095	0.086	0.086	-0.008
4	-0.003	0.063	0.057	0.069	-0.008
5	-0.019	0.234	0.212	0.254	-0.034
6	-0.002	0.041	0.037	0.044	-0.368
7	0.025	1.246	2.131	0.806	-0.062
8	-0.002	0.049	0.045	0.048	-0.007
9	-0.001	0.032	0.029	0.034	-0.003
10	-0.017	0.119	0.107	0.130	-0.024
11	-0.008	0.176	0.253	0.191	-0.019
12	-0.001	0.120	0.037	0.044	-0.006
13	-0.005	0.132	0.119	0.142	-0.012
14	-0.018	0.464	0.420	0.500	-0.049
15	-0.003	0.078	0.071	0.084	-0.007
16	-0.003	0.084	0.075	0.090	-0.008
17	-0.003	0.085	0.077	0.092	-0.008
18	-0.003	0.067	0.061	0.073	-0.003
19	-0.002	0.046	0.042	0.050	-0.007
20	-1.370	0.402	0.364	0.434	-0.042
21	-0.001	0.025	0.022	0.027	-0.002
22	-0.001	0.031	0.028	0.033	-0.003
23	-0.001	0.323	0.320	0.028	0.289
24	-0.001	0.036	0.032	0.020	-0.006
25	-0.002	0.062	0.058	0.066	-0.010
26	-0.017	0.445	0.419	0.480	-0.046
27	-0.003	0.092	0.087	0.100	-0.010
28	-0.001	0.019	0.018	0.020	-2.671
29	-0.001	0.018	0.016	0.019	-0.002
30	-0.001	0.021	0.019	0.023	-0.002
31	-0.003	0.088	0.080	0.095	-0.009
32	-0.002	0.042	0.038	0.045	-0.004
33	-0.004	0.095	0.088	0.064	-0.009
34	-0.274	0.220	0.175	0.257	-0.305
35	-0.001	0.035	0.031	0.037	-0.004
36	-0.014	0.377	0.341	0.407	-0.060
37	-0.037	0.970	0.916	1.047	-0.097
38	-0.022	0.583	0.528	0.629	-0.055
39	-0.001	0.014	0.016	0.019	-0.002
40	-0.067	1.787	1.618	1.929	-0.190
average:	-0.047	0.207	0.230	0.217	-0.097

Table 5.10. Sum of absolute Residuals (SAR) and total sum of absolute residuals (TSAR).

Storm	SCS	Average Snyder	Calibrated Snyder	Clark	SDUH
1	1.073	0.612	0.739	0.994	0.776
2	2.481	8.385	3.840	2.011	3.630
3	6.241	1.345	2.883	5.004	4.055
4	7.303	4.570	4.885	6.482	6.216
5	13.250	3.828	9.013	11.035	13.765
6	3.877	1.631	2.263	3.511	2.996
7	35.566	36.631	31.859	37.163	31.452
8	0.745	1.710	1.011	1.019	0.561
9	1.662	0.736	0.903	1.201	0.776
10	7.365	12.726	5.258	6.116	3.574
11	6.159	7.827	7.515	7.456	8.263
12	2.424	4.035	3.659	2.727	3.228
13	6.604	6.632	8.450	5.615	6.697
14	30.367	44.327	40.108	33.992	31.203
15	2.311	5.703	4.046	3.424	2.761
16	2.860	5.049	2.869	3.217	3.081
17	2.308	3.245	2.008	2.716	1.858
18	1.875	4.140	2.427	0.750	1.557
19	1.147	2.180	1.303	1.099	2.271
20	19.881	24.228	24.423	17.307	19.522
21	1.223	0.348	0.699	1.045	0.640
22	2.280	0.564	1.218	1.798	1.450
23	1.172	2.115	1.727	1.099	1.441
24	1.509	1.124	1.164	1.172	0.895
25	1.237	3.123	2.059	0.923	1.750
26	9.854	29.942	18.219	8.450	8.325
27	3.486	7.490	4.500	2.515	3.947
28	0.269	1.070	0.816	0.504	3.418
29	0.555	0.915	0.920	0.255	0.753
30	1.382	1.824	0.796	0.909	0.617
31	3.520	2.393	2.619	2.869	3.687
32	1.427	1.331	1.039	1.368	1.481
33	3.234	3.095	9.132	3.070	2.648
34	15.421	30.364	20.830	9.970	15.521
35	0.521	1.784	3.384	0.651	1.345
36	27.915	23.775	24.862	27.215	24.231
37	37.291	50.073	36.387	21.915	29.359
38	9.401	30.319	19.029	14.934	30.497
39	0.818	0.262	0.524	0.566	0.476
40	68.807	62.683	70.566	67.969	65.395
TSAR:	346.821	434.134	379.952	322.035	346.116

Table 5.11. Sum of squared residuals (SSR) and total sum of squared residuals (TSSR).

Storm	SCS	Average Snyder	Calibrated Snyder	Clark	SDUH
1	4.97	1.13	1.25	4.74	2.13
2	26.04	237.68	56.65	19.12	67.29
3	122.86	5.04	28.31	91.41	55.60
4	126.27	36.05	58.38	114.90	102.40
5	617.38	69.63	217.81	398.99	682.61
6	43.63	6.40	16.43	40.84	32.03
7	2765.89	3231.69	2396.82	3541.23	2319.76
8	3.10	12.96	6.60	4.74	2.01
9	12.18	2.21	2.09	7.38	2.47
10	116.32	12.73	57.92	78.25	28.88
11	100.63	228.73	218.39	151.24	156.16
12	38.85	87.85	65.27	38.93	54.83
13	133.06	242.89	311.54	133.01	228.67
14	3613.23	6163.73	5446.04	4932.83	3870.20
15	33.26	145.46	84.36	46.60	25.70
16	35.33	84.35	36.43	62.16	40.82
17	17.83	38.25	19.72	34.40	20.18
18	18.99	66.70	21.24	3.08	9.22
19	5.34	16.71	5.95	8.26	25.78
20	1123.08	1829.53	1130.66	614.94	784.78
21	5.71	0.39	1.37	4.99	1.43
22	18.36	0.93	5.15	12.73	8.43
23	8.80	20.55	11.53	6.07	11.80
24	7.39	3.90	4.03	8.32	5.09
25	6.50	35.24	13.05	6.67	14.76
26	594.72	2982.00	1100.65	360.73	481.08
27	69.45	213.01	79.59	28.94	70.98
28	0.35	4.52	2.32	1.72	12.88
29	1.73	4.21	4.89	0.26	2.17
30	6.16	10.24	1.65	2.79	0.99
31	51.55	22.25	32.48	41.92	79.67
32	9.65	5.69	2.40	9.18	8.27
33	32.41	39.18	271.53	37.56	33.76
34	1557.74	3447.03	1342.59	445.24	876.74
35	1.54	11.49	42.14	1.99	5.84
36	2031.81	1612.86	1940.09	2093.93	1999.87
37	5761.69	13522.34	9817.43	4613.23	513.26
38	429.53	2946.77	1662.39	1285.34	7680.43
39	2.84	0.63	0.63	1.33	0.73
40	10887.35	16029.69	15483.31	10787.52	10024.14
TSSR:	30443.48	53432.60	42001.07	30077.51	30343.81

5.1.6 Analysis Based on Storm Size

The predictions of the five unit hydrograph techniques for each of the forty storm events were analyzed based on the rainfall volume. In general, there was no obvious trend between the storm sizes. Among the five unit hydrograph techniques, the Clark method predicted the peak flow rate most accurately for the largest 25% of the storms (rainfall greater than 49 mm). The calibrated Snyder technique predicted the peak flow rate most accurately for the remainder of the storms. With the exception of the average Snyder method, each technique predicted the peak flow rate more accurately for the large and small storms than they did for the storms with rainfall between 18 mm and 49 mm. The two Snyder techniques predicted the peak flow rate more accurately for the storms with less than 18 mm of rainfall than they did for storms with at least 49 mm of rainfall. The SCS, Clark, and SDUH methods predict the peak flow rate for large storm events more accurately than they do for small storms.

With the exception of the SCS method, each of the unit hydrograph techniques predicted the time to peak better for the largest and smallest storms than they did for the medium-sized events (Table 5.13). Among the five techniques, the average Snyder method predicted the time to peak most accurately for the smallest 25% of the storms, while the SCS method predicted the time to peak most accurately for the remainder of the events. The SDUH and two Snyder methods predicted the time to peak more accurately for storms with less than 18 mm of rainfall than they did for storms with more than 49 mm of rainfall. The SCS and Clark methods predicted the time to peak more accurately for large storms than for small ones.

All five unit hydrograph techniques had lower average model efficiencies for mid-sized storms than they did for storms with less than 18 mm or more than 49 mm of rainfall (Table 5.14). The SDUH and two Snyder techniques had higher model efficiencies for small storms than for the large events. The SCS and Clark models had higher average model efficiencies when there was at least 49 mm of rainfall than when the rainfall was less than 18 mm. Between the five techniques, the SDUH model had the highest model efficiency for the smallest 25% of the storms, while the Clark method had the highest model efficiency for the largest 25% of the storm events.

Table 5.12. Relative error in peak flow rate based on rainfall volume.

	RV ≤ 18mm		18mm ≤ RV ≤ 49mm		49mm ≤ RV	
	(n = 10)		(n = 20)		(n = 10)	
	<i>MARE</i>	<i>LMARE</i>	<i>MARE</i>	<i>LMARE</i>	<i>MARE</i>	<i>LMARE</i>
SCS	0.303	-0.678	0.410	-0.757	0.235	-0.717
average Snyder	0.213	-0.796	0.348	-0.538	0.416	-0.409
calibrated Snyder	0.167	-0.854	0.330	-0.672	0.297	-0.590
Clark	0.292	-0.679	0.397	-0.784	0.225	-0.836
SDUH	0.249	-0.835	0.342	-0.808	0.246	-0.754

RV: rainfall volume

Table 5.13. Relative error in the time to peak based on rainfall volume.

	RV ≤ 18mm		18mm ≤ RV ≤ 49mm		49mm ≤ RV	
	(n = 10)		(n = 20)		(n = 10)	
SCS	0.240		0.230		0.151	
average Snyder	0.173		0.307		0.256	
calibrated Snyder	0.454		0.679		0.542	
Clark	0.223		0.267		0.163	
SDUH	0.298		0.385		0.321	

RV: rainfall volume

Table 5.14. Average model efficiency (R^2) based on rainfall volume.

	RV ≤ 18mm		18mm ≤ RV ≤ 49mm		49mm ≤ RV	
	(n = 10)		(n = 20)		(n = 10)	
SCS	0.726		0.309		0.786	
average Snyder	0.866		0.671		0.743	
calibrated Snyder	0.827		0.717		0.813	
Clark	0.765		0.435		0.794	
SDUH	0.888		0.570		0.806	

RV: rainfall volume

The results from the forty storm events were also analyzed based on the average intensity of the rainfall excess. When the storms were divided this way, there was very little difference in each technique's ability to predict the peak flow rate (Table 5.15). The SCS, calibrated Snyder and Clark methods more accurately predicted the peak flow rate for the higher intensity storms than they did with the lowest intensity events. The average Snyder and SDUH methods did a slightly better job predicting the peak flow rates for the lower intensity events than they did for the high intensity storms.

There was no trend in the prediction of the time to peak. With the exception of the Clark technique, each unit hydrograph model had a higher MARE for the medium sized events than they did for the larger and smaller storms (Table 5.16). With the exception of the average Snyder method, each technique had higher model efficiencies for the larger and smaller events than they did for the medium sized storms (Table 5.17).

Based on both the rainfall volume and rainfall excess intensity, each technique seems to have the most difficulty representing the watershed response for medium-sized events with a rainfall volume between 18 mm and 49 mm and an average rainfall intensity between 1.1 mm/hr and 3.1 mm/hr.

Table 5.15. Error in peak flow rate based on average rainfall excess intensity.

	REI ≤ 1.1 mm/hr (n = 10)		1.1mm/hr ≤ REI ≤ 3.1 mm/hr (n = 20)		3.1mm/hr ≤ REI (n = 10)	
	<i>MARE</i>	<i>LMARE</i>	<i>MARE</i>	<i>LMARE</i>	<i>MARE</i>	<i>LMARE</i>
SCS	0.371	-0.609	0.399	-0.734	0.189	-0.832
average Snyder	0.231	-0.804	0.356	-0.510	0.381	-0.457
calibrated Snyder	0.257	-0.632	0.314	-0.706	0.238	-0.743
Clark	0.361	-0.603	0.375	-0.848	0.201	-0.784
SDUH	0.201	-0.843	0.352	-0.821	0.274	-0.719

REI: average rainfall excess intensity

Table 5.16. Error in time to peak based on average rainfall excess intensity.

	REI ≤ 1.1 mm/hr (n = 10)		1.1mm/hr ≤ REI ≤ 3.1 mm/hr (n = 20)		3.1mm/hr ≤ REI (n = 10)	
SCS	0.252		0.239		0.122	
average Snyder	0.208		0.296		0.235	
calibrated Snyder	0.459		0.646		0.602	
Clark	0.277		0.253		0.138	
SDUH	0.305		0.370		0.342	

REI: average rainfall excess intensity

Table 5.17. Average model efficiency (R^2) based on average rainfall excess intensity.

	REI ≤ 1.1 mm/hr (n = 10)		1.1mm/hr ≤ REI ≤ 3.1 mm/hr (n = 20)		3.1mm/hr ≤ REI (n = 10)	
SCS	0.500		0.417		0.797	
average Snyder	0.767		0.731		0.722	
calibrated Snyder	0.848		0.693		0.840	
Clark	0.676		0.456		0.841	
SDUH	0.889		0.601		0.743	

REI: average rainfall excess intensity

5.1.7 Analysis Based on Season

There was a substantial seasonal difference in each technique's predictive capabilities. The storms were divided into two seasons: Spring (April to mid-June) and Summer/Fall (mid-June through November). All of the unit hydrograph techniques were more accurate in the summer and fall than they were in the spring.

With the exception of the average Snyder technique, the error in the peak flow rate predictions for the summer storms were approximately half that of the spring storms (Table 5.18). In addition, the LMARE statistic indicated that the error in the peak flow rate prediction was much larger for the spring storms than it was for the summer and fall events. According to both the MARE and LMARE statistics, the average Snyder method did the best job of predicting the peak flow rate for the spring events. The calibrated Snyder technique had the lowest MARE statistic for the summer and fall storms, however each of the techniques were similar. The LMARE statistic indicated that the Clark method, followed closely by the SDUH method did the best job of predicting the peak flow rate. The seasonal effects were more significant than the effects of the different techniques.

The differences in the time to peak prediction are not as dramatic as they were for the peak flow rate prediction (Table 5.19). The SCS, Clark, and SDUH models predicted the time to peak slightly better in the summer than in the spring; the two Snyder methods predicted the time to peak better for the spring storms than for the summer and fall events.

The average model efficiency was also compared between the seasons. In general, the average model efficiencies were significantly better for the summer and fall storms than they were for the spring storms (Table 5.20). The SCS method showed the largest seasonal difference. Both Snyder techniques showed little difference between the seasons. The average Snyder method had the highest model efficiency for the spring storms, while the SDUH technique had the highest model efficiency for the summer and fall events. Because the model efficiencies for storm #4 were so low, that storm was

Table 5.18. Seasonal effects on the prediction of peak flow rate.

	Spring (n = 15)		Summer/Fall (n = 25)	
	MARE	LMARE	MARE	LMARE
SCS	0.530	-0.481	0.212	-0.891
average Snyder	0.346	-0.596	0.321	-0.553
calibrated Snyder	0.404	-0.527	0.199	-0.810
Clark	0.512	-0.494	0.205	-0.955
SDUH	0.428	-0.579	0.206	-0.949

Table 5.19. Seasonal effects on time to peak prediction (MARE).

	Spring (n = 15)	Summer/Fall (n = 25)
SCS	0.219	0.209
average Snyder	0.166	0.321
calibrated Snyder	0.491	0.653
Clark	0.246	0.220
SDUH	0.372	0.330

Table 5.20. Seasonal effects on average model efficiency.

	Spring (n = 15)		Summer/Fall (n = 25)
	w/ Storm #4	w/o Storm #4	
SCS	0.169	0.405	0.775
average Snyder	0.735	0.801	0.740
calibrated Snyder	0.658	0.770	0.843
Clark	0.288	0.506	0.820
SDUH	0.451	0.651	0.880

removed from the analysis and the remaining model efficiencies were averaged again. Once storm #4 was removed, each of the average model efficiencies improved; the SCS, Clark and SDUH methods improved the most. Without storm #4, the average model efficiencies were still higher for the summer and fall events than they were for the spring storms.

Based on the relative error in the peak flow rate, the time to peak and the average model efficiencies, there is a difference in how well each unit hydrograph model performs based on the season. One possible explanation is based on the phi-index line that was used to separate the rainfall into losses and rainfall excess. Novotny and Olem (1994) report that depression storage in agricultural watersheds is highest in the spring months. Because the phi-index line does not account for initial losses, there may be substantial errors when it is applied to agricultural watersheds, especially in the spring. There is most likely the largest difference between predicted and observed rainfall excess during this time.

5.1.8 Summary

The SDUH model does a good job of predicting the peak flow rate and shape of the observed hydrograph. Among the five techniques investigated, it had the lowest relative error in the peak flow rate for 12 of the 40 storms, and overall, had the lowest LMARE value and one of the lowest MARE values. The SDUH model generally had high model efficiencies for each storm, with an R^2 value of at least 0.90 for 21 storms. It also had one of the smallest values for the bias, TSAR, and TSSR statistics.

The two Snyder methods did not predict the observed hydrographs very well. Based on a visual evaluation, they frequently showed too much attenuation. Both had relatively high LMARE statistics for the peak flow rate predictions, indicating that neither predicted the peak flow rate very accurately. In general, both Snyder methods tended to underpredict the peak flow rates, especially for the larger storms (Figure 5.4). The calibrated Snyder method had the highest average relative error (MARE) among the five unit hydrograph techniques; it was almost double the averages for the other methods.

The average and calibrated Snyder methods also had the lowest R^2 values for 22 of the 40 storms, and they had the highest values for the bias, TSAR, and TSSR statistics, indicating that they did not predict the hydrograph shape very well.

There was a substantial difference in each of the techniques predictive capabilities based on the season. The average Snyder method was clearly the most accurate model for the spring storms. It had the lowest error in the peak flow rate and the time to peak. The average Snyder method also had the largest model efficiency for the spring storms. The calibrated Snyder, Clark and SDUH techniques all perform well for the summer and fall storm events.

Each of the unit hydrograph techniques perform equally well in comparing small versus large storm events.

5.2 Multiple Watershed Comparison

In order to evaluate the accuracy of the SDUH model at different spatial scales, it was applied to subwatersheds C and D in Owl Run (Figure 4.3). The two subwatersheds are described in section 4.1. The resulting predictions are compared based on the relative error in the peak flow rate, relative error for the time to peak, and model efficiency. The shape statistics such as bias, SSR, and SAR were not used because they are dimensional and dependent on the number of hydrograph ordinates.

Because the two subwatersheds are smaller and have shorter times of concentration than the entire watershed, a 10-minute time step was used to develop the hydrographs for each of the subwatersheds. In addition, storm #13 and storm #23 were omitted from the analysis of subwatershed C because there were errors in the observed hydrographs at that station for each of those storm events.

5.2.1 Visual Comparison

In order to get an overall "feel" for how well the SDUH model performed on watersheds of various sizes, the hydrographs from the whole watershed, subwatershed C,

and subwatershed D were visually compared with the observed hydrographs at each of those gauge sites. The same three example storms are used in this discussion as are in the discussion of the five synthetic unit hydrograph techniques. These storms were chosen because they represent a range of seasons and storm sizes. Hydrographs for all 40 storm events may be found in Appendix D.

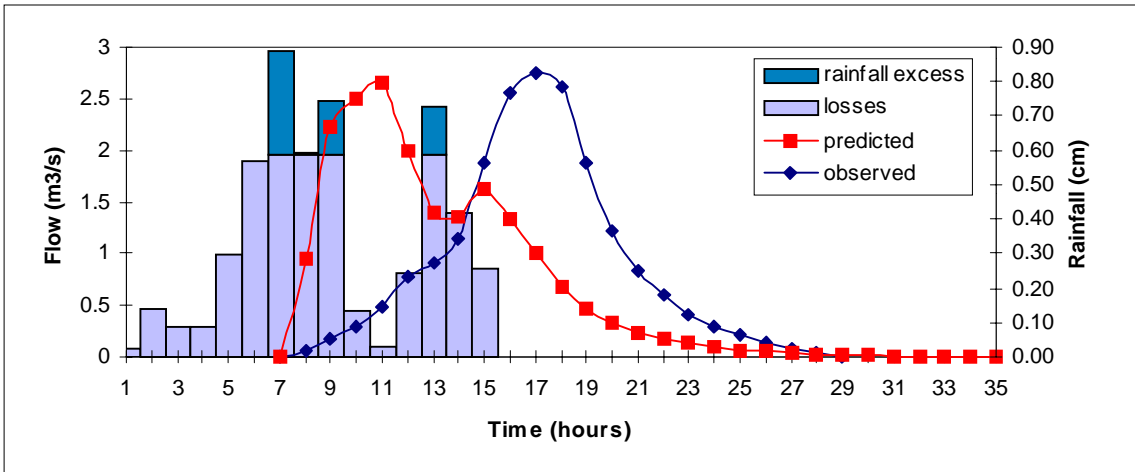
In general, the SDUH model tends to overpredict the peak flow rate and underpredict the time to peak. While the hydrographs for subwatershed D and the entire watershed tend to have the same shape, the hydrograph at the outlet of subwatershed C does not always follow the shape of the other two hydrographs.

Storm #11, November 9-10, 1990:

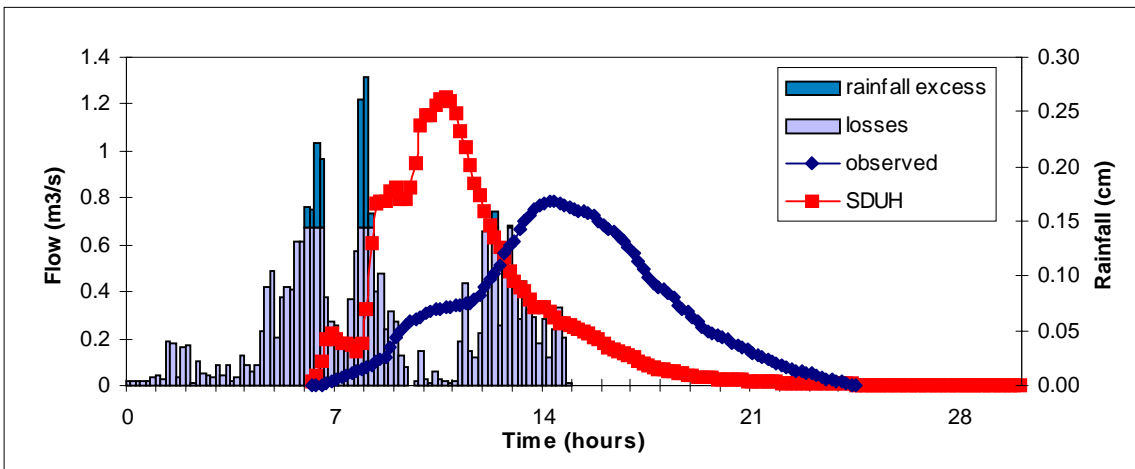
Each subwatershed and the entire watershed show a similar hydrograph shape. They each have “knee” in the rising limb of the observed hydrograph (Figure 5.5). It is most pronounced in subwatershed D, where the hydrograph starts to take on the characteristics of two separate runoff events. The “knee” is the least prominent in the response from the whole watershed. There is only a slight inflection in the rising limb of the hydrograph for the entire watershed.

In subwatershed C, the observed hydrograph showed much more attenuation than the prediction. Both the observed and predicted hydrographs start to rise at the same time, however, predicted hydrograph rises much faster than the observed hydrograph. In addition, the predicted hydrograph peaks much earlier than the observed hydrograph.

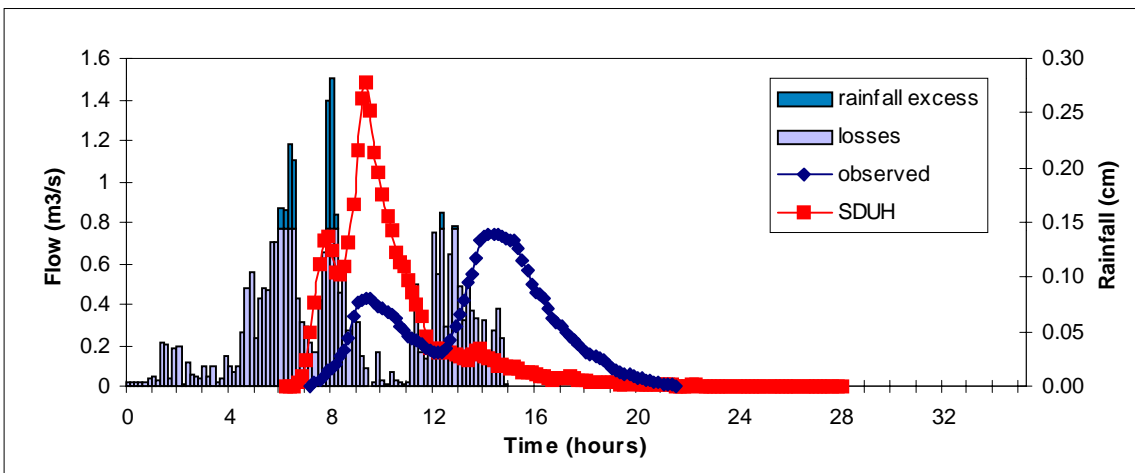
In subwatershed D, there is a poor fit between the predicted and observed values. The time to peak for the predicted hydrograph corresponds well with the peak in the first phase of the observed hydrograph. The simulated peak flow rate is significantly higher than the observed peak flow rate. The simulated hydrograph only has one real peak,



(a) Owl Run watershed



(b) subwatershed C



(c) subwatershed D

Figure 5.5. Observed and predicted hydrographs for storm #11 (Nov. 9-10, 1990).

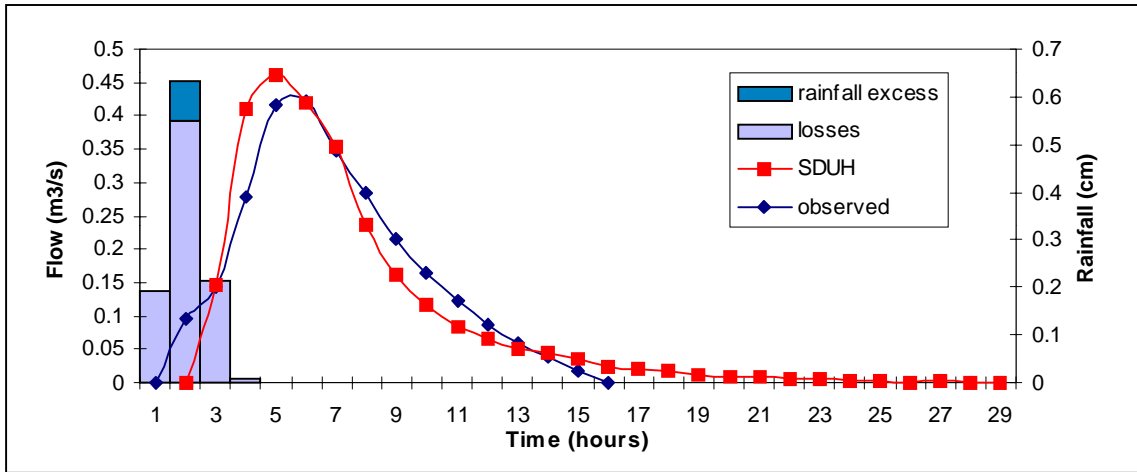
unlike the observed hydrograph that shows two separate peaks. The observed hydrograph resembles a bimodal distribution.

The predicted hydrograph for the whole watershed fits the observed data fairly well. Both of the hydrographs have similar amounts of attenuation. Although they have similar peak flow rates, the simulated hydrograph predicts that the peak will occur 6 hours before the observed peak flow rate. While the hydrograph shapes are similar, they are not identical. The simulated hydrograph has a short rising limb and a long falling limb, while the observed hydrograph has a long rising limb and a short falling limb.

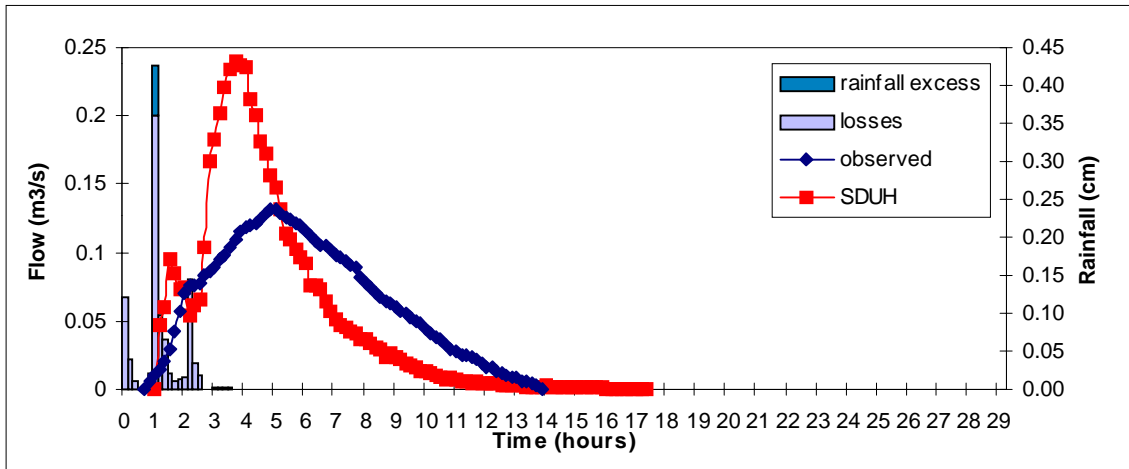
Storm #21: May 8, 1992

For storm #21 (Figure 5.6), the SDUH model predicts the observed hydrograph shape more accurately for the entire watershed than it does for either subwatershed. In subwatershed C, the observed hydrograph showed much more attenuation than the predicted hydrograph. The predicted hydrograph was also shifted so that it forecasted a slightly earlier peak flow rate than was observed.

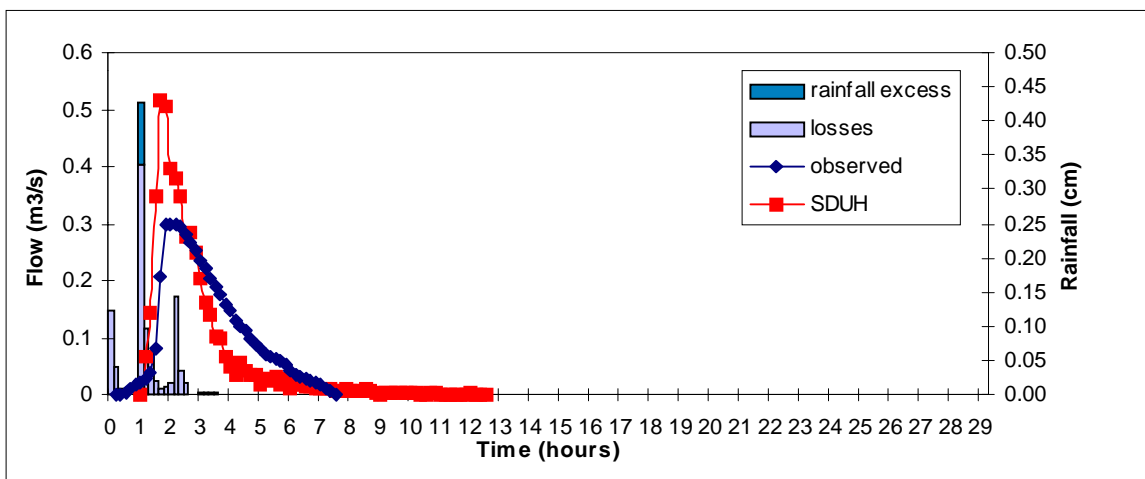
For subwatershed D, the observed hydrograph had a quick rising limb and a longer falling limb. It also showed much more attenuation than the predicted hydrograph. Although the predicted peak flow rate was much higher than the observed value, there was generally good agreement between the observed and predicted hydrographs. The observed hydrograph falls off much more slowly than the predicted hydrograph, however the predicted hydrograph had a longer falling limb.



(a) Owl Run watershed



(b) subwatershed C



(c) subwatershed D

Figure 5.6. Observed and predicted hydrographs for storm #21 (May 8, 1992).

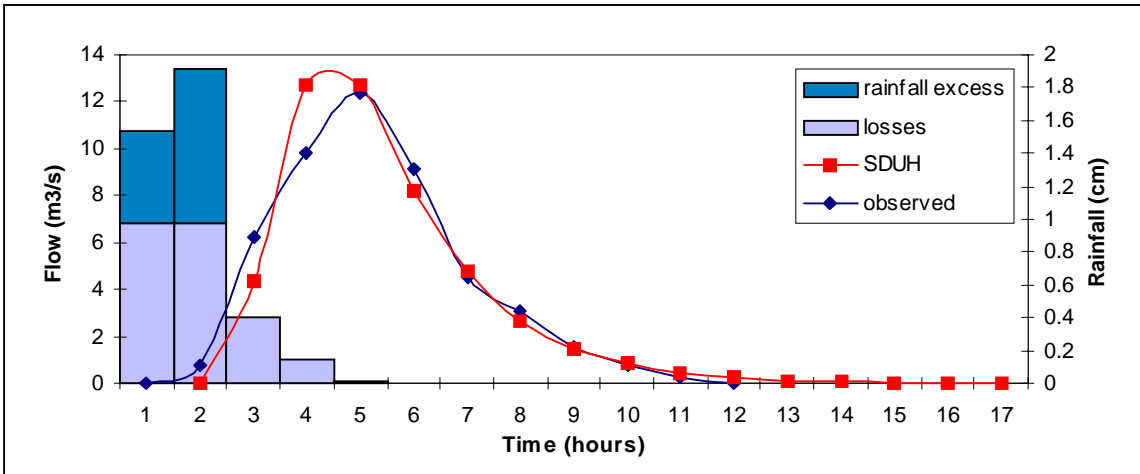
For the entire watershed, there was a fairly good agreement between the observed and predicted hydrographs. They both had similar peak flow rates and times to peak. The observed and predicted hydrographs show similar amounts of attenuation and have similar shapes.

Storm #26: July 27, 1992

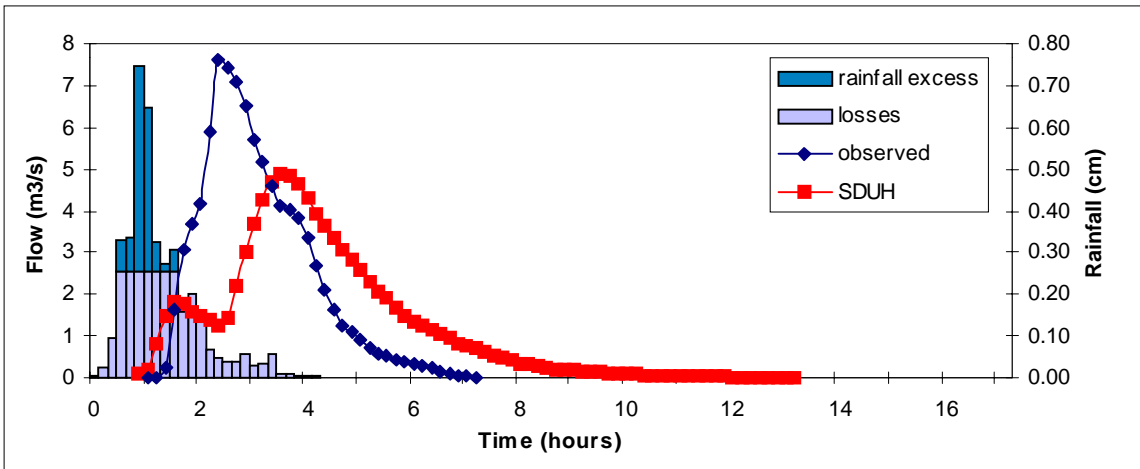
For storm #26, the predicted hydrograph for the entire watershed matched the observed hydrograph much more closely than for any of the subwatersheds (Figure 5.7). The predicted hydrograph for subwatershed C showed more attenuation than the observed hydrograph. Both start at approximately the same time. The observed hydrograph was a smooth curve, while the predicted hydrograph shows a pronounced “knee” after 1 hour. The predicted hydrograph has a much longer falling limb than the observed hydrograph.

For subwatershed D, the observed hydrograph showed more attenuation than the predicted hydrograph. Both hydrographs rise at the same rate for the first hour, then the observed hydrographs stops rising as quickly. The observed hydrograph has a much shorter falling limb than the predicted hydrograph.

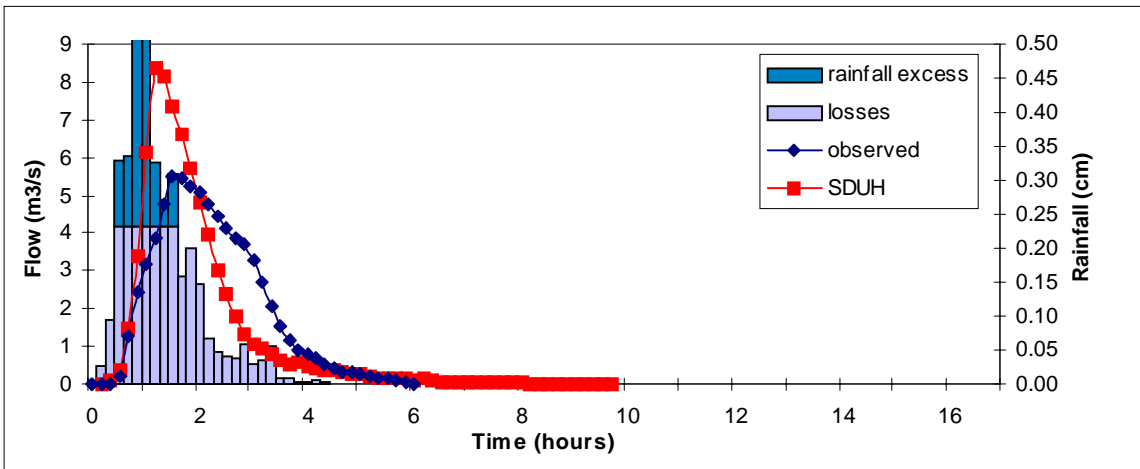
The observed and predicted hydrographs from the entire watershed have similar shapes, peak flow rates and times to peak. The observed hydrograph rises slightly faster than the prediction; however, they both have similar falling limbs.



(a) Owl Run watershed



(b) subwatershed C



(c) subwatershed D

Figure 5.7. Observed and predicted hydrographs for storm #26 (July 27, 1992).

5.2.2 Peak Flow Rate

The observed and predicted peak flow rates for each of the subwatersheds and the entire watershed are summarized in Table 5.21. The SDUH model did a better job of predicting the peak flow rate for the whole watershed than for the subwatersheds. The MARE for subwatershed C is more than twice the MARE for the entire watershed (Table 5.22). The LMARE values also indicate that the SDUH method works best on the entire watershed area. The SDUH model results in a relative error less than 10% for 11 events for the whole watershed, but there are only 3 events for each subwatershed that meet this cutoff.

Scatterplots of the peak flow rates for the entire watershed and the two subwatersheds are in Figures 5.8 - 5.10. In Figure 5.10, subwatershed D shows good scatter around the line. On subwatershed D, the SDUH model overpredicts and underpredicts the peak flow rate equally. For the whole watershed and subwatershed C, the SDUH model tends to underpredict the peak flow rate for the larger storms. This may be due to the effects of the largest pond that is along the main channel in subwatershed C. The pond is a complex watershed feature that does not behave linearly. The pond outflow is based not only on the inflow, but also on the storage available within the pond. The Muskingum method used to route the runoff hydrograph through the pond may not be sensitive to the changes in the hydrologic response to different sizes of runoff events. There seems to be too much attenuation in the largest runoff events. The hydraulic residence time (Muskingum K value) may change based on the size of the runoff event. If there is more runoff, the average residence time may be shorter than it is during small runoff events.

Table 5.21. Predicted and observed peak flow rates (m³/s).

Storm	subwatershed C		subwatershed D		whole watershed	
	obs.	pred.	obs.	pred.	obs.	pred.
1	0.140	0.214	0.278	0.340	0.496	0.515
2	0.838	1.201	1.045	0.867	3.132	3.794
3	0.287	0.438	0.365	0.501	1.342	2.118
4	0.229	0.731	0.442	0.566	0.597	1.642
5	1.029	0.566	1.979	3.129	4.250	6.796
6	0.104	0.460	0.275	0.719	0.442	0.858
7	4.297	2.880	3.760	2.699	11.018	8.475
8	0.432	0.606	2.135	2.373	1.220	1.206
9	0.307	0.827	0.671	0.411	0.578	0.609
10	0.521	0.691	0.521	0.439	1.472	1.894
11	0.789	1.227	0.742	1.484	2.747	2.656
12	1.041	0.247	2.585	1.713	1.708	0.864
13	<i>omitted</i>	<i>omitted</i>	0.765	0.960	3.019	4.335
14	7.197	3.006	5.949	3.381	12.947	9.231
15	0.281	0.037	2.047	1.540	2.566	2.234
16	0.291	0.158	1.631	2.260	2.206	2.469
17	0.125	0.128	1.028	1.385	1.931	2.520
18	0.118	0.175	0.801	1.059	1.920	1.855
19	0.184	0.312	0.433	0.966	1.119	1.127
20	3.854	3.339	3.489	4.327	8.996	8.158
21	0.132	0.240	0.300	0.515	0.422	0.462
22	0.142	0.206	0.371	0.462	0.462	0.583
23	<i>omitted</i>	<i>omitted</i>	1.702	1.294	0.988	1.589
24	0.139	0.195	0.660	0.651	0.762	0.750
25	0.407	0.711	0.776	0.835	1.659	1.589
26	7.601	4.902	5.527	8.385	12.349	12.734
27	2.270	0.597	1.741	1.127	3.067	2.752
28	0.213	0.251	0.555	0.682	0.535	0.430
29	0.105	0.133	0.507	0.844	0.462	0.340
30	0.108	0.155	0.450	0.430	0.382	0.430
31	0.268	0.391	0.762	1.688	1.597	2.631
32	0.258	0.601	0.365	1.036	0.830	1.042
33	0.477	0.838	1.127	2.016	1.903	0.634
34	7.161	5.390	6.133	7.691	13.199	11.035
35	0.273	0.576	0.447	0.668	0.920	0.634
36	1.495	1.419	1.487	1.127	6.626	3.928
37	13.293	11.793	11.678	15.906	32.256	29.464
38	9.606	10.077	5.474	8.147	13.776	23.248
39	0.117	0.299	0.360	0.292	0.351	0.331
40	14.525	9.362	10.067	8.379	35.175	30.577

Table 5.22. Percent error in peak flow rate for subwatersheds C and D and the whole watershed.

<i>Storm</i>	<i>subwatershed C</i>	<i>subwatershed D</i>	<i>whole watershed</i>
1	-0.522	-0.224	-0.040
2	-0.432	0.171	-0.212
3	-0.530	-0.372	-0.578
4	-2.185	-0.282	-1.749
5	0.450	-0.581	-0.599
6	-3.443	-1.619	-0.942
7	0.330	0.282	0.231
8	-0.404	-0.111	0.012
9	-1.698	0.388	-0.054
10	-0.326	0.158	-0.287
11	-0.555	-1.000	0.033
12	0.762	0.337	0.494
13	<i>omitted</i>	-0.256	-0.436
14	0.582	0.432	0.287
15	0.869	0.248	0.129
16	0.455	-0.385	-0.119
17	-0.023	-0.347	-0.305
18	-0.486	-0.322	0.034
19	-0.691	-1.229	-0.008
20	0.133	-0.240	0.093
21	-0.826	-0.717	-0.094
22	-0.454	-0.244	-0.264
23	<i>omitted</i>	0.240	-0.607
24	-0.401	0.013	0.015
25	-0.746	-0.077	0.043
26	0.355	-0.517	-0.031
27	0.737	0.353	0.102
28	-0.178	-0.230	0.196
29	-0.270	-0.665	0.264
30	-0.445	0.044	-0.126
31	-0.458	-1.216	-0.647
32	-1.327	-1.837	-0.256
33	-0.756	-0.789	0.667
34	0.247	-0.254	0.164
35	-1.113	-0.494	0.311
36	0.051	0.242	0.407
37	0.113	-0.362	0.087
38	-0.049	-0.488	-0.688
39	-1.553	0.189	0.056
40	0.355	0.168	0.131
MARE:	0.666	0.453	0.295
LMARE:	-0.354	-0.497	-0.801

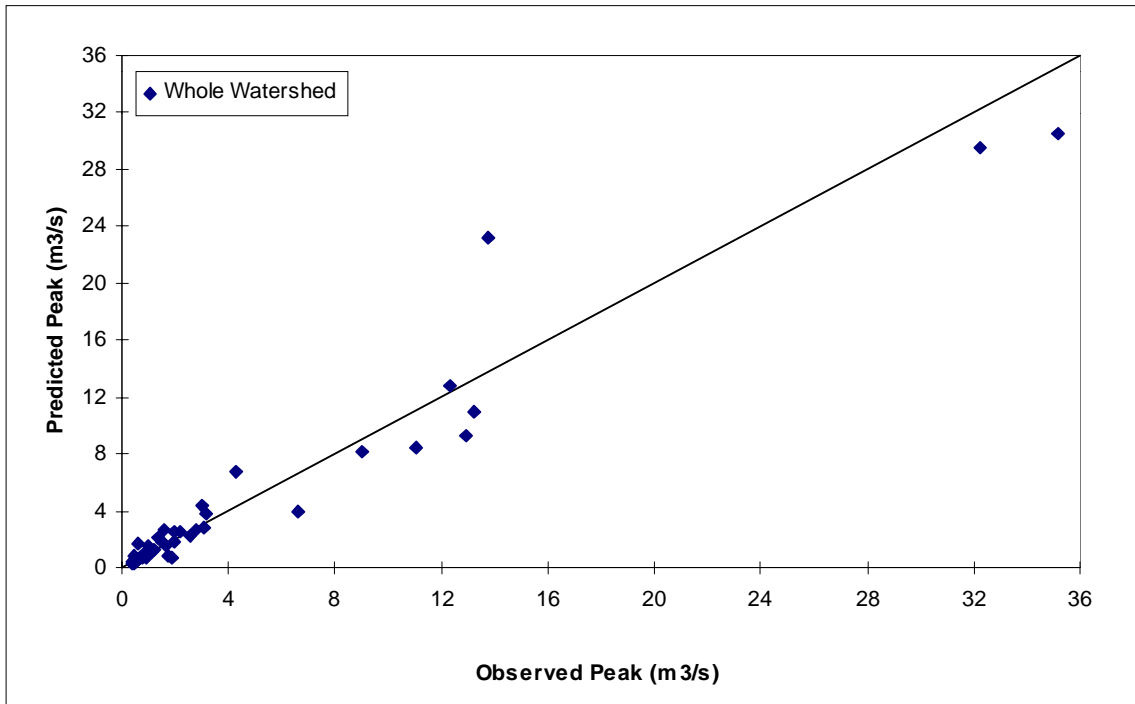


Figure 5.8. Predicted vs. observed peak flow rates, entire Owl Run watershed.

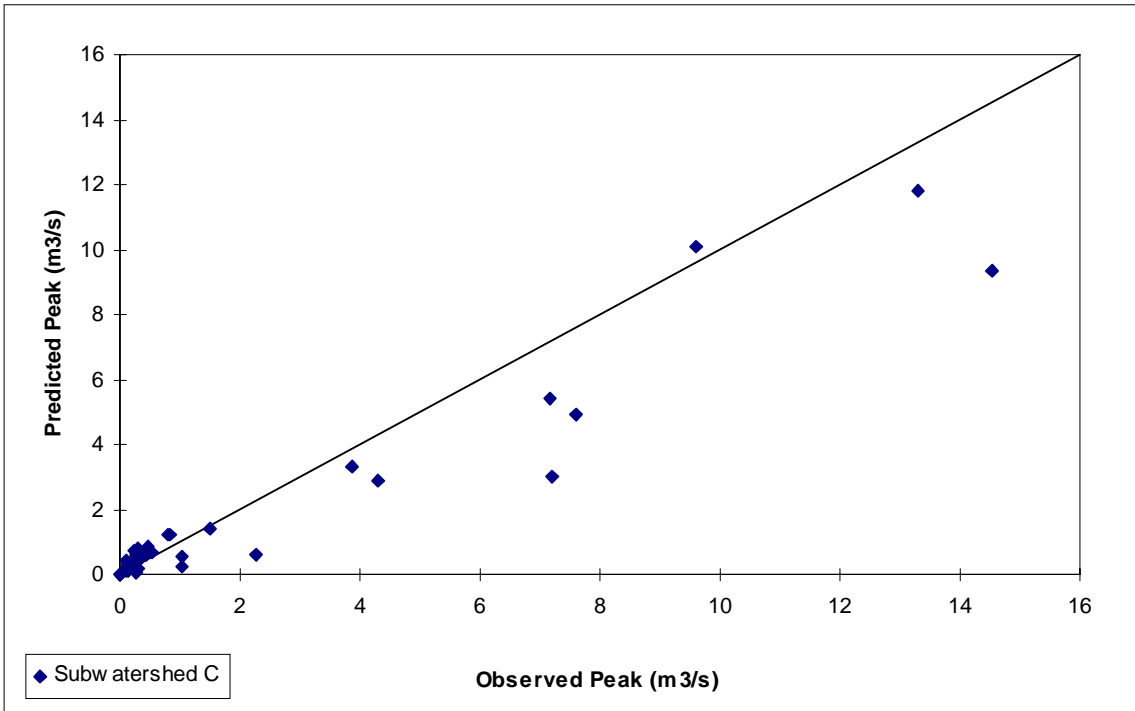


Figure 5.9. Observed vs. predicted peak flow rates for subwatershed C.

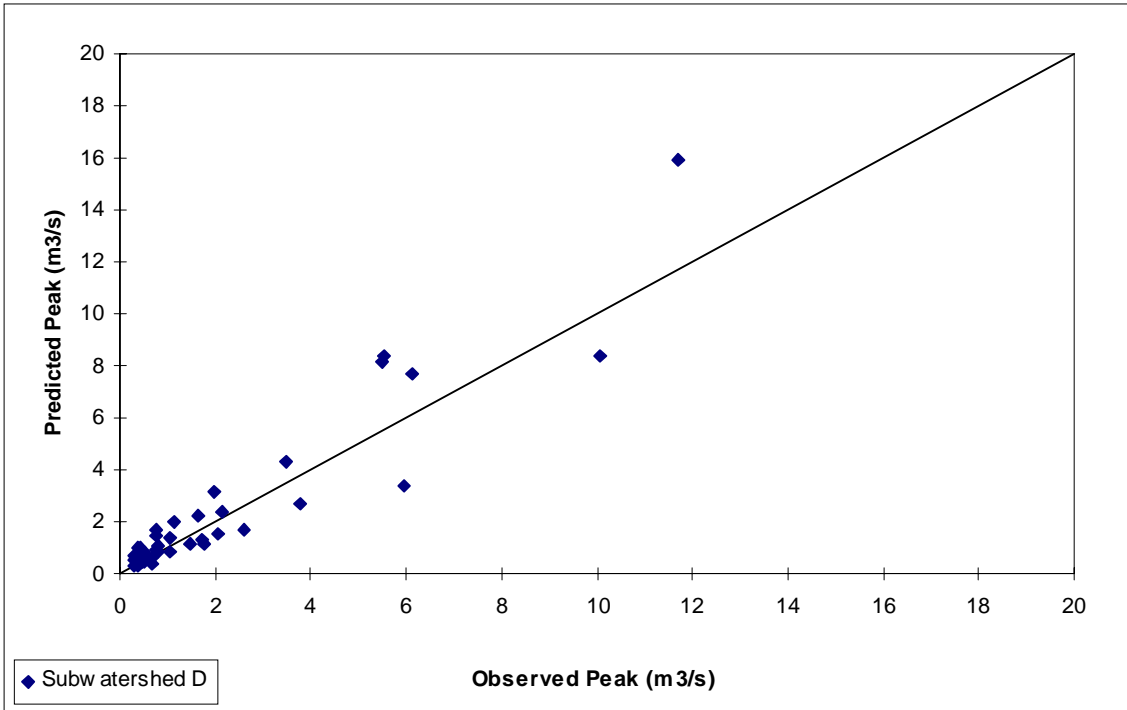


Figure 5.10. Observed vs. predicted peak flow rates for subwatershed D.

5.2.3 Time to Peak

The observed and predicted times to peak flow rate are summarized in Table 5.23. The whole watershed was modeled with a 1-hour time step, while the subwatersheds were modeled with a 10-minute time step. The SDUH model predicted the time to peak flow rate equally well for the entire watershed and subwatershed D (Table 5.24). They each had a MARE value of approximately 0.34. The time to peak prediction for subwatershed C was not as good as the predictions for the entire watershed and subwatershed D. The MARE value for subwatershed C was 0.52. One possible explanation for the differences in the time to peak prediction between subwatershed C and the other watersheds is the existence of the large pond in the middle of subwatershed C.

The SDUH model tended to underpredict the time to peak flow rate for both subwatershed D and the entire watershed. For subwatershed C, the model overpredicted and underpredicted the time to peak flow rate equally.

Table 5.23. Time to Peak (hours).

Storm	Whole Watershed		Subwatershed C		Subwatershed D	
	obs.	pred.	obs.	pred.	obs.	pred.
1	5	3	3.5	3.67	1.67	1.33
2	4	2	2.83	2.67	1.17	1.33
3	6	3	5.67	4.17	5.00	2.67
4	4	2	5.33	4.17	2.17	1.17
5	4	3	2.5	3	2	1.33
6	5	2	4.5	3.5	2	1.33
7	17	15	25.17	16.66	24.67	24.5
8	3	2	3.5	3.83	1.67	0.5
9	4	3	2.83	0.83	1.17	1.5
10	12	6	11.83	7.83	7.33	6.17
11	10	4	8.33	4.67	8.33	3.33
12	3	2	1.17	3.5	2.33	1.83
13	6	2	<i>omitted</i>	<i>omitted</i>	4.67	1.17
14	8	6	5.83	7	7.17	6
15	3	2	0.33	2.33	5.33	4
16	5	2	3.33	2.83	3.17	0.67
17	2	2	2.5	3	1.83	4
18	2	2	3.33	1.67	1.33	1.17
19	3	2	5	6.5	2.67	1.83
20	14	13	12.33	14	12.5	12.67
21	5	4	4.17	3	1.83	1.5
22	5	3	7.17	5.17	3	2.5
23	3	4	<i>omitted</i>	<i>omitted</i>	0.83	0.67
24	4	3	3.67	3	2.33	0.83
25	3	2	2.83	2.5	1	0.67
26	4	3	1.67	2.83	1.67	1
27	4	3	1	2.5	1	0.67
28	3	3	1.67	3	1.33	1
29	7	3	6.33	2.67	5.67	0.67
30	6	3	6.33	5.33	3	2.83
31	5	2	3.33	3.33	1.17	0.83
32	6	3	4.67	2.83	2.83	1.33
33	8	7	5.67	6.17	7	5.67
34	4	5	2.33	3.83	2.33	2.17
35	4	4	4.67	5	2	1.5
36	13	3	2	4.33	4.33	3.17
37	4	3	3	4.67	2.67	3.17
38	3	1	3.17	3.5	2.33	2
39	5	3	5.83	3.17	2.33	0.83
40	11	10	11.33	12.17	9.17	10.83

Table 5.24. Relative error and MARE for time to peak predictions; Owl Run and subwatersheds C and D.

Storm	Owl Run	Subwatershed C	Subwatershed D
1	0.400	-0.048	0.200
2	0.500	0.059	-0.143
3	0.500	0.265	0.467
4	0.500	0.219	0.462
5	0.250	-0.200	0.333
6	0.600	0.222	0.333
7	0.118	0.620	0.007
8	0.333	-0.095	0.700
9	0.250	0.706	-0.286
10	0.500	0.338	0.159
11	0.600	0.440	0.600
12	0.333	-2.000	0.214
13	0.667	<i>omitted</i>	0.750
14	0.250	-0.200	0.163
15	0.333	-6.000	0.250
16	0.600	0.150	0.789
17	0.000	-0.200	-1.182
18	0.000	0.500	0.125
19	0.333	-0.300	0.313
20	0.071	-0.135	-0.013
21	0.200	0.280	0.182
22	0.400	0.279	0.167
23	-0.333	<i>omitted</i>	0.200
24	0.250	0.182	0.643
25	0.333	0.118	0.333
26	0.250	-0.700	0.400
27	0.250	-1.500	0.333
28	0.000	-0.800	0.250
29	0.571	0.579	0.882
30	0.500	0.158	0.056
31	0.600	0.000	0.286
32	0.500	0.393	0.529
33	0.125	-0.088	0.190
34	-0.250	-0.643	0.071
35	0.000	-0.071	0.250
36	0.769	-1.167	0.269
37	0.250	-0.556	-0.188
38	0.667	-0.105	0.143
39	0.400	0.457	0.643
40	0.091	-0.074	-0.182
MARE:	0.347	0.521	0.342

5.2.4 Model Efficiency

The model efficiencies were compared for the entire Owl Run watershed and the subwatersheds C and D. The model efficiency for each storm is summarized in Table 5.25. The model efficiencies for subwatershed C are significantly lower than the model efficiencies for the entire watershed and subwatershed D. The average model efficiencies for the whole watershed and subwatershed D are close (0.708 and 0.711, respectively), however the average model efficiency for subwatershed C was only 0.069. This value was affected by the extremely poor prediction for storm #6 (subwatershed C $R^2 = -11.817$). Without this event the average model efficiency for subwatershed C rises to 0.390, which is still substantially lower than the other averages. For the entire watershed and subwatershed D, over half of the events have a model efficiency of at least 0.85, while only 10 events for subwatershed C have a model efficiency that is that high. Subwatershed C also has 8 events with a model efficiency of less than zero, while the whole watershed and subwatershed D have 2 and 3 events, respectively, that are less than zero. The median R^2 values were also calculated. The whole watershed has a substantially higher median R^2 value than the two subwatersheds.

Table 5.25. Model efficiencies for Owl Run and subwatersheds C and D.

Storm	Owl Run	subwatershed C	subwatershed D
1	0.942	0.862	0.981
2	0.909	0.798	0.906
3	0.693	-0.178	-0.496
4	-2.547	-1.762	0.912
5	0.407	0.289	0.810
6	-0.959	-11.817	-0.529
7	0.808	0.836	0.881
8	0.984	0.730	0.915
9	0.948	-3.441	0.871
10	0.896	0.829	0.795
11	0.831	0.755	0.505
12	0.873	0.833	0.935
13	0.520	<i>omitted</i>	0.884
14	0.776	0.751	0.742
15	0.949	0.885	0.854
16	0.886	0.836	0.816
17	0.916	0.911	0.918
18	0.922	0.524	0.928
19	0.921	-0.133	0.389
20	0.923	0.939	0.936
21	0.942	0.498	0.797
22	0.629	0.817	0.959
23	0.897	<i>omitted</i>	0.956
24	0.905	0.921	0.802
25	0.938	0.347	0.978
26	0.953	0.875	0.670
27	0.918	0.782	0.924
28	0.727	0.609	0.942
29	0.932	0.910	0.585
30	0.946	0.933	0.953
31	0.709	0.866	0.035
32	0.913	-0.344	-0.382
33	0.911	0.066	0.585
34	0.943	0.892	0.892
35	0.959	-0.054	0.910
36	0.544	0.351	0.594
37	0.875	0.809	0.690
38	0.250	0.691	0.822
39	0.966	-1.620	0.975
40	0.883	0.822	0.804
average:	0.708	0.069	0.711
median:	0.907	0.769	0.863

5.2.5 Summary

The SDUH model does a substantially better job on subwatershed D and the entire watershed than it does for subwatershed C. The error in the peak flow rate is substantially lower for the entire watershed than it is for the two subwatersheds. Subwatershed D and the entire watershed have similar errors in the time to peak prediction and similar average model efficiency values. Subwatershed C has a good deal more error in the prediction of the peak time and a lower model efficiency than either subwatershed D or the whole area.

One likely explanation for the poor predictions for subwatershed C may be the existence of the large pond along the main channel near the center of the watershed. The effects of the pond would be expected to have a much greater impact on the hydrograph from subwatershed C than it would have on the entire watershed.

The SDUH model predicts the peak flow rate for the entire watershed better than it does for the two subwatersheds; however there is very little difference in the prediction of the time to peak and the model efficiency. The model efficiency and time to peak predictions are equally accurate for subwatershed D and the entire watershed; this would indicate that scale does not have a major impact on the accuracy of the SDUH model.

5.3 Sensitivity Analysis

In order to evaluate how well the SDUH model responds to different input parameters, a series of sensitivity analyses were performed. The 'base' values that were used in this study were presented in Table 3.1.

5.3.1 Channel Flow Threshold

The effects of the channel flow threshold (CFT) on the resulting runoff hydrograph were examined. The channel flow threshold was allowed to vary from 10 cells up to 60 cells. As the CFT increased, the number of cells designated as overland flow cells increased; the cumulative travel times to the watershed outlet also increased. As the CFT increased, the runoff hydrograph showed more attenuation and a much lower peak discharge than at lower CFT values (Figure 5.11). With an increase in CFT from 10 to 60, the peak discharge rate decreased by approximately 34%. In addition, the hydrographs resulting from lower CFT values show less attenuation than the hydrographs resulting from the higher CFT values. The higher CFT hydrographs also show a less sharply defined peak discharge rate, tending to be relatively flat at the top of the hydrograph.

The CFT does have a significant impact on the predicted hydrograph. It has a significant impact on the cumulative travel time estimates. The lower CFT values result in a hydrograph shape that resembles the traditional hydrograph shape better than the higher CFT values. Because overland flow is generally restricted to distances less than 100 m and few areas will have the idealized semi-circular geometry discussed in Section 4.3, a CFT between 10 cells (0.9 ha) and 20 cells (1.8 ha) may be the most appropriate choice.

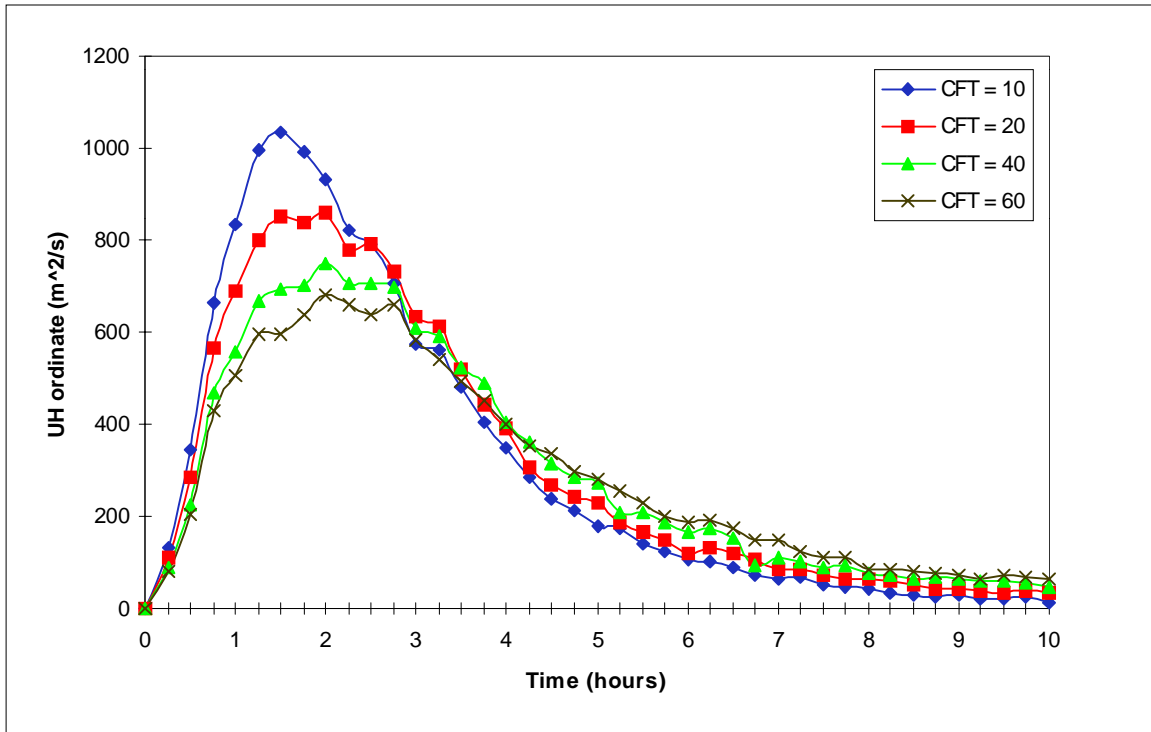


Figure 5.11. Sensitivity of model response to variations in the channel flow threshold (CFT).

5.3.2 Channel Velocity

The channel velocity estimate is an important variable in estimating the time-area curve and the resulting runoff hydrograph. The channel velocity was varied from 50% to 200% of the base channel velocities calculated in section 4.4. Despite the large changes in the channel velocities, the peak flow rate varied less than 10% (Figure 5.12). The changes in the channel velocity did have an impact on the hydrograph timing. As the channel velocity increased, the hydrograph shifted to the left and occurred earlier. This difference may be important when the unit hydrograph is convoluted with multi-period rainfall events. As the channel velocity increased, the time to the peak discharge decreased from 2.75 hours to 0.75 hours. Using the ‘base’ channel velocity estimates, the SDUH model already underpredicted the time to peak. If higher channel velocities were used, the time to peak predictions would be shorter.

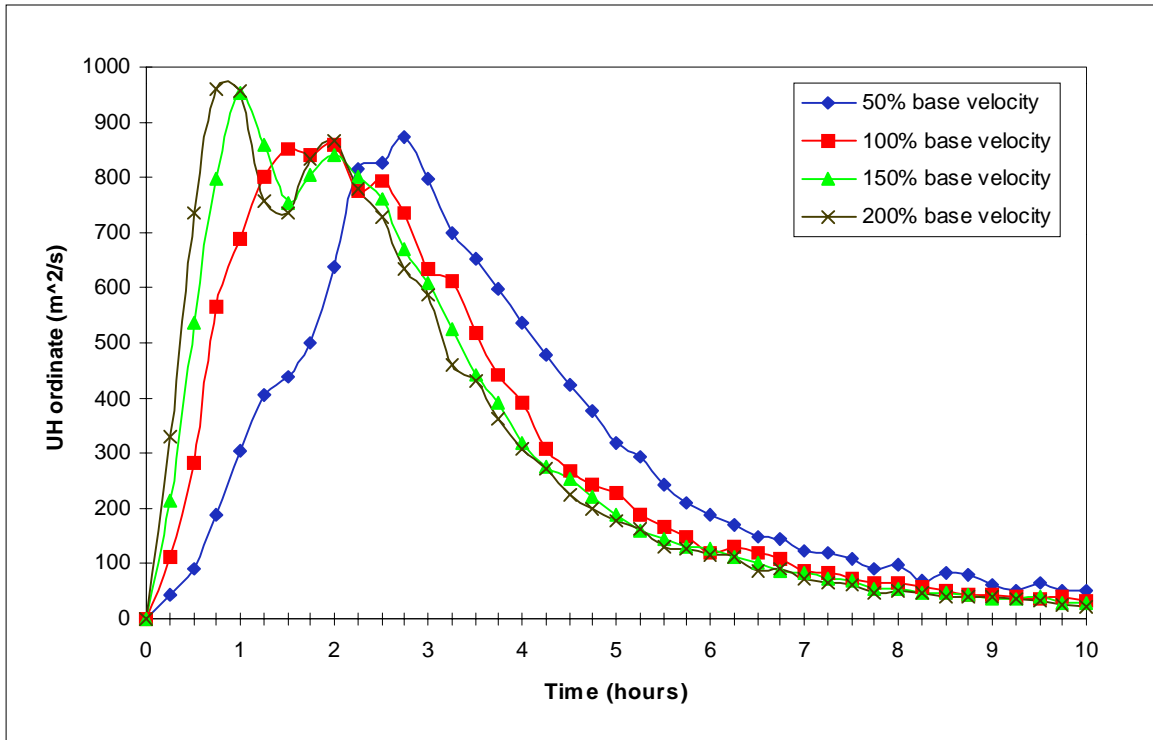


Figure 5.12. Sensitivity of model response to variations in channel velocity.

5.3.3 Overland Flow Velocity

In order to investigate the importance of the overland flow velocity, it was varied from 50% below the base value up to 200% above the original velocities. The overland flow velocity had a large impact on the hydrograph shape (Figure 5.13). As the overland velocity changed from 50% below the original value up to 200% above the original value, the peak flow rate almost tripled. There was substantially more attenuation in the 50% hydrograph than in the 200% hydrograph. In addition the 50% hydrograph had a much longer tail than the hydrographs resulting from faster overland flow velocities. While the overland flow velocity had an enormous impact on the shape of the resulting hydrographs, it had a minor impact on the time to the peak flow rate. The overland flow velocity parameter is much more important than the channel flow velocity estimate in predicting the peak flow rate; however, the channel velocity estimate has a greater impact on the time to peak estimate.

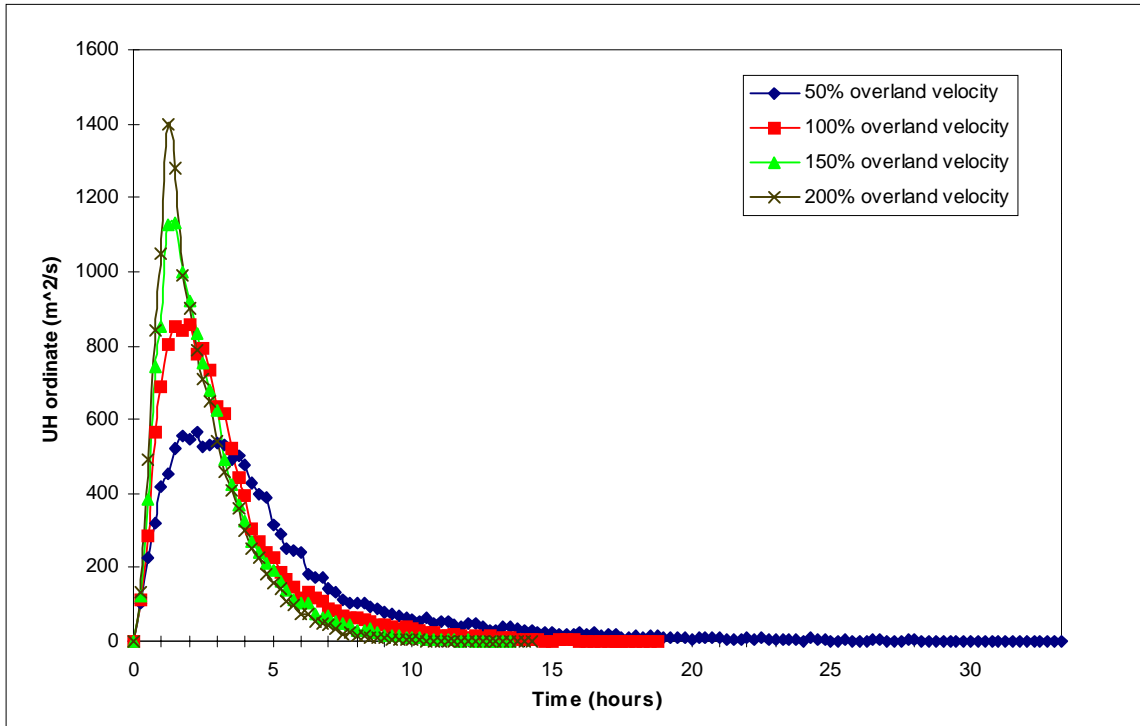


Figure 5.13. Sensitivity of model response to variations in overland flow velocity.

5.3.4 Channel Width

Because there is a good deal of uncertainty in the channel dimension estimates, model sensitivity to channel width was examined. Channel width was varied from 50% to 200% of the bottom width used in the base model formulation. The peak flow rate did not vary much over the range of channel widths (Figure 5.14). As the bottom width increased, the hydrograph shifted to the right, resulting in a slightly longer time to the peak flow rate. There was little change in the hydrograph shapes or peak flow rates as the bottom width was increased. While an increased channel width may slightly delay the resulting runoff hydrograph, there is very little impact on the peak flow rate prediction or on the overall hydrograph shape.

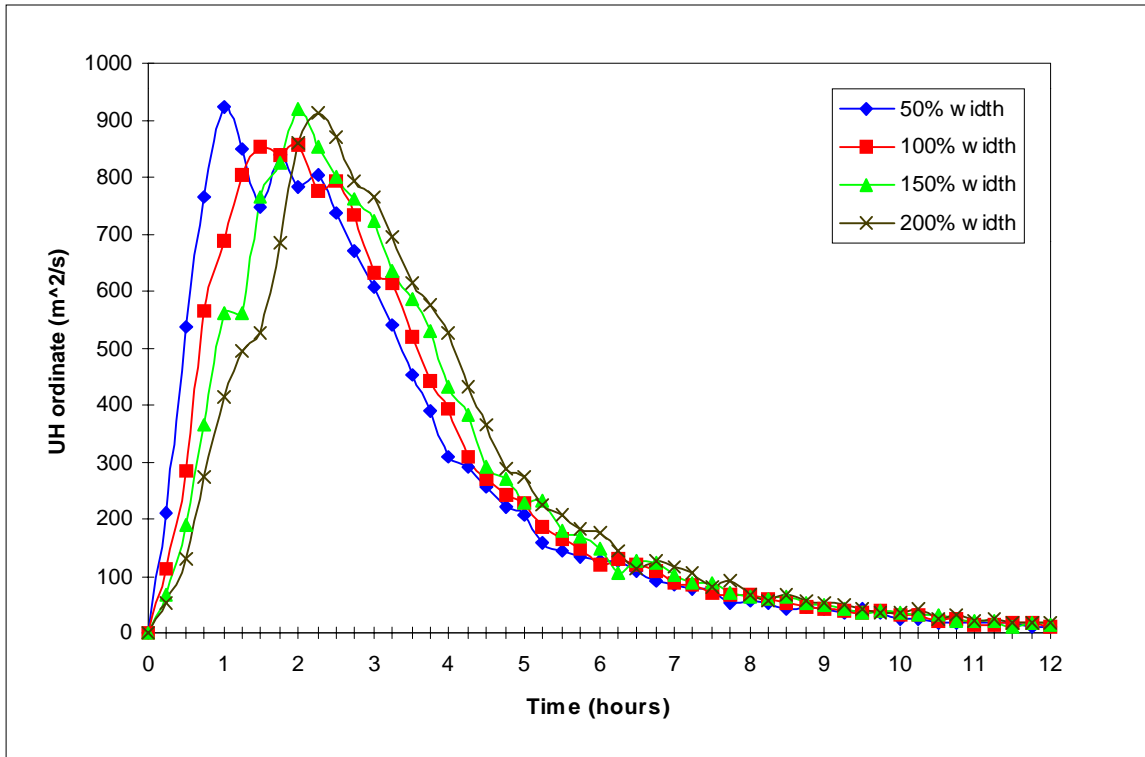


Figure 5.14. Sensitivity of model response to variations in channel bottom width.

5.3.5 Rainfall Excess Intensity

Because there is a good deal of uncertainty in the estimate of the rainfall excess intensity, the effects of different rainfall excess intensities was investigated by allowing the intensity to vary from 1.27 mm/hr (0.05 in./hr) to 5.08 mm/hr (0.20 in./hr). As the intensity of rainfall excess increased, the resulting hydrographs showed less attenuation and a higher, faster peak flow rate (Figure 5.15). As the rainfall excess intensity increased, the time to peak decreased from 2.5 hours to 1.5 hours. The peak flow rate increased by approximately 31% as the rainfall excess intensity varied from 1.27 mm/hr to 5.08 mm/hr. The rainfall excess intensity is an important parameter for estimating the peak flow rate and the time to peak. Care should be taken when selecting a technique to estimate the rainfall excess.

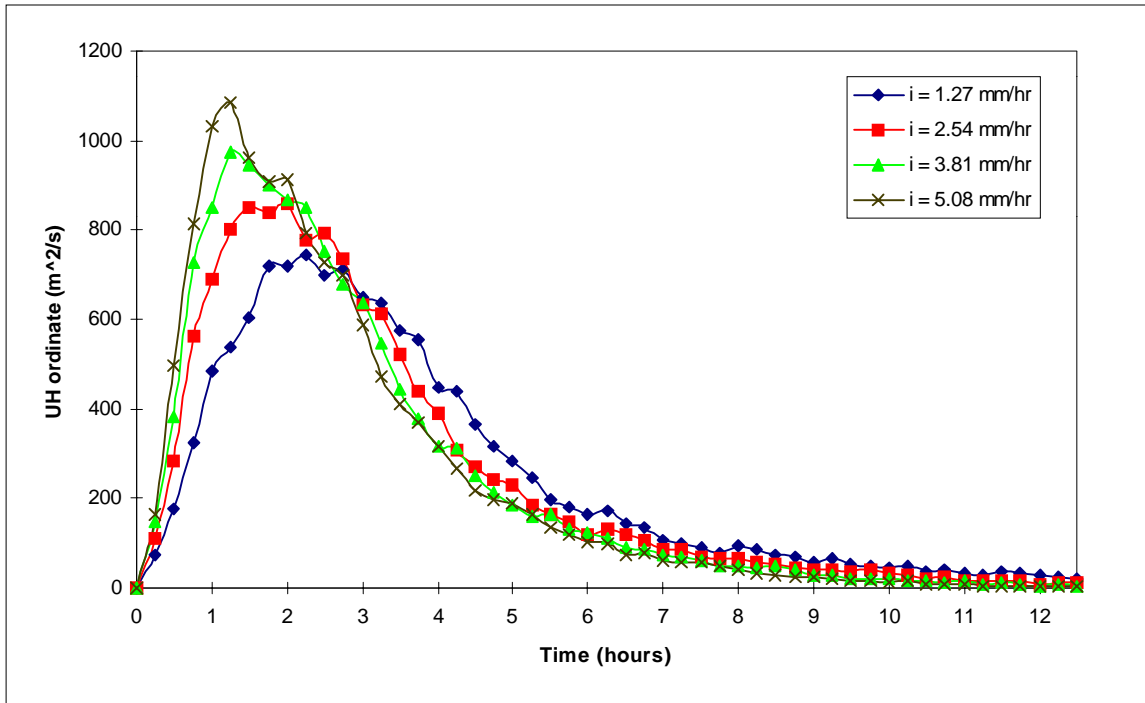


Figure 5.15. Sensitivity of model response to variations in rainfall excess intensity.

5.3.6 Hydraulic Residence Time in Ponds

To investigate the effects of the pond routing, the hydraulic residence time in the pond was varied from 30 minutes up to 2 hours. The hydrographs show no difference for the first hour of runoff (Figure 5.16), but after that point, the shorter hydraulic residence times resulted in hydrographs that had a higher peak flow rate. With a longer hydraulic residence time, the hydrograph shows more attenuation and a smaller peak flow rate. The largest differences between the hydrographs occur around the peak flow rate; the tails of each hydrograph are very similar. There is a slight time shift in the hydrographs. If a longer hydraulic residence time was assumed, the SDUH model would have underpredicted the peak flow rate more often.

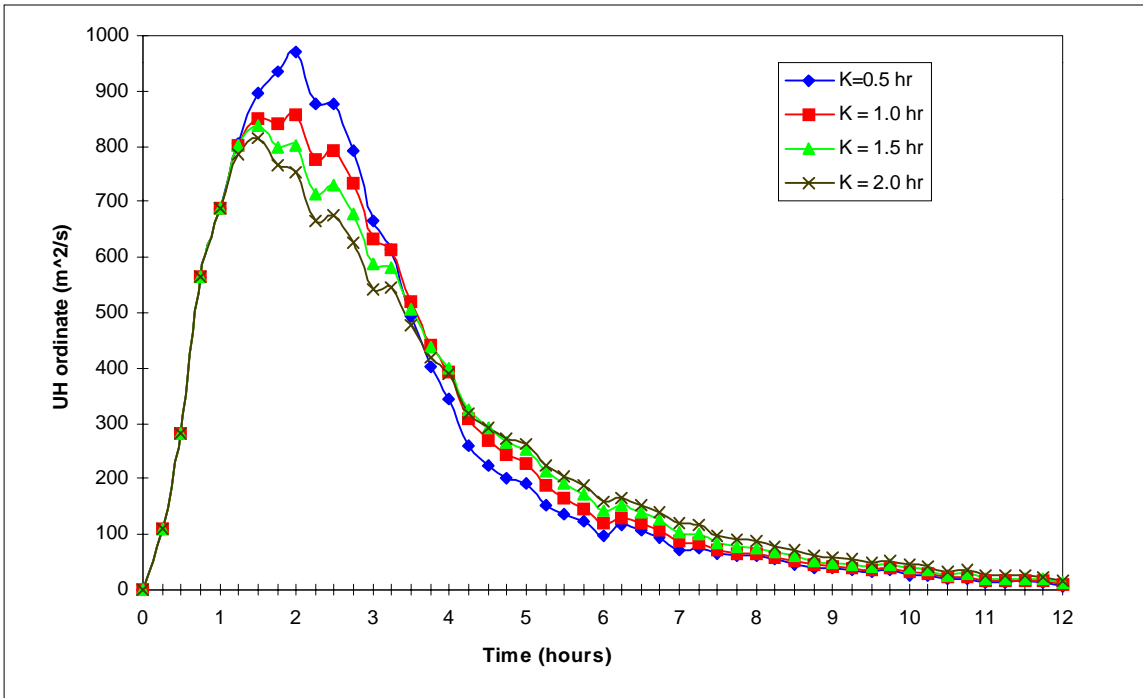


Figure 5.16. Sensitivity of model response to variations in hydraulic residence time in the pond.

5.3.7 Time Step

Because the time step used in hydrologic modeling may have a significant impact on the accuracy of the results, a sensitivity analysis was performed on the time step used in this study. The unit hydrographs resulting from 20-minute, 40-minute, and 60-minute time intervals were compared (Figure 5.17). Although the time interval tripled, there was very little change in the peak flow rate or in the hydrograph shape. The time interval does not seem to be a significant parameter in the SDUH model.

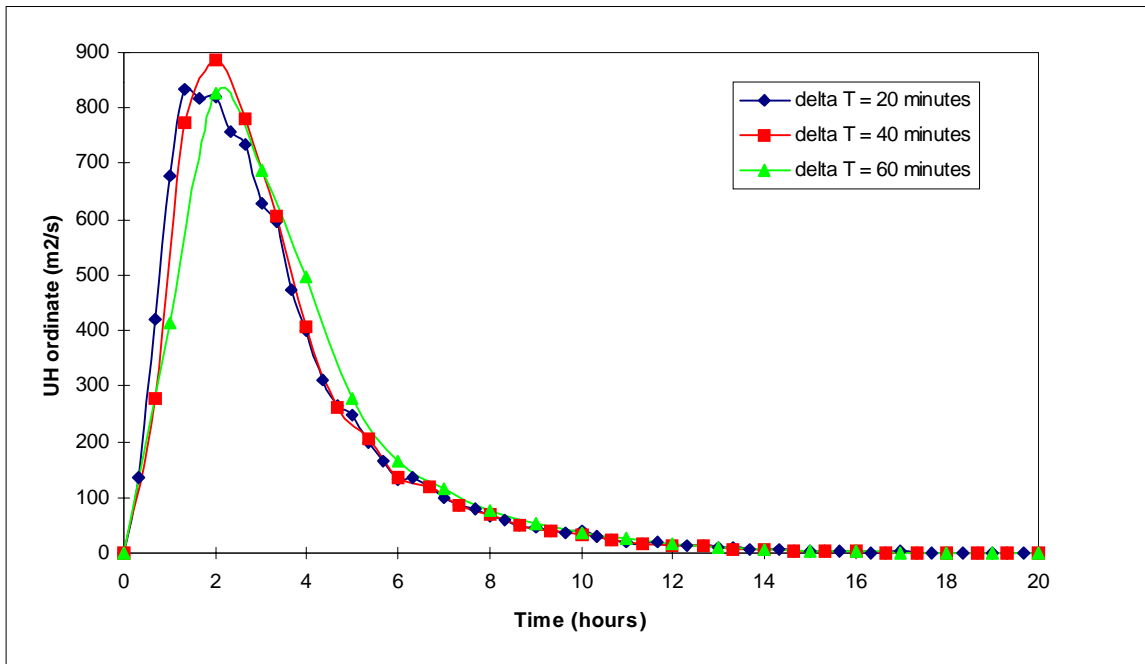


Figure 5.17. Sensitivity of model response to variations in the time interval.

5.3.8 Summary

The estimates of the channel flow threshold, the overland velocity, and the rainfall excess intensity had the biggest impact on the peak flow rate prediction. The time to peak flow rate is affected most by the channel velocity, the rainfall excess intensity, and the hydraulic residence time in the largest pond. The time interval used did not influence the peak flow rate or time to peak predictions.

The SDUH model underpredicted the time to peak for 34 of 40 storm events. Based on the results of the sensitivity analyses, the estimates of the channel dimensions and velocities may need to be refined. Because there was a good deal of uncertainty in the channel dimension estimates, a complete channel survey would improve the channel dimension estimates and may improve the time to peak predictions.

5.4 Discussion

A major source of error in this study is in the determination of rainfall excess. A phi-index method was used to identify the periods of rainfall excess in this study. The volume of runoff under the observed hydrograph was determined, then used to back solve for the best phi-index line. While this insured that the volume of runoff was correct, it did not account for the time distribution of the rainfall excess. Some of the errors in the model predictions are a result of the errors in determining the time distribution of the rainfall excess. For many of the storms with more than one period of rainfall excess (storms #7 and #14), it is apparent that the distribution of rainfall excess was in error. For both storms it seems that the volume of rainfall excess should be redistributed so that more of the rainfall is allocated to losses in the beginning of the storm, leaving more rainfall excess volume for the end of the storm (Figures 5.18 and Figure 5.19). For short storms where the phi-index line seems to accurately predict the pattern of rainfall excess (storm #18 and #27), the unit hydrograph predictions are generally good (Figure 5.20 and 5.21).

All of the unit hydrograph techniques did a similar job of predicting the observed

runoff hydrograph. The two Snyder models did slightly worse than the other techniques in general. Although the SDUH model was not superior to the traditional synthetic unit hydrographs, it was not inferior either. It produced a slightly better than average prediction.

Owl Run is smaller than most watersheds that are modeled with unit hydrographs; Ponce (1989) recommended that unit hydrographs only be applied to watersheds that were between 2.5 km² and 250 km². The SDUH model may perform better on larger watersheds that are more suitable for unit hydrograph analysis. When Ajward (1996) performed a similar study on two large watersheds, his relative error in the peak flow rate was usually less than 10% and always under 30%.

The SDUH model is an improvement over traditional synthetic unit hydrographs because it is based on physical, hydrologic relationships instead of empirical equations. In addition, it can account for watershed features such as ponds or wetlands, which traditional unit hydrograph techniques neglect. The SDUH model is conceptually and mathematically simple, requiring little input data.

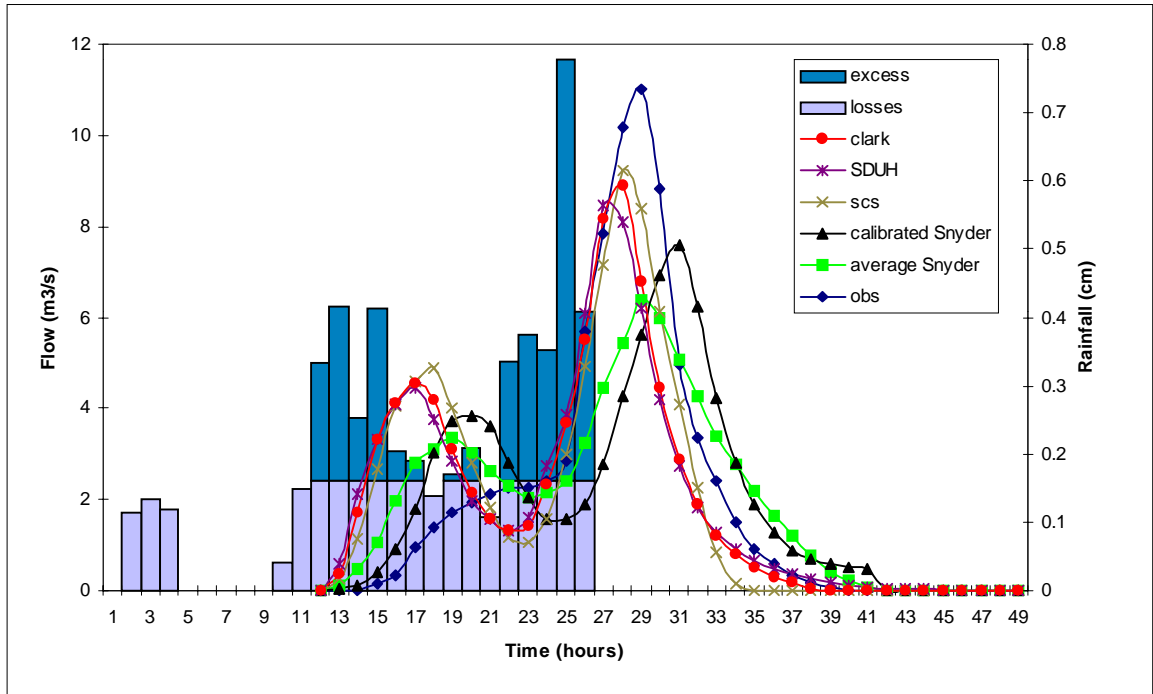


Figure 5.18. Observed and predicted hydrographs for storm #7 (May 28-29, 1990).

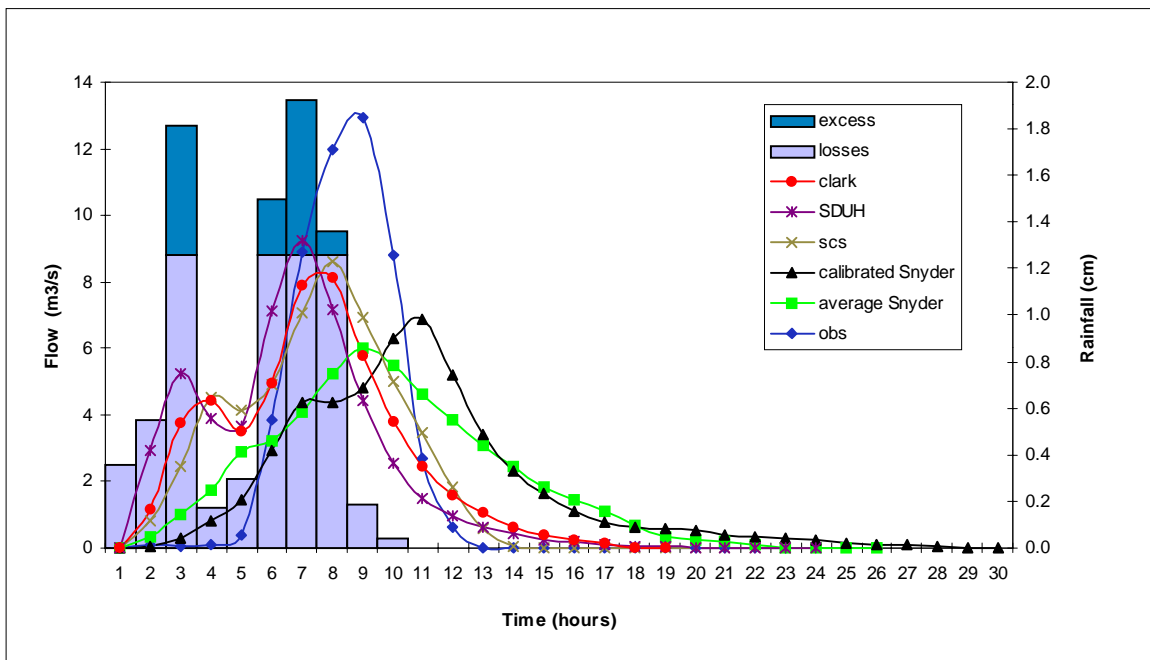


Figure 5.19. Observed and predicted hydrographs for storm #14 (August 9-10, 1990).

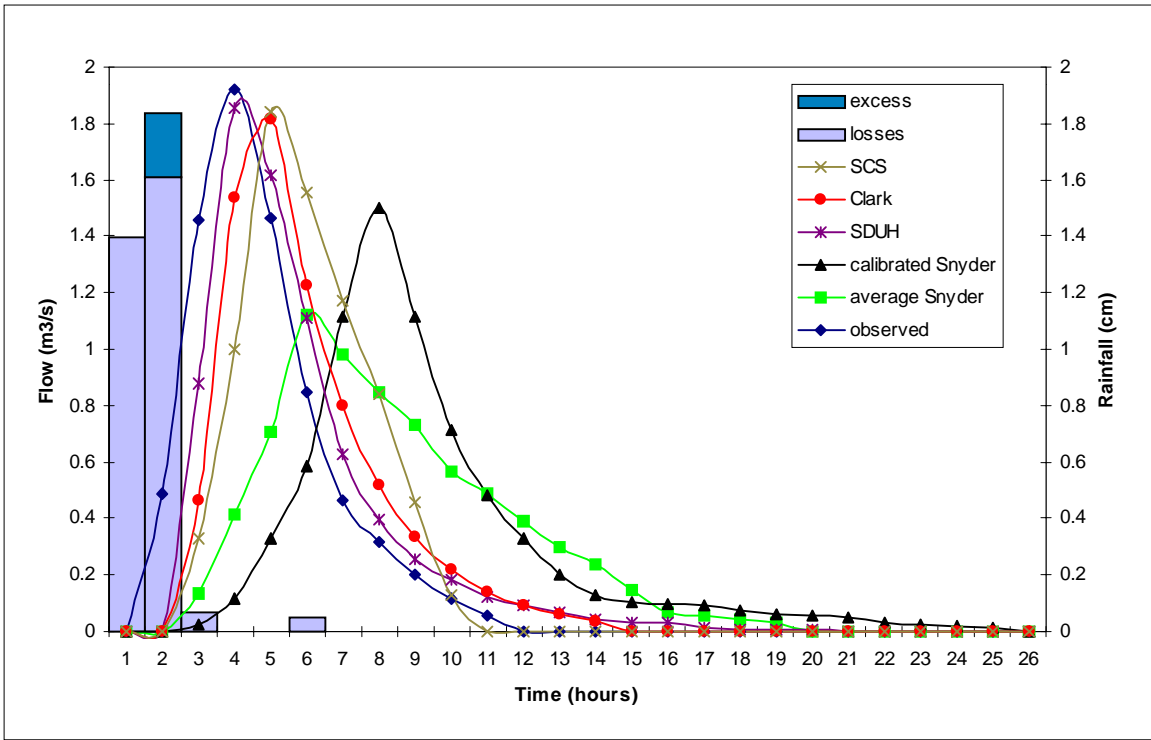


Figure 5.20. Observed and predicted hydrographs for storm #18 (October 5-6, 1991).

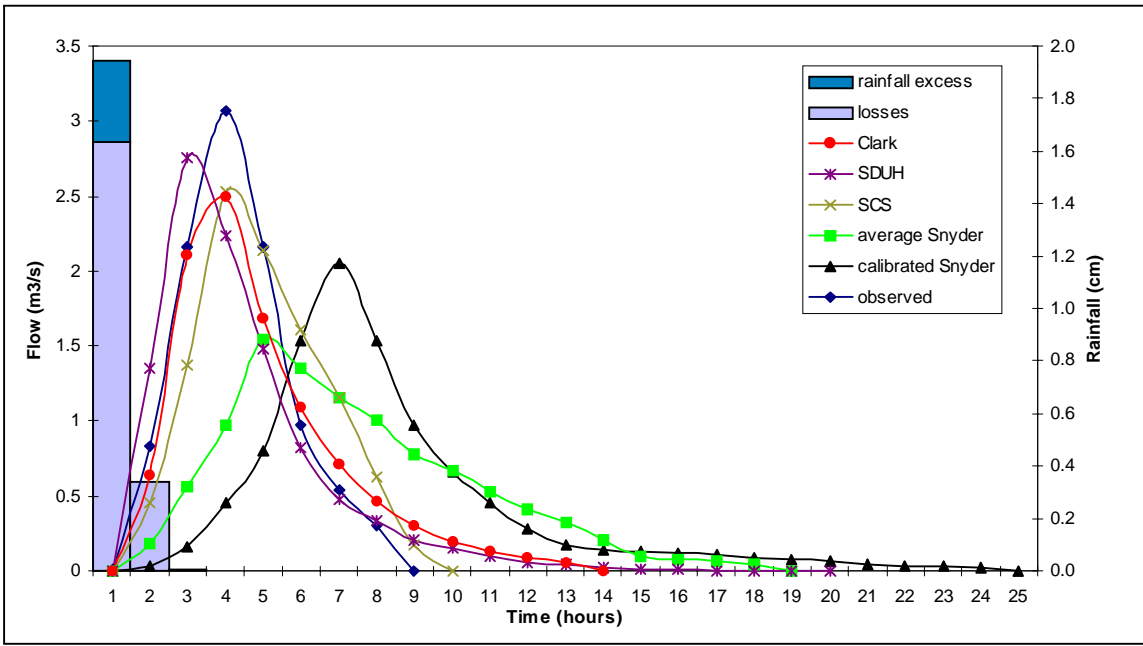


Figure 5.21. Observed and predicted hydrographs for storm #27 (July 31, 1992).

Most unit hydrograph models are “black box” models that directly transform rainfall into a runoff hydrograph at the watershed outlet (Bedient and Huber, 1992). The SDUH model can model the hydrologic response throughout the watershed. With the spatially distributed capabilities, the SDUH model may be coupled with distributed nonpoint source pollution models in the future.

One of the largest drawbacks of the SDUH model is that it relies on the traditional unit hydrograph assumptions of superposition and watershed linearity. There are a number of parameters that the SDUH model does not include that could significantly improve the hydrograph predictions. Currently, the SDUH model does not account for spatial variability in rainfall or runoff generation. If these two components were introduced the SDUH model may be applicable to a wider range of watersheds. The prediction of the SDUH model could also be improved if the variations of the rainfall excess intensity during the storm event were considered. The present model uses an average rainfall excess intensity for the entire storm.

6.0 Summary and Conclusions

6.1 Summary

A spatially distributed unit hydrograph model was developed using digital DEM elevation data and land use data collected during a field survey. The model's predictive capabilities were compared with four existing synthetic unit hydrograph techniques.

The SDUH model was applied to a 1153-ha agricultural watershed in the Piedmont region of Virginia. The USGS DEM (30-m) resolution was used to estimate the slope, aspect, flow distance and upstream area for each cell. The watershed was divided into "overland" and "channel" flow cells based on the area upstream above each cell. If the area was larger than the threshold of 1.8 ha (20 cells), the cell was assumed to be dominated by channel flow. The flow velocity for the overland cells was estimated using a kinematic wave approximation. Channel velocities were predicted by estimating the channel dimensions and combining the equilibrium flow rate with Manning's equation. Small ponds in the watershed were assigned a high roughness coefficient, and treated like regular channel sections. The largest pond in the watershed was modeled using Muskingum routing. The cumulative travel time to the watershed outlet was estimated by routing runoff over the elevation surface and summing the travel time through each cell along the runoff flow path.

The SDUH model was compared with the SCS, Clark, and two Snyder synthetic unit hydrographs. Based on a visual comparison, the SDUH model predicted the observed hydrograph shape better than the other types of synthetic unit hydrographs. There was very little difference in how well each of the unit hydrograph techniques predicted the peak flow rate; however, the calibrated Snyder and SDUH models

performed slightly better than the other methods. The SDUH had difficulty predicting the time to peak; it underpredicted the time to peak for 34 of 40 storms. According to the model efficiency statistic, the SDUH model predicted the hydrograph shape well. It had the highest model efficiency, among the 5 unit hydrograph techniques studied, for 12 storms. In addition, it had a model efficiency of at least 0.90 for 21 storms. The bias, TSAR, and TSSR statistics indicate that the SCS, Clark, and SDUH models were comparable in predicting the observed hydrograph shape, while the two Snyder methods do poorly.

In order to assess the impacts of scale on the SDUH model, it was applied to two subwatersheds within Owl Run. A visual comparison indicates that the predictions for subwatershed D and the entire watershed are generally similar, while the prediction for subwatershed C is not as good. The model predicts the peak flow rate more accurately for the entire watershed than for either subwatershed; the average relative error for the two subwatersheds is almost double the average for the entire watershed. The SDUH model tends to underpredict the peak flow rates for the entire watershed and for subwatershed C; the model overpredicts and underpredicts the peak flow rates for subwatershed D equally. The SDUH model tends to predict the time to peak equally well for the entire watershed and subwatershed D, while the prediction for subwatershed C is worse. When the average model efficiencies were compared, the SDUH model performs comparably on the entire watershed and subwatershed D, while the predicted hydrograph for subwatershed C does not fit the observed data as well.

In order to identify the input parameters that had the biggest impact on the SDUH model, a series of sensitivity analyses were performed. The channel flow threshold, overland velocity, and rainfall excess intensity had the biggest influence on the peak flow rate. The channel width, channel velocity, and rainfall excess intensity had the greatest effect on the time to peak prediction.

6.2 Conclusions

1. The SDUH predicted the peak flow rate and the shape of the observed hydrograph well; overall the predictions were comparable to the other synthetic unit hydrograph techniques.
2. There is a seasonal factor in how well each of the unit hydrograph models perform. The predictions were generally substantially worse in the spring than they were for summer and fall events.
3. The SDUH model predicted the observed hydrograph equally well for large and small storm events.
4. The SDUH model performed slightly better on the entire watershed than it did for either of the two smaller subwatersheds. In addition, there was a substantial difference in the model results between the two subwatersheds. The large pond in subwatershed C probably caused the difference between the two subwatersheds.
5. The division of the rainfall into losses and rainfall excess has a significant impact on the model predictions. Care should be taken when determining rainfall excess.
6. When a sensitivity analysis was performed, the channel flow threshold and the overland flow velocity had the largest impact on the peak flow rate. The channel velocity had the most influence over the time to peak.

6.3 Recommendations for Future Research

- Develop a technique to include spatially distributed rainfall excess in the model.
- Include an infiltration model to determine the time distribution of the rainfall excess.
- Develop a method to account for pond effects within the GIS model itself.
- Apply the SDUH model to watersheds with different characteristics and land uses, such as urban or tropical areas.
- Apply the SDUH model to a watershed with significant storage effects. Unit hydrographs are typically not applied to watersheds with large amounts of storage effects; however, the SDUH model may be able to include significant channel storage effects.
- Further investigation is needed into the seasonal changes that affect the accuracy of the unit hydrograph models.

7.0 References

- ASCE Task Committee of the Watershed Management Committee. 1993. Criteria for evaluation of watershed models. *J. Irrig. Drainage Eng.* 119(3):429-443.
- Ajward, M. H. 1996. A spatially distributed unit hydrograph model using a geographical information system. Ph.D. diss. Civil Engineering Dept., University of Calgary, Calgary.
- Arnold, J. G., P. M. Allen and G. Bernhardt. 1993. A comprehensive surface-groundwater flow model. *J. Hydrol.* 142(4):47-69.
- Beasley, D. B. and L. F. Huggins. 1981. ANSWERS Users Manual, EPA 905/9-82-001. U. S. Environmental Protection Agency, Chicago, IL.
- Bedient, P. B. and W. C. Huber. 1992. *Hydrology and Floodplain Analysis*. 2nd edition. New York: Addison-Wesley Publishing Company.
- Bhaskar, N. R., W. P. James and R. S. Devulapalli. 1992. Hydrologic parameter estimation using geographic information system. *J. Water Resources Planning and Management* 118(5):492-512.
- Brater, E. F. and H. W. King. 1976. *Handbook of Hydraulics for the Solution of Hydraulic Engineering Problems*. New York: McGraw-Hill Book Company.
- Chieng, S. and J. Luo. 1993. Application of GIS to peak flow estimation. In *Applications of Advanced Information Technologies: Effective Management of Natural Resources*. ed. C. D. Heatwole. 279-289. St. Joseph, Mich.: ASAE.
- Chow, V. T., D. R. Maidment, and L. W. Mays. 1988. *Applied Hydrology*. New York: McGraw-Hill Book Company.
- Clark, C. O. 1945. Storage and the unit hydrograph. *Trans. ASCE* 110:1419-1446.

- DeVantier, B. A. and A. D. Feldman. 1993. Review of GIS applications in hydrologic modeling. *J. Water Resources Planning and Management* 119(2): 246-261
- Drayton, R. S., B. M. Wilde and J. K. Harris. 1992. Geographical information system approach to distributed modeling. *Hydrological Processes* 6(3):361-368.
- Eastman, J. R. 1995. IDRISI for Windows, Users Guide, Version 1.0, Clark University, Worcester, Mass.
- Engman, E. T. 1986. Roughness coefficients for routing surface runoff. *J. Irrig. Drainage Eng.* 112(1):39-53.
- Gray, D. M. 1973. *Handbook on the Principles of Hydrology*. Syosset, N.Y.: Water Information Center, Inc.
- Green, I. R. A. and D. Stephenson. 1986. Criteria for comparison of single event models. *Hydrological Sci. J.* 31(3):395-411.
- Gurnell, A. M., D. Simmons, P. J. Edwards, J. Ball, J. Feaver, A. McLellan, and C. Ogle. 1993. GIS and multivariate ecological analysis: an input to integrated river channel management. In *HydroGIS 93: Application of Geographic Information Systems in Hydrology and Water Resources, Proceedings of the Vienna Conference*. eds. K. Dovar and H. P. Natchnebel, 363 - 374. Vienna: Int. Assoc. of Hydrological Sci.
- Gustafsson, P. 1993. High resolution satellite imagery and GIS as a dynamic tool in groundwater exploration in a semi-arid area. In *HydroGIS 93: Application of Geographic Information Systems in Hydrology and Water Resources, Proceedings of the Vienna Conference*. eds. K. Dovar and H. P. Natchnebel, 93-100. Vienna: Int. Assoc. of Hydrological Sci.
- Hill, J. M., V. P. Singh and H. Aminian. 1987. A computerized data base for flood prediction modeling. *Water Resources Bull.* 23(1):21-27.
- Huggins, L. F. and J. R. Burney. 1982. Surface runoff, storage, and routing. In *Hydrologic Modeling of Small Watersheds*, eds. C. T. Haan, H. P. Johnson, D. L. Brakensiek, ch. 5, 169-225. St. Joseph, Mich.: ASAE.
- Jenson, S. K. and J. O. Domingue. 1988. Extracting topographic structure from digital elevation data for geographic information system analysis. *Photogrammetric Engineering and Remote Sensing* 54(11):1593-1600.
- Jeton, A. E. and J. L. Smith. 1993. Development of watershed models for two Sierra Nevada basins using a geographic information system. *Water Resources Bull.* 29(6):923-932.

- Julien, P. Y., B. Saghafian and F. L. Ogden. 1995. Raster-based hydrologic modeling of spatially-varied surface runoff. *Water Resources Bull.* 31(3):523-536.
- Kao, J. J. 1992. Determining drainage pattern using DEM data for nonpoint source water quality modeling. *Water Sci. Technol.* 26(5):1431-1438.
- Kopp, S. M. 1996. Linking GIS and hydrologic models: where we have been, where we are going? In *HydroGIS 96: Application of Geographic Information Systems in Hydrology and Water Resources Management*, 133-139. Vienna, Austria.
- Larson, C. L., C. A. Onstad, H. H. Richardson, and K. N. Brooks. 1982. Some particular watershed models. In *Hydrologic Modeling of Small Watersheds*, eds. C. T. Haan, H. P. Johnson, D. L. Brakensiek, ch. 10, 409-434. St. Joseph, Mich.: ASAE.
- Lee, M. T., J. J. Kao, and Y. Ke. 1990. Integration of GIS, remote sensing, and digital elevation data for a hydrologic model. In *Hydraulic Engineering: Proceedings of the 1990 National Conference*. eds. H. H. Chang and J. C. Hill, 427-432. New York: ASCE.
- Linsley, R. K., M. A. Kohler, and J. H. Paulhus. 1975. *Hydrology for Engineers*. New York: McGraw Hill Book Company.
- Maidment, D. R. 1993a. GIS and hydrologic modeling. In *Environmental Modeling with GIS*. eds. M. F. Goodchild, B. O. Parks, L. Steyaert, New York: Oxford University Press.
- Maidment, D. R. 1993b. Developing a spatially distributed unit hydrograph by using GIS. In *HydroGIS 93: Application of Geographic Information Systems in Hydrology and Water Resources, Proceedings of the Vienna Conference*, eds. K. Dovar and H. P. Natchnebel, 181 - 192. Vienna: Int. Assoc. of Hydrological Sci.
- Mark, D. M. 1984. Automated detection of drainage networks from digital elevation models. *Cartographica* 21(2):168-178.
- Martz, L. W. and J. Garbrecht. 1993. Automated extraction of drainage network and watershed data from digital elevation models. *Water Resources Bull.* 29(6):901-908.
- Martz, L. W. and J. Garbrecht. 1992. Numerical definition of drainage network and subcatchment areas from digital elevation models. *Computers and Geosciences* 18(6):747-761.

- McCuen, R. H. 1989. *Hydrologic Analysis and Design*. Englewood Cliffs, N.J.: Prentice-Hall.
- McCuen, R. H., W. J. Rawls and S. L. Wong. 1984. SCS urban peak flow methods. *J. Hydraulic Eng.* 110(3):290-299.
- McDonnell, R. A. 1996. Including the spatial dimension: Using geographical information systems in hydrology. *Prog. Physical Geography* 20(2):159-177.
- Mostaghimi, S., P. W. McClellan, U. S. Tim, J. C. Carr, R. K. Byler, T. A. Dillaha, V. O. Shanholtz, and J. R. Pratt. 1989. Watershed/water quality monitoring for evaluating animal waste BMP effectiveness: Owl Run watershed. Pre-BMP evaluation final report. Report No. 0-P1-8906. Agricultural Engineering Department. Virginia Polytechnic Institute and State University, Blacksburg, VA.
- Mostaghimi, S., S. Shukla and R. B. Reneau. 1997. A mass balance study for investigating N retention and cycling in mixed and forested watersheds in the Chesapeake Bay drainage basin. Unpublished manuscript, Biological Systems Engineering Dept. Virginia Polytechnic Institute and State University.
- Muzik, I. 1988. Applications of GIS to SCS procedure for design flood hydrographs. In *Modeling Agricultural, Forest and Rangeland Hydrology*, 494 - 499. Chicago, Ill., 12-13 Dec.
- Muzik, I. 1995. GIS derived distributed unit hydrograph, a new tool for flood modeling. In *Developments in Computer Aided Design and Modeling for Civil Engineering*, ed. B. H. V. Topping, 243-247. Edinburgh, UK: Civil-Comp Press.
- Nash, J. E. and J. V. Sutcliffe. 1970. River flow forecasting through conceptual models. Part I - A discussion of principles. *J. Hydrol.* 10(3):282-290.
- Novotny, V. and H. Olem. 1994. *Water Quality: Prevention, Identification, and Management of Diffuse Pollution*. New York: Van Nostrand Reinhold.
- Overton, D. E. and M. E. Meadows. 1976. *Stormwater Modeling*. New York: Academic Press.
- Ponce, V. M. 1989. *Engineering Hydrology: Principles and Practices*. Englewood Cliffs, N.J.: Prentice Hall.
- Rewerts, C. C. and B. A. Engel. 1991. ANSWERS on GRASS: integrating a watershed simulation with a GIS. ASAE paper 91 - 2621. St. Joseph, Mich.: ASAE.
- Rodriguez-Iturbe, I. and J. B. Valdes. 1979. The geomorphological structure of hydrologic response. *Water Resources Res.* 15(6):1409-1420.

- Rosenthal, W. D., R. Srinivasan and J. G. Arnold. 1995. Alternative river management using a linked GIS-hydrology model. *Trans. ASAE* 38(3):783-790.
- Sasowsky, K. C. and T. W. Gardner. 1991. Watershed configuration and geographic information system parameterization for SPUR model hydrologic simulations. *Water Resources Bull.* 27(1):7-18.
- Shamsi, U. M. 1996. Stormwater management implementation through modeling and GIS. *J. Water Resources Planning and Management* 122(2):114-127.
- Sherman, L. K. 1932. Streamflow from rainfall by the unit-graph method. *Eng. News Record* 108:501-505.
- Singh, V. P. 1988. *Hydrologic Systems: Rainfall-Runoff Modeling*. vol. 1. Englewood Cliffs, N.J.: Prentice Hall.
- Singh, V. P., A. Banijkiewicz, and R. S. Ram. 1981. Some empirical methods of determining the unit hydrograph. In *Rainfall-Runoff Relationship*, ed. V. P. Singh, 67 - 90. Littleton, Colo.: ASAE.
- Snyder, F. F. 1938. Synthetic unit-graphs. *Transactions, American Geophysics Union* 19:447-454.
- Soil Conservation Service. 1986. *Urban Hydrology for Small Watersheds (TR-55)*. Washington, D. C.: USDA.
- Soil Conservation Service. 1972. *Hydrology: National Engineering Handbook*, section 4. Washington, D. C.: USDA.
- Srinivasan, R. and B. A. Engel. 1991. A knowledge-based approach to extract input data from a GIS. ASAE paper no. 91-7045. St. Joseph, Mich.: ASAE.
- Srinivasan, R. and J. G. Arnold. 1994. Integration of a basin scale water quality model with GIS. *Water Resources Bull.* 30(3):453-462.
- Tim, U. S. and R. Jolly. 1994. Evaluating agricultural nonpoint source pollution using integrated geographic information systems and hydrologic water quality model. *J. Environ. Qual.* 23(1):25-35.
- Todini, E. 1988. Rainfall-runoff modeling-- past, present, and future. *J. Hydrol.* 100: 341 - 352.
- Viessman, W., J. W. Knapp, G. L. Lewis and T. E. Harbaugh. 1977. *Introduction to Hydrology*. 2nd edition. New York: Harper-Row Publishers.

- Wang, Yang. 1991. Application of a nonpoint source pollution model to a small watershed in Virginia. M.S. thesis. Blacksburg: Virginia Polytechnic Institute and State University.
- Wolfe, M. L. 1992. GIS-assisted input data set development for the finite element storm hydrograph model (FESHM). *Appl. Eng. Agric.* 8(2):221-227.
- Yen, B. C. and K. T. Lee. 1997. Unit hydrograph derivation for ungauged watersheds by stream-order laws. *J. Hydrologic Eng.* 2(1):1-9.
- Young, R. A., C. A. Onstad, D. D. Bosch and W. P. Anderson. 1985. Agricultural nonpoint surface pollution models (AGNPS) I and II, model documentation. St. Paul: Minn. Pollution control Agency and Washington, D. C.: USDA-ARS.
- Zollweg, J. A., W. J. Gburek and T. S. Steenhuis. 1996. SMoRMod- a GIS-integrated rainfall-runoff model. *Trans. ASAE* 39(4):1299-1307.